

Analysis of the connection between primary sclerosing cholangitis and inflammatory bowel disease

Dissertation with the aim of achieving a doctoral degree at the Faculty
of Mathematics, Informatics and Natural Sciences

Department of Biology, University of Hamburg

Submitted by

Friederike Stumme

Hamburg, March 2022

Reviewers:

Prof. Dr. Samuel Huber

I. Department of Medicine

University Medical Center Hamburg-Eppendorf

Martinistraße 52

20251 Hamburg

Prof. Dr. Julia Kehr

Department of Biology

University of Hamburg

Ohnhorststraße 18

22609 Hamburg

Date of disputation 17.06.2022

Table of Content

1	Summary	8
2	Zusammenfassung	10
3	Introduction.....	12
3.1	Primary sclerosing cholangitis.....	12
3.1.1	Pathogenesis and epidemiology.....	12
3.1.2	Inflammatory bowel disease and its association to PSC	13
3.2	The microbiome	14
3.2.1	The intestinal microbiota.....	14
3.2.2	The role of the intestinal microbiota in PSC and PSC-associated IBD	14
3.3	Synthesis of bile acids and enterohepatic circulation	15
3.3.1	Biosynthesis of bile acids	15
3.3.2	Enterohepatic circulation	16
3.3.3	Bile acids in PSC	17
3.4	The immune system in PSC.....	18
3.4.1	The innate immune system in PSC	19
3.4.2	The adaptive immune system in PSC.....	20
3.4.2.1	Generation and differentiation of T cells	20
3.4.2.2	Role of T cells in PSC.....	21
3.4.2.3	Generation and differentiation of B cells.....	22
3.4.2.4	Role of B cells in PSC and PSC-associated IBD.....	23
3.5	Genetic predispositions in PSC	24
3.5.1	Function of the IL-2R α	24
3.5.2	SNPs in the <i>IL2RA</i> gene are associated with PSC and IBD	25
3.6	Experimental mouse model of PSC.....	26
3.6.1	<i>Mdr2</i> -deficient mouse model.....	26
3.6.2	DDC induced liver pathology	27
3.7	Experimental mouse models of colitis.....	27
3.7.1	DSS colitis.....	27
3.7.2	Infection with <i>Citrobacter rodentium</i>	27

3.8	Aim of the study.....	29
4	Material and Methods	30
4.1	Material.....	30
4.1.1	Consumables.....	30
4.1.2	Equipment	31
4.1.3	Reagents	32
4.1.4	Buffers and solutions.....	33
4.1.5	Animals	35
4.1.6	Antibodies.....	35
4.1.7	Kits	36
4.1.8	Software.....	36
4.2	Methods.....	37
4.2.1	Genotyping	37
4.2.2	Mouse experiments.....	41
4.2.2.1	Acute and chronic DSS colitis	41
4.2.2.2	<i>Citrobacter rodentium</i> infection.....	42
4.2.2.3	DDC as a model of chemical induced sclerosing cholangitis.....	42
4.2.2.4	Fecal microbiome transplantation in germ-free mice	42
4.2.2.5	<i>In vivo</i> depletion of different immune cell subsets.....	43
4.2.3	Mouse endoscopy.....	43
4.2.4	Isolation and preparation of organs and blood samples.....	43
4.2.4.1	Isolation of lymphocytes from the liver	44
4.2.4.2	Isolation of lymphocytes from the colon	44
4.2.4.3	Isolation of lymphocytes from the spleen.....	45
4.2.4.4	Erythrocyte lysis	45
4.2.4.5	Extraction of blood serum and plasma	45
4.2.5	Blood analysis	45
4.2.6	Histology of tissue samples	46
4.2.6.1	H&E and Sirius red staining	46
4.2.7	Measurement of bile acids in serum and stool	46
4.2.8	Flow cytometry (FACS).....	47
4.2.8.1	Live dead staining.....	47

4.2.8.2	Extracellular staining	47
4.2.8.3	Intracellular staining.....	47
4.2.8.4	Cell counting for FACS	48
4.2.9	Fluorescence-activated cell sorting (FACS-sort)	48
4.2.10	<i>In vitro</i> suppression Assay	48
4.2.10.1	Isolation of CD4 ⁺ T cells and APCs using Magnetic activated cell sorting (MACS)	48
4.2.10.2	Labeling of CD4 ⁺ T cells with proliferation dye	49
4.2.10.3	Isolation of Foxp3 ⁺ Treg.....	49
4.2.10.4	Pipetting scheme of <i>in vitro</i> suppression assay	49
4.2.11	Statistical analysis.....	50
5	Results.....	51
5.1	Analysis of the mechanism(s) of how colitis affects PSC	51
5.1.1	Induction of colitis in an experimental mouse model of PSC, leads to reduced liver pathology.....	51
5.1.2	Role of the microbiota in the protective effect of colitis on PSC development.....	58
5.1.2.1	The protective effect of colitis on the liver pathology was not transferable via fecal microbiota transplantation	58
5.1.3	Role of bile acids in the protective effect of colitis on PSC development.....	61
5.1.3.1	Unconjugated bile acids were reduced in the gut microbiota of <i>Mdr2</i> -deficient mice with DSS colitis.....	61
5.1.4	The innate immune system was not the major driver of the observed reduction in liver pathology in the presence of colitis	63
5.1.4.1	Impairment of the phagocytosis during PSC-associated colitis still resulted in reduced liver pathology.....	63
5.1.4.2	The reduced liver pathology during colitis was not dependent on neutrophils and granulocytes	66
5.1.4.3	A mouse model without T and B cells suggested a non-essential role of the innate immune system in the protective effect.....	69
5.1.5	Role of T and B cells in the protection.....	71
5.1.5.1	CD8 ⁺ T cells were not the major driver of the observed protection of colitis in <i>Mdr2</i> -deficient mice	71
5.1.5.2	Role of CD4 ⁺ Foxp3 ⁺ regulatory T cells in the protective effect.....	75

5.1.5.3B cells might be one major player in the protection of colitis on liver pathology	78
5.2 Role of an <i>Il2ra</i> ^{SNP} in disease development of PSC	81
5.2.1 Generation of <i>Il2ra</i> ^{SNP} mice	81
5.2.2 <i>Il2ra</i> ^{SNP} <i>ex vivo</i> Treg show a reduced suppressive capacity <i>in vitro</i>	82
5.2.3 Characterization of <i>Il2ra</i> ^{SNP} mice (comparison HH vs. Marson)	84
5.2.4 <i>Il2ra</i> ^{SNP} mice develop more severe sclerosing cholangitis compared to <i>Il2ra</i> ^{wt} mice in a chronic state of disease	86
5.2.5 The <i>Il2ra</i> ^{SNP} has no impact on the protective effect of colitis on PSC development in the model of acute DSS colitis.....	89
6 Discussion	92
6.1 Colitis protects against PSC in different experimental mouse models.....	92
6.2 An indirect effect of the microbiota by a change in the fecal bile acid composition, could play a role in the protection of colitis on PSC development.....	95
6.3 The major driver of the observed protection is not the innate immune system	98
6.4 The cells of the adaptive immune system are involved in the protective effect of IBD on PSC development.....	100
6.4.1 Depletion of T cells does not ameliorate the protective effect of IBD on PSC development	101
6.4.2 B cells are an important player in the observed protection.....	103
6.5 Role of an <i>Il2ra</i> SNP on the disease severity of PSC and PSC-associated IBD, as well as the protective effect of IBD on PSC development	105
6.5.1 <i>Il2ra</i> ^{SNP} mice have impaired Treg function and develop more liver pathology in a mouse model of sclerosing cholangitis	105
6.5.2 The protective effect of IBD on PSC development is not impaired due to the <i>Il2ra</i> ^{SNP} in a mouse model of DSS colitis.....	106
7 Conclusion and Outlook	109
8 Appendix	110
8.1 References	110
8.2 List of abbreviations.....	115
8.3 List of figures.....	118
8.4 List of tables	120
8.5 Acknowledgment	121
8.6 Curriculum vitae.....	122

8.7	Eidesstattliche Erklärung.....	124
8.8	Statement under oath.....	124
8.9	Confirmation of linguistic correctness.....	124

1 Summary

Primary sclerosing cholangitis (PSC) is a chronic cholestatic disease affecting the intra- and extra-hepatic bile ducts, which progresses to end-stage liver disease. The etiology of PSC is still not fully understood and there is no effective medical treatment available. Two potential factors, impacting PSC are concomitant inflammatory bowel disease (IBD) and genetic predispositions. PSC is highly associated with IBD, where 50-80 % of PSC patients show co-occurrence of IBD, but it is unknown how PSC and IBD affect each other. Furthermore, multiple genetic risk factors were already identified to be associated with PSC. One of the most frequent ones are polymorphisms in the *IL2RA* gene, which are highly associated with PSC patients.

The first aim of this study was to understand how colitis affects the disease development of PSC. Therefore, different experimental models of colitis (DSS, *Citrobacter rodentium* infection) were induced in experimental mouse models of sclerosing cholangitis (*Mdr2*^{-/-}, DDC). Surprisingly, induction of colitis resulted in reduced liver pathology in experimental mouse models for sclerosing cholangitis. This protective effect of colitis on PSC severity was further investigated. It was highly suggested, that the gut-liver axis plays an important role in the disease development of PSC and PSC-associated IBD. Therefore, influences of the intestinal microbiota, the bile acid composition and different immune cell subsets were analyzed. The protective effect of colitis on PSC development was not transferable via the fecal microbiota transplantation. Indeed, fecal microbiota transplantation from mice with PSC and colitis into germ-free mice had a rather pathogenic effect on the liver pathology compared to fecal microbiota transplantation from mice with PSC without colitis. Analysis of the bile acids revealed that colitis induction led to decreased unconjugated bile acids in the stool of an experimental mouse model of sclerosing cholangitis. But the relevancy of this findings requires further studies. The most crucial impact in the protective effect of colitis on PSC development was found for B cells. Depletion of B cells resulted in the absence of the protective effect of colitis on PSC development, while an effect of T cells and innate immune cells was not found.

The second aim of this study was to investigate the role of the rs61839660 *IL2RA* single nucleotide polymorphism (SNP) in the progression of PSC and PSC-associated colitis. To this end, the disease development of sclerosing cholangitis in *Mdr2*-deficient mice with the

corresponding SNP in the *Il2ra* gene was analyzed, with and without induction of colitis. Additionally, Foxp3⁺ Treg function, which is dependent on a functional IL-2 receptor, was analyzed *in vitro*. A defect in the suppressive capacity of Foxp3⁺ Treg with the SNP in the *Il2ra* gene was found. Furthermore, it led to increased disease susceptibility in an experimental mouse model of sclerosing cholangitis. No effect of the SNP was identified in the protective effect of colitis on PSC development in an acute model of colitis.

Overall, our data indicate that B cells mediated the protective effect of colitis on PSC development. However, the detailed mechanism is not clear yet. The investigated *Il2ra* SNP had no impact on the protective effect of colitis on PSC development. However, increased disease susceptibility for sclerosing cholangitis was found, which might be due to impaired suppressive capacity of Foxp3⁺ Treg.

2 Zusammenfassung

Die Primär sklerosierende Cholangitis (PSC) ist eine chronische Entzündung der intra- und extra-hepatischen Gallengänge, welche sich zu einer Lebererkrankung im Endstadium entwickelt. Die Ätiologie der PSC ist noch nicht vollständig verstanden und eine medizinische Behandlung ist derzeit nicht verfügbar. Zwei potentielle Risikofaktoren, welche zu einer PSC beitragen können, sind chronisch entzündliche Darmerkrankungen (CED) und genetische Prädispositionen. Das Auftreten einer PSC ist stark mit dem Auftreten einer CED assoziiert. Ungefähr 50-80 % der PSC Patienten haben eine begleitende CED. Bisher ist nicht bekannt wie die Krankheiten sich gegenseitig beeinflussen. Ein weiterer Risikofaktor sind genetische Prädispositionen. Single Nukleotid Polymorphismen (SNPs) im *IL2RA* Gen gehören zu den am häufigsten auftretenden Mutationen, die mit einer PSC assoziiert sind.

Das erste Ziel dieser Arbeit befasste sich damit, zu verstehen wie eine Kolitis das Auftreten einer PSC beeinflusst. Dafür wurden zwei Kolitis-Mausmodelle (DSS, *Citrobacter rodentium* Infektion) in unterschiedliche Mausmodelle für sklerosierenden Cholangitis (*Mdr2*^{-/-}, DDC) induziert. Überraschenderweise führte die Induktion einer Kolitis zu einer verminderten Leberpathologie in Mäusen mit einer experimentellen sklerosierenden Cholangitis. Dieser protektive Effekt wurde weitergehend untersucht. Es wird angenommen, dass die Darm-Leber Achse eine entscheidende Rolle für die Entwicklung einer PSC und PSC-assoziierten CED spielt. Daher wurden die Rolle des intestinalen Mikrobioms, die Zusammensetzung der Gallensäuren, sowie die Rolle unterschiedlicher Immunzellen untersucht.

Die Protektion der Kolitis auf die PSC war nicht durch eine Stuhltransplantation transferierbar. Tatsächlich hatte die Stuhltransplantation mit Mikrobiota von Mäusen mit PSC und Kolitis in keimfreie Mäuse eher einen pathogenen Effekt auf die Leberpathologie im Vergleich zu Stuhltransplantation mit Mikrobiota von Mäusen mit PSC ohne Kolitis. Die Analyse der Gallensäuren zeigte, dass eine Kolitis zur Verringerung der unkonjugierter Gallensäuren im Stuhl von Mäusen mit einer experimentellen sklerosierenden Cholangitis führt. Allerdings bedarf die Relevanz dieser Ergebnisse weitere Untersuchungen. Der größte Einfluss auf den protektiven Effekt einer Kolitis auf die PSC konnte für B Zellen gezeigt werden. Die Depletion von B Zellen führte zu dem Ausbleiben des protektiven Effekts der Kolitis auf die PSC, während

kein Effekt für T Zellen und Immunzellen des angeborenen Immunsystems beobachtet werden konnten.

Das zweite Ziel dieser Arbeit war es, die Rolle des rs61839660 *IL2RA* SNP im Verlauf einer PSC und PSC-assoziierten CED zu untersuchen. Zu diesem Zweck wurde der Krankheitsverlauf der sklerosierenden Cholangitis in *Mdr2*-defizienten Mäusen mit und ohne den SNP im *Il2ra* Gen, sowie mit und ohne assoziierter Kolitis untersucht. Zusätzlich wurde die Funktion von Foxp3⁺ Treg *in vitro* untersucht, welche von einem funktionalen IL-2 Rezeptor abhängt. Dabei wurde ein Defekt in der suppressiven Kapazität der Foxp3⁺ Treg mit einem SNP im *Il2ra* Gen festgestellt. Des Weiteren führte der SNP zu einer verstärkten Erkrankung in einem experimentellen Mausmodell der sklerosierenden Cholangitis. Es konnte kein Effekt des SNPs auf den protektiven Effekt von Kolitis auf die PSC festgestellt werden.

Insgesamt zeigen unsere Daten, dass der protektive Effekt der Kolitis auf die Entwicklung einer PSC von B Zellen vermittelt wird. Allerdings ist der detaillierte Mechanismus noch nicht verstanden. Der untersuchte *Il2ra* SNP hatte hingegen keinen Einfluss auf den protektiven Effekt der Kolitis auf die Entwicklung einer PSC. Jedoch führte der *Il2ra* SNP zu einer verstärkten Krankheitsentwicklung einer sklerosierenden Cholangitis, welche mit der verminderten suppressiven Kapazität der Foxp3⁺ Treg in Zusammenhang gebracht werden könnte.

3 Introduction

3.1 Primary sclerosing cholangitis

3.1.1 Pathogenesis and epidemiology

Primary sclerosing cholangitis (PSC) is a cholestatic liver disease, characterized by inflammation of the intra- and extra-hepatic bile ducts, chronic bile duct destruction, which leads to sclerosis and cholestasis, and progresses to end-stage liver disease (1). At present, no effective medical treatment is available (2-4). As a consequence, disease progression to end-stage liver disease are inevitable in most patients (5). In 1983, liver transplantation was established as the only potentially curative treatment option for advanced disease (6, 7), however, at least 25% of patients develop recurrent disease afterwards (8). In addition to cirrhosis, approximately 10-15 % of PSC patients will develop cholangiocarcinoma during their lifetime (9). PSC is likely to have an underlying multifactorial etiology, with a predominant immune-mediated process (10).

The disease often develops asymptotically (11, 12), however, possible symptoms include fatigue, pruritus, and right upper quadrant pain. Characteristics of the progression of biliary epithelia disorders, so-called cholangiopathies, are mild epithelial changes with few infiltrating lymphocytes in early lesions that evolve into substantial concentric layers of fibrosis circumferential to the cholangiocyte lining of the bile ducts, also referred to as onion-skin-like fibrosis (13). Cholangiopathies are diagnosed histopathologically and radiologically by magnetic resonance cholangiopancreatography (MRCP) or endoscopic retrograde cholangiopancreatography (ERCP), which enable visualization of dominant strictures of the bile ducts with associated dilatation in between the strictures. In addition, cholestatic biochemical profiles show elevated levels of alkaline phosphatase (ALP) and gamma-glutamyl transferase (GGT).

Published reports show a difference in the incidence regarding the geographical location. In northern Europe it is at 1.3 per 100 000 people per year. The prevalence of PSC is with up to 16.2 per 100 000 people, the highest in northern Europe and markedly lower in Asia (1, 14, 15). With a prevalence of less than 50 per 100 000 people, PSC is classified as a rare disease.

More than 60 % of PSC patients are men and the median age at onset is 30-40 years (14, 16, 17).

The pathogenesis of PSC is still not fully understood. Different hypothesis have attempted to explain the etiology and pathogenesis of PSC (e.g. a role of different immune subsets, the microbiota and genetic predispositions). Treatment with corticosteroids and immunosuppressant agents have not demonstrated any improvement in disease activity or outcome of PSC, suggesting that it does not arise exclusively due to inflammation, but that it is a multifactorial disease (2).

3.1.2 Inflammatory bowel disease and its association to PSC

Inflammatory bowel disease (IBD) is a chronic idiopathic inflammatory disease of the gastrointestinal tract. Differences in the clinical presentation divides them into two subtypes, ulcerative colitis (UC) and Crohn's disease (CD). UC is a relapsing non-transmural inflammation that is mostly restricted to the colon. The inflammation starts in the rectum and continues throughout the colon. Inflammation of the whole colon is referred to as pancolitis, and inflammation of the terminal ileum is termed backwash ileitis. CD is a relapsing transmural inflammation of the gastrointestinal mucosa that can affect the entire gastrointestinal tract from the mouth to the anus. Typically, it can be described as a discontinuous inflammation, where regions of inflamed and uninflamed tissues can be found simultaneously (18).

For the purpose of this study, the strong association between PSC and IBD is particularly important (19, 20). Around 50-80 % of patients with PSC have, or subsequently develop colonic IBD (21). On the other hand, only 5-10 % of IBD patients develop PSC (22, 23). PSC-associated IBD presents differently to UC or CD. PSC-associated IBD is typically a mild pancolitis with a right-sided predominance, backwash ileitis and rectal sparing (24). PSC patients with associated IBD also have an increased risk of developing colorectal cancer (19, 24, 25).

PSC and IBD are interrelated conditions that may share an underlying predisposition (26). Different hypotheses suggest a role of the gut-liver axis and involvement of the immune system and the gut microbiota. It was shown that activated T cells can migrate from the gut to the liver of PSC patients and localize around bile ducts (27). It was also described that the liver may act as a firewall, mediating mutualism between the host and its gut commensal

microbiota (28). In addition, it was found that specific gut bacteria can disrupt the gut barrier integrity and initiate an inflammatory response in the liver following translocation (29). Unfortunately, it is still not understood how these two diseases affect each other.

3.2 The microbiome

The microbiome describes the genome of all the microorganisms and includes bacteria, fungi, parasites and viruses. The microbiome can be symbiotic and pathogenic. In this work, it was focused on the commensal microbiota of the gastrointestinal tract, describing the symbiotic microorganisms per se. A disturbance in that balance can lead to a change in the composition of the microbiota (dysbiosis), stopping these normal interactions. As a result, the body may become more susceptible to disease (30).

3.2.1 The intestinal microbiota

The intestinal microbiota describes all the microorganisms in the intestinal tract. It contains up to 1 000 different species of known bacteria. Most of the species belong to the phyla *Firmicutes* and *Bacteroides*. The composition of the intestinal microbiota can change due to different factors, such as genetic predispositions, diet, age but also underlying medical conditions as well as medications and antibiotics. The intestinal microbiota plays an important role in the maintenance of homeostasis in the intestinal tract. It is an important player in the synthesis of vitamins, amino acids and other nutrients crucial for host health. A dysbiosis of the intestinal microbiota is often associated with chronic diseases due to reduced bacterial diversity (31).

3.2.2 The role of the intestinal microbiota in PSC and PSC-associated IBD

PSC and IBD are both characterized by a dysbiosis. The gut-liver axis is suggested to play a role in the disease development of PSC and PSC-associated IBD. During intestinal inflammation, the gut barrier becomes leaky such that gut microbes, their metabolites, and immune cells, can pass the gut barrier and translocate via the portal vein to the liver, where they can induce inflammation (32-35). Different studies investigating the microbiome in PSC patients were able to show that a dysbiosis, characterized by reduced diversity in the fecal microbiota, occurred compared to controls (36, 37). Although some differences in the composition of the PSC microbiota were detected in these studies, it was overall characterized by an increase of

Veillonella, *Enterococcus*, *Streptococcus*, *Lactobacillus* and *Enterobacter*, as well as a depletion of *Firmicutes*, producing anti-inflammatory short chain fatty acids (SCFA), *Faecalibacterium* and *Coprococcus* (38).

In addition, it was shown in a mouse model of experimental PSC that inoculation of germ-free mice with fecal microbiota from PSC-IBD patients leads to increases susceptibility to DDC-induced sclerosing cholangitis. *Klebsiella pneumoniae* was identified to disrupt the intestinal epithelium to initiate bacterial translocation and liver inflammatory responses (29). Members of the Enterobacteriaceae family, including *K. pneumoniae*, were often observed in the microbiota of individuals with hepatobiliary diseases such as liver cirrhosis and primary biliary cirrhosis (PBC) (39, 40).

A recent study further investigated the fecal microbiota of patients with PSC compared to PSC-IBD, UC and healthy controls. It was shown that the microbial alterations found in PSC patients were independent from associated colitis, medication, or grade of colonic inflammation. In addition, significant differences between PSC and UC in microbial abundance and diversity were found, indicating that PSC drives the dysbiosis observed in both patient groups with PSC only, as well as in those with PSC-IBD (41). The same was shown in other studies as well (36, 37, 42).

3.3 Synthesis of bile acids and enterohepatic circulation

3.3.1 Biosynthesis of bile acids

Two major classes of bile acids (BAs) exist in mammals: primary and secondary BAs. Primary BAs are synthesized from cholesterol in hepatocytes in the liver, while secondary BAs are derivatives of primary BAs generated by microbial metabolisms in the intestine (43, 44). The two primary BAs in human are colic acid (CA) and chenodeoxycholic acid (CDCA), whereas rodent hepatocytes produce CA, muricholic acid (MCA), and ursodeoxycholic acid (UDCA). In humans, UDCA is a secondary bile acid and MCAs are generally not detected (45). Bile acid synthesis proceeds via the “classical” or the “alternative” pathway. Cytochrome P450 (CYP) enzymes are the key regulators for BAs synthesis.

The classical pathway, defined by the activities of CYP7A1, CYP8B1, and CYP27A1, is thought to account for the majority of primary BAs that are produced in steady state (43, 46). The

classical pathway is initiated by 7 α -hydroxylation of cholesterol catalyzed by CYP7A1 (47). CYP7A1 is the rate-limiting enzyme and determines the amount of bile acids produced (45). The alternative pathway is upregulated during periods of hepatic stress and synthesizes predominantly CDCA (48). It is a mitochondrial-based process, therefore, all cells and tissues have the potential to produce CDCA. The alternative pathway begins with the hydroxylation of the cholesterol side chain by CYP27A1 in extrahepatic sites, followed by 7 α -hydroxylation of the oxysterol intermediates by CYP7B1 (49).

In both pathways, the final step of BA synthesis is the conjugation of primary BAs to the amino acids taurine or glycine. For this process the key enzymes are the bile acid:amino acid transferase (BAT) and the bile acid:CoA synthase (BACS). Conjugation to taurine or glycine increases the solubility and decreases the toxicity on the biliary epithelium and the hepatocytes. Next, the BAs are actively transported into the bile via the bile salt export pump (BSEP) and stored in the gallbladder (46). The gallbladder contracts during food intake and BAs are released into the duodenum.

Many bacterial taxa in the colon express bile salt hydrolase (BSH) enzymes, which deconjugate taurine- and glycine-conjugated BAs (43, 44). The hydroxysteroid dehydrogenase (HSDH) enzyme, also produced by enteric bacteria, converts primary BA into secondary BA products. The most common secondary BA are deoxycholic acid (DCA; the 7-dehydroxylation product of CA) and lithocholic acid (LCA; the 7-dehydroxylation product of CDCA). The 7-dehydroxylation of the primary murine α MCA and β MCA results in the formation of murideoxycholic acid (MDCA) (45). Omega-MCA (ω MCA) is a major metabolite of β MCA. Other metabolites from β MCA are hyodeoxycholic acid (HDCA) and hyocholic acid (HCA). By further isomerization, iso- and allo- BAs are generated. Through gut microbial oxidation, oxo- BAs are generated (45).

3.3.2 Enterohepatic circulation

The enterohepatic circulation describes the path of BAs from synthesis, secretion, absorption to recirculation. BAs are synthesized by hepatocytes via the classical or alternative pathway. BAs are conjugated to glycine or taurine, which enables their active transport into bile ducts and storage in the gallbladder (45). During food intake, the BAs are secreted from the gallbladder into the duodenum. This is important for the digestion of fat and protein, and the uptake of liposoluble vitamins. In addition, BAs increase the pH in the duodenum to buffer the

acidic chymus from the stomach. The majority of BAs (90-95 %) are actively reabsorbed in the terminal ileum. Some of the recirculating BAs are directly circulating back to the liver and restrict *de novo* BA synthesis in the liver by suppressing expression of CYP7A1, the rate limiting enzyme in the classical BA biosynthetic pathway (43). The other recirculating BAs activate FXR in ileal epithelial cells, which induces fibroblast growth factor (FGF)-15/19. FGF-15/19 is secreted into portal circulation, which also leads to suppressed expression of CYP7A1 in the liver, and therefore, *de novo* BA synthesis (43). Such tight and integrated control over BA synthesis and circulation serves as a rheostat to maintain a functional, but not toxic, circulating BA pool (43). A small part of BAs (5-10 %) escape the reabsorption in the ileum and enters the large intestine for bacterial metabolism into secondary BAs. These are either passively reabsorbed in the colon to re-enter the enterohepatic circulation, or are excreted with the feces (43).

3.3.3 Bile acids in PSC

The close association of PSC and IBD points towards a potential role of the gut-liver axis in the disease development of PSC and PSC-associated IBD. Thereby, interactions between the gastrointestinal microbiota and the hepatic bile acid metabolism could play an important part in the development of disease. A bidirectional interaction between the intestinal microbiota and the hepatic BA metabolism exists (50). BAs have antimicrobial capacity and can damage the bacterial cell membrane. Therefore, BAs can inhibit bacterial outgrowth (34, 51). On the other hand, intestinal microbiota also alters BAs (52).

Treatments which are effective in other cholestatic liver diseases have been tested in PSC with a limited degree of success (2, 53). The bile acid Ursodeoxycholic acid (UDCA) is an effective treatment of primary biliary cirrhosis (PBC). Whether PSC patients benefit from UDCA treatment remains controversial (54). Initial data showed an improvement in serum liver biochemistry and histology measurements (1, 55, 56), and a double-blinded, randomized, placebo control trial of 13-15 mg/kg of UDCA suggested improvement in serum liver tests but not in symptoms, and most importantly, not in difference in treatment failure (defined as death, liver transplantation, histologic progression or progression to cirrhosis) (57). A long-term, randomized, placebo-controlled study of high doses UDCA was terminated after 6 years because, despite improved biochemical test results, the frequency of adverse events (death,

liver transplantation, cirrhosis) was significantly higher in the active group compared to the placebo group (58). Histological data suggest a benefit of UDCA in the prevention of cholangiocarcinoma (59), but these data are not supported by randomized, placebo-controlled trials (60). Therefore, no substantive recommendation can be given for normal doses, but high-doses should be avoided (1).

Defects in mechanisms protecting against bile acid toxicity have been proposed as possible key players in PSC development (55, 61, 62). One example is the bicarbonate umbrella hypothesis. It describes that bicarbonate ions, secreted by cholangiocytes and hepatocytes form a defensive barrier on the apical side of the hepatocytes (63). Malfunctioning of this system results in the crossing of glycine-conjugated bile acids of the cholangiocyte membrane, bypassing membrane transporters. This phenomenon leads to cholangiocyte apoptosis and senescence (62). There is evidence supporting the concept that in cholangiopathies like PSC and PBC, the biliary bicarbonate umbrella is defective. It can be stabilized through 24-*nor*ursodeoxycholic acid (*nor*UDCA), due to its ability of undergoing cholehepatic shunting (64). The relative resistance of unconjugated *nor*UDCA to N-acyl-amidation with taurine or glycine, leads to reabsorption by the cholangiocytes, returning to the sinusoids and hepatocytes via the periductular capillary plexus, and is re-secreted into the bile. This results in ductal targeting and leads to profound stimulation of cholangiocellular bicarbonate secretion, and consequently, induction of BA-independent bile flow and flushing of bile ducts (65).

A double-blinded, randomized, placebo-controlled, phase II study evaluating *nor*UDCA in PSC patients, showed that *nor*UDCA significantly reduced ALP values dose-dependently in the treatment groups. The safety profile was excellent and comparable to the placebo, justifying a phase III trial of *nor*UDCA in PSC patients (65).

3.4 The immune system in PSC

The association of PSC and IBD suggests that, like IBD, PSC is not a classical autoimmune disease with respect to a targeted destruction of tissue promoted by immune responses to self-antigens (9). IBD is at least in part the result of an exaggerated innate immune response to antigens of the intestinal microbiota, which activates an immune response (66). As a hepatobiliary manifestation of IBD, gut primed adaptive and innate immune cells contribute

to chronic and progressive biliary inflammation (1). Biliary infiltrates are mainly activated effector or memory T cells, but also include B cells, NK cells, macrophages, and neutrophils (67, 68).

3.4.1 The innate immune system in PSC

It is suggested that the gut-liver axis is involved in the disease development of PSC and PSC-associated IBD (38, 69). Bacterial components, like pathogen-associated molecular patterns (PAMS), can leak from the colon to the liver due to barrier defects during colitis. These bacterial components can be delivered to the liver via the portal vein and activate innate immune cells through pattern recognition receptors (9). Accordingly, it was proposed that the liver may act as a functional vascular firewall that clears commensals that have penetrated the intestinal vascular circuits (28). In case the commensals cannot be cleared, this results in activation of the innate immune system in the liver, which has been proposed by several investigators as a primary inciting event of PSC (9, 70). As a first line of defense macrophages and neutrophils play an important role in orchestrating the immune response and induce inflammation (71, 72).

Macrophages phagocyte bacteria and secrete both pro-inflammatory and antimicrobial mediators (71). They are resident in almost all tissues. Many tissue resident macrophages arise during embryonic development. Macrophages are the mature form of bone marrow-derived monocytes, which circulate in the blood and continually migrate into tissues, where they differentiate.

A potential role of macrophages in PSC has already been shown. A three-fold increase in relative numbers of macrophages were found in the sinusoidal and perisinusoidal spaces in PSC patients, but not in PBC or other biliary tract disease patients. The accumulation was independent of necrosis, cholestasis, and neutrophil infiltration. The perisinusoidal macrophages were increased in all patients, whereas IBD was only present in 60 % of the PSC patients. This suggests that the accumulation of macrophages in PSC might be independent of IBD (73). In accordance, the contribution of macrophages on the pathogenesis of PSC was also shown in an experimental mouse model of PSC. The pharmacological inhibition of macrophage recruitment reduced the PSC-like liver pathology in mice (74).

Neutrophils are the most abundant cells in the innate immune response and next to macrophages the second major population of the innate immune system. Neutrophils mature in the bone marrow and their production increases during immune responses. They migrate via the bloodstream and extravasate into the tissue to sites of infection or inflammation (75). Neutrophils take up a variety of microorganisms by phagocytosis and efficiently destroy them in intracellular vesicles by using degradative enzymes and other antimicrobial substances stored in their cytoplasmic granules (72). A recent study investigated the immune cell composition of the biliary system in PSC patients. Major differences in immune cell composition in bile ducts compared to the blood were revealed. The biliary inflammation in patients with PSC was characterized by a high presence of neutrophils and T cells, as compared to control individuals without PSC (68).

3.4.2 The adaptive immune system in PSC

3.4.2.1 Generation and differentiation of T cells

T cells are a major subset of the adaptive immune system. Their progenitor cells migrate from the bone marrow via the bloodstream to the thymus, where they mature. Their main characteristic is the expression of a T cell receptor (TCR). Most T cells express a TCR consisting of α - and β -chains. A small fraction expresses γ - and δ - chains. These γ : δ T cells do not belong to the conventional T cells (α : β T cells), but are considered as part of the innate immune system. T cells undergo a strict selection in the thymus before they are released in the periphery. Positive selection tests for the potential usefulness of the antigen receptor to recognize foreign antigens. Negative selection removes self-reactive cells from the lymphocyte repertoire, which could cause autoimmunity, or converts them into regulatory T cells (Foxp3⁺ Treg). T cells fall into two major classes distinguished by the expression of the cell-surface proteins, CD4⁺ and CD8⁺. Positive selection also coordinates the choice of co-receptor expression. The distinction is based on the ability of T cells to recognize MHC molecules. CD8⁺ T cells recognize MHC class I molecules, expressed on all nucleated cells. CD4⁺ T cells recognize MHC class II molecules on antigen presenting cells (APCs). T cells are a very heterogeneous cell population. Different subsets are important for the defense against pathogens (e.g. bacteria, virus or fungi), prevent cancer, and maintain immune homeostasis.

This selection process in the thymus is called central tolerance and is an essential step in programming T cells to only react against foreign antigens, and not against self-antigens. However, this central tolerance is not sufficient to maintain immune homeostasis alone. Another mechanism to induce peripheral tolerance is through regulatory T cells. Regulatory T cells can not only control effector T cells, but can also modulate APCs and B cells. An imbalance in effector and regulatory T cells can impair the immune homeostasis and lead to autoimmunity and chronic inflammation.

Once T cells have completed their primary development in the thymus, they enter the bloodstream and migrate into secondary lymphoid organs. Mature recirculating T cells that have not yet encountered their specific antigens are known as naïve T cells. A naïve T cell must meet its specific antigen to be activated, presented to it as a peptide:MHC complex. Thereby, it is induced to proliferate and differentiate into progeny with new activities that contribute to removal of antigens. These progeny cells are called effector T cells. Because of their requirement to recognize peptide antigens presented by MHC molecules, all effector T cells act on other host cells, not on the pathogen itself.

After recognizing its specific antigen, T cells differentiate into several functional classes of effector T cells that are specialized for different activities. Naïve CD8⁺ T cells differentiate into cytotoxic effector T cells that recognize and kill infected cells. CD4⁺ T cells are more diverse in its effector subsets. The main effector subsets of CD4⁺ T cells are Th1, Th2, Th17 and TFH cells, and the regulatory subsets Treg and Tr1 cells, which control immune activation.

A broad generalization segregates helper and regulatory function to CD4⁺ T cells and cytotoxic functionality to CD8⁺ T cells. But numerous exceptions to these rules have been documented, and in any setting, the potential of cytokine-producing or regulatory CD8⁺ T cells and/or cytotoxic CD4⁺ T cells must be considered (76).

3.4.2.2 Role of T cells in PSC

An imbalance of effector and regulatory T cells affects the immune homeostasis and is associated with autoimmunity and chronic inflammation. In PSC patients, an imbalance of the Th17 – Foxp3⁺ Treg axis in the liver is described, which is also known to play a key role in intestinal inflammation (35). An increased production of interleukin (IL)-17, the main cytokine produced by Th17 cells, by PBMCs was observed after pathogen stimulation in patients with

PSC, further supporting an immune imbalance in PSC (77). During colitis development an influx of Th17 cells to the liver was observed in mice (35). On the other hand, a reduced number, and possibly impaired function of Treg was described in patients with PSC (78). In addition, a colitis induction in a mouse model without Treg leads to a mild inflammation of the liver (35). Furthermore, it was shown in a mouse model of PSC, that *in vivo* enrichment of Treg in the liver is not sufficient to provide effective control of cholangitis. The suppressive functionality of hepatic Treg was significantly limited due to increased IL-12 signaling and increased upregulation of the IL-12 receptor (79). This shows a potential role of reduced numbers of Treg in the disease development of PSC.

Also, a direct effect of bile acid (BA) metabolites on the immune system has already been shown (80). Hang *et al.* identified two distinct derivatives of LCA, 3-oxo-LCA and iso-allo-LCA, as T-cell regulators in mice. 3-oxo-LCA inhibits the differentiation of Th17 cells by directly binding to the key transcription factor, retinoid-related orphan receptor- γ t (ROR γ t). Iso-allo-LCA increases the differentiation of Treg through the production of mitochondrial reactive oxygen species (mitoROS), which leads to increased expression of FOXP3 (80). In a follow up, iso-allo-LCA producing bacteria were identified from human stool isolates. A gene cluster consisting of a 5 β -reductase, 5 α -reductase, and 3 β -HSDH, was identified to be responsible for iso-allo-LCA production from the gut bacterial phylum, Bacteroidetes. These two publications suggest that iso-allo-LCA production by gut bacteria induces host immune tolerance through Treg induction, an immune regulatory response that may benefit the host in the context of autoimmune and inflammatory diseases including IBD (81).

Also, a possible role of interferon (IFN)- γ producing CD8⁺ T cells was described in the disease development of PSC. An increased IFN γ response was observed in patients with PSC and in a mouse model of sclerosing cholangitis. IFN γ changed the phenotype of hepatic CD8⁺ T cells, towards increased cytotoxicity, and its absence decreased liver cell death, reduced frequencies of inflammatory macrophages in the liver, and attenuated liver fibrosis (82).

3.4.2.3 Generation and differentiation of B cells

B cells are generated in the bone marrow from common lymphoid progenitor cells. They undergo different precursor stages until they are classified as immature B cells that bear intact IgM molecules. At this time point, the antigen receptor is tested for reactivity to self-antigens,

or autoreactivity. Autoreactive B cells will be eliminated to ensure that B cell populations are tolerant of self-antigens. The tolerance produced at this stage of B cell development is known as central tolerance because it arises in a central lymphoid organ, the bone marrow. When B cells migrate from the bone marrow to the peripheral lymphoid tissues, they are still functionally immature. Immature B cells express high levels of IgM, but little IgD, whereas long-lived mature B cells express low levels of IgM and high levels of IgD. Transitional B cells that have left the bone marrow must complete their maturation in the B cell follicles of the spleen, where they receive necessary maturation and survival signals. There are three main subsets of mature naïve B cells: B1 B cells, marginal zone B cells and follicular B cells. Residing predominantly in the peritoneal cavity and at the mucosal sites, B1 cells provide rapid first-line response to the so-called T-independent antigens, such as bacterial components. Marginal zone B cells carry out a similar function located in the marginal sinus of the spleen. While follicular B cells can also respond to T-independent antigens, they are considered to be specialized responding cells to antigens that demand help from CD4⁺ T cells (83).

The follicular B cell response leads to production of high-affinity plasma cells and memory B cells, which are vital for the humoral immunity. Follicular B cells are activated by exogenous antigens and differentiate into plasma cells. Plasma cells are the effector form of B cells. Their function is to secrete antibodies that have the same antigen specificity as their BCR. Therefore, the antigen that activates a given B cell becomes the target of the antibodies produced by that B cells progeny. In addition to this well studied function, more B cell characteristics have been described in the last decades. These functions include antigen presentation, the production of multiple cytokines, and a suppressive capacity that is ascribed chiefly to the secretion of IL-10 (84-86).

3.4.2.4 Role of B cells in PSC and PSC-associated IBD

B cells may contribute to liver pathology by recognizing shared antigens in the gut and liver (87). It was shown that a proportion of gut and liver B cells in PSC and PSC-IBD patients originate from a mutual clonal origin (i.e., likely to recognize the same antigen), which suggests that B cell antigens are shared across the gut-liver axis (87).

Bacterial translocation from the gut to the liver activates the innate immune system in the liver. Antigen presenting cells (APCs) of the innate immune system activate T and B cells by

antigen presentation. The biliary infiltrates in PSC patients are mainly T cells, but also include B cells (67, 68). Additionally, T and B cells are detected in discrete tertiary lymphoid structures associated with small bile ducts, the so-called portal-associated lymphoid tissues, which are portals for lymphocyte recruitment (1, 88).

B cells play an important role in the immune homeostasis of the intestine. They produce secretory immunoglobulin A (IgA), which binds commensals and preserves a healthy microbial ecosystem (89). It was shown that the IgA-coating of bacteria in the microbiota especially identifies inflammatory commensals that preferentially drive intestinal disease (90).

3.5 Genetic predispositions in PSC

Siblings of patients with PSC and IBD have an enhanced risk of developing PSC (11-fold and 8-fold respectively) indicating that genetic factors are involved in disease development (91). Genome-wide case-control comparisons of the frequency of genetic variants (genome wide association studies [GWAS]) have provided means of the frequency of genetic variants in PSC (92). For PSC patients more than twenty robust PSC genes were identified (92-96). The predominant genetic findings localize within the human leukocyte antigen (HLA) complex. The non-HLA findings are almost without exception associated with one or more other immune-mediated or autoimmune conditions. Around half of the PSC associated genes show associations with IBD (13). One of these genes is the *IL2RA* gene, where single nucleotide polymorphisms (SNPs) are associated with both PSC and IBD.

3.5.1 Function of the IL-2R α

The IL-2R α chain (CD25) is mainly expressed on T cells, but also on natural killer (NK) cells, B cells and some innate lymphoid cells (ILCs). The high-affinity IL-2 receptor (IL-2R) comprises of three polypeptides: the IL-2R α chain, IL-2R β chain (CD122) and γ subunit (γ_c , or CD132) (97-99). Upon early activation, naïve T cells express a receptor composed of the β and γ chain, which has only moderate affinity for IL-2 binding. Within hours of activation, naïve T cells upregulate the expression of the IL-2R α in addition. Consequently, the IL-2R α chain associates with the β and γ heterodimer, resulting in a receptor with a much higher affinity for IL-2, allowing the T cell to respond to low concentrations of IL-2. Binding of IL-2 by activated naïve

T cells triggers signaling that supports their activation and differentiation, and can enhance their proliferation (100).

Regulatory T cells (Treg) are crucial in maintaining immune homeostasis and in prevention of autoimmune diseases (101). Treg constitutively express the high affinity IL-2R. Therefore, they can outcompete T cells that express only the low affinity form of the receptor, in binding of the limited quantities of IL-2 that are available early in the response to antigen. IL-2 is essential for the maintenance of Treg, which do not produce their own IL-2. IL-2 is a key cytokine for Treg cell differentiation, survival, and function (100, 102, 103). Binding of IL-2 to the high affinity IL-2R induces, among others, the phosphorylation of STAT5, resulting in increased expression of IL-2R α and Foxp3 on Treg and activation of their suppressive activity (104).

3.5.2 SNPs in the *IL2RA* gene are associated with PSC and IBD

GWAS found non-coding SNPs in the *IL2RA* gene to be associated with PSC, IBD, type 1 diabetes and other autoimmune disorders, underlining the important role of *IL2RA* regulation in human immune homeostasis (94, 95, 105, 106). Aberrant IL-2R signaling in CD4⁺ T cells in type 1 diabetes subjects was shown to decrease persistence of *FOXP3* expression in CD4⁺CD25⁺ Treg, which may impact the establishment of tolerance (107). PSC patients with an *IL2RA* gene polymorphism present reduced numbers of FOXP3⁺ Treg in the liver (78)

In this study it was focused on the rs61839660 SNP, located in the first intron of the *IL2RA* gene. This area of the gene is highly conserved between human and mouse. Taking advantage of CRISPR Cas9 genome editing, a mouse model with this SNP known from human was generated in the mouse *Il2ra* gene.

It was shown that the rs61839660 SNP, and other SNPs in the first intron of the *IL2RA* gene, affect transcription factor binding and enhancer activity *in vitro* (108). The rs61839660 SNP was also further investigated by Simeonov *et al.* (109). They showed that it alters the transcriptional response to stimulation in anti-CD3/CD28 stimulated human CD4⁺ T cells. The minor variant for the SNP was associated with reduced levels of *IL2RA* transcripts in stimulated T cells, confirming the functional effect of sequence variation on human T-cell gene regulation (109).

In vivo phenotyping of mice with the rs61839660 SNP revealed no evidence of overt immune dysregulation. *In vitro* activation of naïve CD4⁺ T cells from SNP or wild type (wt) mice with anti-CD3/CD28 antibodies showed reduced IL-2R α surface expression 24h after activation. After three days of stimulation, the percentage of SNP cells expressing IL-2R α was similar to the wild type levels. The disease associated SNP has subtle effects on final levels of IL-2R α , but on the other hand exerts a pronounced effect on the timing of induction (109).

3.6 Experimental mouse model of PSC

3.6.1 *Mdr2*-deficient mouse model

The *Mdr2*^{-/-} mouse model is a well-established genetic, experimental mouse model for PSC (110). The *Mdr2* (*Abcb4*) gene, is the mouse homolog to the human *MDR3* gene (61). It encodes for an ATP-dependent transport protein of p-glycoproteins. It is responsible for the active transport of phospholipid, especially phosphatidylcholine, from the liver into the bile duct. The lack of biliary phospholipids in the bile ducts of *Mdr2*-deficient mice, leads to insufficient solution of the BAs. Increased concentrations of BAs in the biliary tract have a toxic effect on the bile duct epithelium, resulting in chronic inflammation around the bile ducts, ultimately leading to sclerosing cholangitis (61, 111, 112).

The serum transaminases (ALT, AST), as well as bilirubin levels, are increased in *Mdr2*-deficient mice compared to wild type (wt) mice. The histopathology of *Mdr2*-deficient mice appears similar to the histopathology of PSC patients. *Mdr2*-deficient mice display age-dependent enlargement of bile ducts, periductular inflammation, and a broad rim of periductular extracellular matrix (111, 112). Additionally, pro-inflammatory and pro-fibrotic genes are elevated in *Mdr2*-deficient mice (111).

Mdr2-deficient mice present a liver pathology directly after birth, which is characterized in the first weeks of age by acute inflammation of the liver and the bile ducts. Between 12-14 weeks of age, the mice transition into a more chronic phase of disease and fibrosis is more pronounced (111, 112).

3.6.2 DDC induced liver pathology

As chemical induced, experimental mouse model for sclerosing cholangitis, the 3,5-diethoxycarbonyl-1,4-dihydrocollidine (DDC) induced liver pathology was used. Mice are fed with a diet containing 0.1 % DDC, which is a porphyrinogenic hepatotoxin. DDC feeding leads to increased biliary porphyrin secretion and induction of vascular cell adhesion molecule, osteopontin, and tumor necrosis factor- α expression in bile duct epithelial cells (113). This results in the formation of porphyrin crystals in the hepatocytes and porphyrin plugs in the bile ducts resembling the PSC phenotype (114, 115). Similar to the *Mdr2*-deficient mice, transaminase levels are increased and liver histology similar to human PSC is detectable (113).

3.7 Experimental mouse models of colitis

3.7.1 DSS colitis

Using dextran sulfate sodium (DSS), acute or chronic colitis can be induced in mice (116). The mechanism by which DSS induces intestinal inflammation, especially in the distal colon, is still not fully understood. One hypothesis is that the DSS forms nanometer-sized vesicles with medium-chain-length fatty acids that are present in the colonic lumen. The vesicles can fuse with colonocyte membranes (117). Damage to the epithelial monolayer lining in the large intestine allows the dissemination of bacteria and their products into underlying tissue, and can lead to an inflammatory response (118). DSS-induced mucosal injury and progression of the disease are dependent on the concentration of the DSS and the length of the treatment. Therefore, an acute DSS colitis can be induced through a single application, or a chronic inflammation of the colon by repetitive administration of the DSS (116).

3.7.2 Infection with *Citrobacter rodentium*

Citrobacter rodentium is a gram negative, facultative anaerobic, mesophilic bacillus. It belongs to the family of enterobacteriaceae. The mouse-restricted pathogen *C. rodentium* and the human enteric pathogens *Escherichia coli* EHEC or EPEH, which are two clinically important human gastrointestinal pathogens, share several pathogenic mechanisms (119). *C. rodentium* infection is used to model several important human intestinal disorders, including Crohn's disease, ulcerative colitis and, colon tumorigenesis (120, 121). *C. rodentium* is transmitted via

the fecal-oral route and causes colitis, which is also known as transmissible murine crypt hyperplasia. Infection with *C. rodentium* results in crypt hyperplasia, loss of goblet cells and an accumulation of undifferentiated colonocytes at the luminal surface, which causes impaired electrolyte absorption and profuse diarrhea (122).

3.8 Aim of the study

Primary sclerosing cholestasis (PSC) is a chronic bile duct obstruction leading to end stage liver disease. The etiology of PSC is still unknown. The only treatment option is liver transplantation with a high risk of recurrent disease. Two of the known risk factors associated with PSC are the co-occurrence of inflammatory bowel disease (IBD) and genetic predispositions. Around 50-80 % of PSC patients have associated IBD, but it still not understood how PSC and IBD affect each other. Additionally, multiple genetic risk loci have been identified to be associated with PSC. Single nucleotide polymorphisms (SNPs) in the *IL2RA* gene are known risk factors of PSC, but exact mechanisms are still obscure.

This thesis is based on two previous studies from our lab. Franziska Mathies found that induction of a DSS colitis in wild type mice, induced a mild liver pathology in the absence of Foxp3⁺ Treg (35). She and Niklas Steffens further investigated the effect of colitis on liver inflammation also in the models of PSC and colitis. They described a protective effect of colitis on PSC development. However, it was unclear if this was only the case in the specific mouse model used or whether this was a general effect. More importantly, the mechanism of this protective effect remained unclear (123, 124).

The first aim of this study was, to further investigate the protective effect of colitis on PSC development in two mouse models of sclerosing cholangitis (*Mdr2*^{-/-}, DDC) and two models of colitis induction (DSS, *Citrobacter rodentium* infection). Furthermore, insights were gained into the mechanism of how colitis affects PSC development. Therefore, three players suggested to be involved in the disease development of PSC were investigated; the intestinal microbiota, the bile acid metabolism and different immune cell subsets.

The second aim of this study was to investigate the role of the rs61839660 *IL2RA* SNP on PSC progression and PSC-associated colitis. To this end, the disease development of sclerosing cholangitis in *Mdr2*-deficient mice with the SNP in the *Il2ra* gene were tested. In addition, an effect of colitis on PSC development in the presence of the *Il2ra* SNP was explored. To further understand the mechanism, a potential role of the *Il2ra* SNP on Foxp3⁺ Treg function was tested.

4 Material and Methods

4.1 Material

4.1.1 Consumables

Table 1: Consumables

Product name	Company
BD Microlance™ 3	BD
Cell strainer 100 µm	Greiner
Cell strainer 70 µm	Greiner
Cell strainer 40 µm	Greiner
Cell culture plate 96 well round bottom	Sarstedt
Cosmetic tissue	Van Merhagen
Embedding cassette	Kabe
Eppi 1.5 ml	Sarstedt
Eppi 1.5 ml RNase-free	Sarstedt
Eppi 2 ml	Sarstedt
Eppi 5 ml	Sarstedt
FACS-tube 5 ml	Sarstedt
Falcon 15 ml	Greiner
Falcon 50 ml	Greiner
Gloves Gr.M	Ansell
Gloves Nitril purple extra-long Gr.M	Halyard
Lidchain for PCR-tubes	Sarstedt
MACS separation column	Miltenyi
PCR-tubes with lid	Sarstedt
PCR-tubes without lid	Sarstedt
Petridish	Sarstedt
Pipetttip 10 µl StackPack	Sarstedt
Pipetttip 200 µl StackPack	Sarstedt
Pipetttip 1250µl	Sarstedt
Serological pipette 5 ml	Greiner
Serological pipette 10 ml	Greiner
Serological pipette 25 ml	Greiner
Serological pipette 50 ml	Greiner
Syringe 1.0 ml	Braun
Syringe 0.5 ml	BD
Syringe 5 ml	BD
Syringe 10 ml	BD

Syringe filter 0.22 µm	Sarstedt
Syringe filter 0.45 µm	Sarstedt

4.1.2 Equipment

Table 2: Equipment

Product name	Company
Axio Cam MRc	Carl Zeiss Microscopy GmbH
Axio Scope. A1	Carl Zeiss Microscopy GmbH
Centrifuge 5424 R	Eppendorf AG
Centrifuge 5427 R	Eppendorf AG
Centrifuge 5810/5427 R	Eppendorf AG
Dissecting set	Fine Science Tools
Embedding System Tissue-Tek® TEC	Sakura Finetek
Flow cytometer LSR II Fortessa	BD Biosciences
Freezer MedLine (-20°C)	Liebherr
Hera Safe Clean bench	Hanau
Hertherm Incubator	ThermoFisher Scientific Inc.
Labor fume hood TEC-Onomic	C+P Möbelsystem GmbH
Microscope DMIL LED	Leica Biosystem
Microtome CUT 5062	SLEE Medical
Neubauer chamber (0.0025mm ²)	Superior Marienfeld
Perfect Blue Gelsystem Maxi	Peqlab Biotechnologie GmbH
Pipettes 10 µl, 20 µl, 200 µl, 1000µl	Eppendorf AG
Practum224-1S	Sartorius
Refrigerator KG KSVV30A	Siemens
Sanyo CO ₂ Incubator	Ewald Innovationstechnik GmbH
Shandon Citadel 1000	Thermo Electron Corporation
Spectrophotometer: Nano-drop	Thermo Fisher Scientific
Thermal cycler C1000	Bio-Rad Laboratories
Thermomixer comfort	Eppendorf AG
Ultra-Low Temperature Freezer MDF-U5386S (-80°C)	Panasonic Healthcare Co.
UV trans-illuminator Gel Doc TM XR+	Bio-Rad Laboratories
Vortex Genie 2	Scientific Industries Inc.
Water bath WNB	Memmert

4.1.3 Reagents

Table 3: Reagents for genotyping

Reagent	Company
Agarose LE	Biozym
dNTP Mix	Thermo Fisher Scientific Inc.
Dream Taq™ DNA Polymerase	Thermo Fisher Scientific Inc.
Dream Taq™ Green Buffer (10X)	Thermo Fisher Scientific Inc.
Ethidium bromide	AppliChem
Gene Ruler DNA ladder Mix	Thermo Fisher Scientific Inc.
Isopropanol	Th. Geyer
Proteinase K recombinant	AppliChem

Table 4: Primer sequences for PCR

Gene	Primer sequence
MDR2 fwd	CCA CAG CCA CAC ACT GAC CT
MDR2 wt rev	CAT CAA ACC ACG TGC AGA AAA
MDR2 m rev	CCA GAC TGC CTT GGG AAA AG
Rag1 WTF	GAG GTT CCG CTA CGA CTC TG
Rag1 R	CCG GAC AAG TTT TTC ATC GT
Rag1 MF	TGG ATG TGG AAT GTG TGC GAG
IL-2RaSeq FW	TCC TCA GGA CCC TGC TAG TC
IL-2RaSeq Rev	GAG AAG CAA AGC AGC AGA CA
FIR1	CAA AAC CAA GAA AAG GTG GGC
FIR2	GGA ATG CTC GTC AAG AAG ACA GG
FIR3	CAT CTT GGA GAG TCG GTG TG
IL10KOF	GTG TGT ATT GAG TCT GCT GGA C
IL10KOR1	GTG TGG CCA GCC TTA GAA TAG
IL10KOR2	GGT TGC CTT GAC CAT CGA TG
GFP IRES1	GGA CGT GGT TTT CCT TTG AA
GFP IRES2	GAA CTT CAG GGT CAG CTT GC
IL-17A KI sense	CAC CAG CGC TGT GTC AAT
IL-17A KI anti sense	ACA AAC ACG AAG CAG TTT GG
IL-17A KI IRES	ACC GGC CTT ATT CCA AGC

Table 5: Reagents for cell isolation and *in vitro* assays

Reagent	Company
Biotin anti mouse CD25 (1:400)	BioLegend
Biotin anti mouse CD44 (1:200)	BioLegend

CD4 microbeads, mouse (1:10)	Miltenyi Biotec
CellTrace Violet dye Proliferation kit (1:500)	ThermoFisher Scientific
Clicks Medium	Irvine Scientific
Collagenase IV (100 U), from Clostridium histolyticum	Sigma-Aldrich
Dithiothreitol (DTT)	AppliChem
DNase I	AppliChem
Dulbecco's Phosphate Buffered Saline (PBS) (1X)	PAA
Fetal bovine serum (FBS)	PAA
Hanks' balanced salt solution (HBSS) (10X)	Gibco
L-Glutamine	Invitrogen
Penicillin/Streptomycin, 10 000 U/ml	Invitrogen
Percoll™	GE Healthcare
RPMI medium	Gibco
Streptavidin microbeads	Miltenyi Biotec
Trypan blue solution, 4 %	Sigma-Aldrich

Table 6: Reagents for flow cytometry

Reagent	Company
SPHERO™ AccuCount Blank Particles	Spherotech Inc.
Ionomycin (1:1000)	Sigma Aldrich
Monensin A (1:1000)	BioLegend
Nonidet P40 (NP40)	Sigma Aldrich
Zombie UV™ Fixable Viability Kit	BioLegend
Phorbol-12-myristat-13-acetat (PMA) (1:20 000)	Merck

4.1.4 Buffers and solutions

Table 7: Buffers and solutions for genotyping

Reagent	Composition
Proteinase K buffer	12.1 g Tris, 10 ml 0.5M EDTA, 11.7 g NaCl, 5 ml SDS (from 20 % Stock), fill up with dH ₂ O to final volume of 1 L
TBE buffer	108 g Tris, 55 g Boric acid, 40 ml 0.5 M EDTA, fill up with dH ₂ O to final volume of 1 L

Table 8: Buffers and solutions for cell isolation and flow cytometry

Reagent	Composition
ACK buffer (10X)	20.05 g NH ₄ Cl, 2.5 g KHCD ₃ , 0.093 g EDTA, ad 250 ml dH ₂ O

Collagenase solution	500 ml RPMI, 55 ml FBS, 5.5 ml 100X HGPG, 1 ml 0.5 M CaCl ₂ , 1 ml 0.5 M MgCl ₂ , 100 U/ml collagenase
DTT solution	50 ml 10X HEPES-bicarbonate buffer, 50 ml HBSS, 50 ml FBS, 350 ml dH ₂ O, 15.4 mg/100 ml DTT
FACS buffer	25 ml FBS, 0.03 % sodium acid, 975 ml 1XPBS
Fix buffer	Prepared from stock (3.65 %) formaldehyde solution using 1XPBS/1 % FBS
Full medium	RPMI, 10 % FBS
Hepes bicarbonate	23.8 g HEPES (100 mM final), 21 g sodium bicarbonate (250 mM final), dH ₂ O to 1 L, adjust pH to 7.2 with HCl
HGPG (100X)	59.6 g HEPES, 14.6 g L-glutamine, 1x10 ⁶ U penicillin, 1 g streptomycin, 2.5 mg gentamicin, RPMI to 500 ml, adjust pH to 7.5 with HCl
MACS buffer	500 ml 1XPBS, 2 mM EDTA, 1 % FBS
Percoll buffer	90 ml Percoll, 10 ml 10X PBS
Perm buffer	0.1 % NP40 solution using 1XPBS/1 %FBS
PBS (10X)	NaCl (1.37 M), KCl (26.8 mM), Na ₂ HPO ₄ x 2 H ₂ O (64.6 mM), KH ₂ PO ₄ (14.7 mM), adjust pH to 7.4 with either HCl or NaOH

Table 9: Buffers and solutions for FMT

Reagent	Company
BHI	Sigma-Aldrich
Glycerol	Carl Roth
Thioglycollate Medium fluid, 8 ml	BD

Table 10: Buffers and solutions for histology

Reagent	Company
Deckgläser 24x50 mm	Th Geyer
Eosin	Leica Biosystems
EuKitt® Quick hardening mounting medium	Sigma-Aldrich

Haematoxinilin	Sigma-Aldrich
Pico Sirius Red	American Mastertech
Xylol-Ersatz XEM-200	DiaTec

4.1.5 Animals

Table 11: Mouse models

Mouse line	Description
<i>C57BL/6J</i>	Wild type mouse line
<i>C57BL/6J</i> germ-free	Germ-free wild type mouse line
<i>Mdr2</i> ^{-/-}	Knockout for the <i>Abcb4</i> gene, experimental model for sclerosing cholangitis
<i>Rag1</i> ^{-/-} <i>Mdr2</i> ^{-/-}	Knockout for the <i>Rag1</i> and the <i>Abcb4</i> gene. Experimental mouse model for sclerosing cholangitis without T and B cells.
<i>Mdr2</i> ^{-/-} <i>DEREG</i>	<i>Mdr2</i> -deficient mouse model with a DTX receptor on Foxp3 ⁺ Treg, DTX induced depletion of Foxp3 ⁺ Treg
<i>AM</i> ^{ff} <i>CSF1R</i> ^{Cre}	Knockout for <i>Axl</i> and <i>MerTK</i> in CSF1R ⁺ cells, impaired phagocytosis
<i>Mdr2</i> ^{-/-} <i>Il2ra</i> ^{SNP_HH}	<i>Mdr2</i> -deficient mouse model with the rs61839660 SNP in the <i>Il2ra</i> gene, generated in the ZMNH, UKE
<i>Mdr2</i> ^{-/-} <i>Il2ra</i> ^{SNP_Mson}	<i>Mdr2</i> -deficient mouse model with the rs61839660 SNP in the <i>Il2ra</i> gene, generated at the UCSF-Gladstone Institute
<i>FirTiger</i> <i>IL-17</i> ^{Kat} <i>Il2ra</i> ^{SNP_HH}	<i>Il2ra</i> ^{SNP} mouse model, with reporter genes for <i>Foxp3</i> ^{mRFP} , <i>Il10</i> ^{eGFP} , <i>Il17a</i> ^{FP635}

Mice were kept under specific pathogen free conditions in the animal research facility of the University Medical Center Hamburg Eppendorf (UKE). Food and water were provided *ad libitum*. Age and sex matched littermates were used. All animals were cared for in accordance with the institutional review board 'Behörde für Soziales, Familie, Gesundheit und Verbraucherschutz' (Hamburg, Germany).

4.1.6 Antibodies

Table 12: Antibodies for surface and intracellular staining

Specificity	Fluorochrome	Clone	Dilution	Company
B220/CD45R	BV650	RA3-6B2	1:400	BioLegend
CD11b	PE-Cy7	M1/70	1:600	BioLegend
CD11c	FITC	HL3	1:400	BD

CD19	BV510	6D5	1:400	BioLegend
CD25	PE	PC61	1:200	BioLegend
CD3	AF700	17A2	1:200	BioLegend
CD4	APC	GK1.5	1:600	BioLegend
CD4	APC-Cy7	GK1.5	1:600	BioLegend
CD4	PacBlue	RM4-5	1:600	BioLegend
CD45	BV510	30-F11	1:800	BioLegend
CD45	BV785	30-F11	1:800	BioLegend
CD8a	BV650	53-6.7	1:800	BioLegend
Foxp3	PE	NRRF-30	1:100	eBioscience
Foxp3	APC	FJK-16s	1:100	eBioscience
IFN γ	BV785	XMG1.2	1:100	BioLegend
IL-17A	AF488	TC11-18H10.1	1:100	BioLegend
Ly6C	PE	AL-21	1:400	BD
Ly6G	BV421	1A8	1:600	BD

Table 13: Antibodies and chemicals for animal experiments and *in vitro* assays

Reagent	Clone	Company
Mouse anti-CD3	2C11	BioLegend
Mouse anti-CD28	37.51	BioLegend
Mouse anti-Gr1	1A8	Bio X Cell
Mouse anti-CD8	T1B105	Hybridoma culture
Mouse anti-CD20	SA271G2	BioLegend
Diphtheria toxin	From <i>Corynebacterium diphtheriae</i>	Sigma-Aldrich

4.1.7 Kits

Table 14: Kits

Product name	Company
GFX™ PCR DNA and Gel Band Purification Kit	Cytiva
Mix2Seq Kit	Eurofins

4.1.8 Software

Table 15: Software

Software	Company
BioRender	BioRender.com
Chromas lite	Technelysium Pty Ltd

EndNote x6	Thomson Reuters
FACS Diva v.6.1.3	BD Pharmingen
FlowJo_V10	FlowJo LLC
GraphPad Prism 7	GraphPad Software, Inc.
Image Lab 5.2.1	Bio-Rad
Microsoft Office 365	Microsoft Corporations
Tbase	Abase

4.2 Methods

4.2.1 Genotyping

Tail biopsies

To extract the genomic DNA from tail biopsies, they were digested overnight at 55 °C, using 3 µl Proteinase K in 80 µl Proteinase K buffer. The enzymatic reaction was stopped by heat-inactivation of the samples for 15 minutes at 95°C. Samples were diluted with 200 µl distilled water. DNA was further used for PCR.

Polymerase chain reactions (PCR) protocols

All reagents used for genotyping are listed in Table 3. To determine the genotype of the genetically modified mice, they were genotyped using polymerase chain reaction (PCR). The master mix for each reaction contained 10x DreamTaq™ master mix buffer, which already contained green loading dye, DreamTaq™ polymerase, dNTPs (10 mM) and specific primers for each gene (10 mM). The total volume of the master mix was brought to 22 µl or 27 µl with dH₂O depending on the protocol. 3 µl of DNA isolated from the tail biopsies was added to the PCR master mix.

Table 16: Master mix *Mdr2*

30 µl	Mdr2 program
10x Dream Taq master mix buffer	3 µl
dNTPs (10 mM)	0.6 µl
Dream Taq polymerase	0.22 µl
MDR2 fwd	0.9 µl
MDR2 wt rev	0.9 µl

MDR2 m rev	0.9 μ l
H ₂ O	20.48 μ l

Wild type band showed a band size of 374bp, knock out showed a band size of 169bp.

Table 17: Master mix *Rag1*

25 μ l	Touchdown
10x Dream Taq master mix buffer	2.5 μ l
dNTPs (10mM)	1.5 μ l
Dream Taq polymerase	0.18 μ l
Rag1 WTF	0.75 μ l
Rag1 R	0.75 μ l
Rag1 MF	0.75 μ l
H ₂ O	15.57 μ l

Wild type band showed a band size of 474bp, knock out showed a band size of 530bp.

Table 18: Master mix *Il2ra*^{SNP}

25 μ l	<i>Il2ra</i> ^{SNP} program
10x Dream Taq master mix buffer	2.5 μ l
dNTPs (10mM)	1.5 μ l
Dream Taq polymerase	0.18 μ l
IL-2RaSeq FW	0.75 μ l
IL-2RaSeq Rev	0.75 μ l
H ₂ O	16.32 μ l

PCR products were purified with the Kit and send to Eurofins for Sanger sequencing as described below.

Table 19: Master mix *Fir*

30 μ l	Touchdown
10x Dream Taq master mix buffer	3 μ l
dNTPs (10mM)	3 μ l
Dream Taq polymerase	0.3 μ l
FIR1	0.9 μ l
FIR2	0.9 μ l
FIR3	0.9 μ l
H ₂ O	18 μ l

Wild type band showed a band size of 692bp, knock out showed a band size of 470bp.

Table 20: Master mix *Tiger (wild type)*

30 μ l	Touchdown
10x Dream Taq master mix buffer	3 μ l
dNTPs (10mM)	1.5 μ l
Dream Taq polymerase	0.22 μ l
IL10KOF	0.9 μ l
IL10KOR1	0.9 μ l
IL10KOR2	0.9 μ l
H ₂ O	19.58 μ l

Wild type band showed a band size of 350bp.

Table 21: Master mix *Tiger (GFP)*

30 μ l	Touchdown
10x Dream Taq master mix buffer	3 μ l
dNTPs (10mM)	0.6 μ l
Dream Taq polymerase	0.22 μ l
GFP IRES1	0.9 μ l
GFP IRES2	0.9 μ l
H ₂ O	21.38 μ l

GFP positive samples showed a band size of 200bp.

Table 22: Master mix *IL17Kat.*

28 μ l	Touchdown
10x Dream Taq master mix buffer	3 μ l
dNTPs (10mM)	0.6 μ l
Dream Taq polymerase	0.22 μ l
IL-17A KI sense	0.9 μ l
IL-17A KI anti sense	0.9 μ l
IL-17A KI IRES	0.9 μ l
H ₂ O	19.48 μ l

Wild type band showed a band size of 370bp, knock out showed a band size of 300bp.

The PCR reaction was performed in the PCR thermocycler using the following programs.

Table 23: Mdr2 program

Step	Temp. [°C]	Time [min.]
1	95	3:00
2	95	0:30
3	60	0:30
4	72	1:00
5	Go to step 2 – 35x	
6	72	10:00
7	12	∞

Table 24: Il2raSNP program

Step	Temp. [°C]	Time [min.]
1	94	5:00
2	94	0:30
3	65	0:30
4	72	0:40
5	Go to step 2 – 35x	
6	72	5:00
7	12	∞

Table 25: Touchdown program

Step	Temp. [°C]	Time [min.]
1	94	5:00
2	94	0:40
3	65	0:40
	-0.3°C / cycle	
4	72	0:55
5	Go to step 2 – 39x	
6	72	5:00
7	4	∞

PCR products were fragmented by electrophoresis on a 1.5 % agarose gel. The gel was prepared using 0.5X TBE buffer, agarose and ethidium bromide. PCR products were loaded on

the gel and separated by electrophoresis running for 30 min at 550 V. Ethidium bromide in the gel matrix intercalated with the DNA and bands were visualized using a UV transilluminator.

*Genotyping of the *Il2ra*^{SNP} mice*

Tail biopsies were digested and PCR was performed as described above. Afterwards the PCR products were purified using the GFX™ PCR DNA and Gel Band purification Kit according to the user manual. Purified samples were diluted to a concentration of 5 ng/μl and the forward primer of the PCR was added for sequencing. Sanger sequencing was performed at Eurofins-Genomics. Sequencing results were analyzed for the *Il2ra*^{SNP} in wild type, homozygous or heterozygous appearance using the Chromas lite software.

*Blood genotyping of the *DEREG* mice*

The appearance of the GFP marked DTX receptor on Foxp3⁺ Treg in *DEREG* mice was analyzed by blood genotyping. Blood was drawn and erythrocytes were lysed as described in 4.2.4.4. Afterwards cells were stained for CD4⁺ T cells in 50 μl antibody cocktail for 5 minutes at 4 °C. After the incubation, 250 μl 1xPBS were added and the samples were analyzed using FACS.

4.2.2 Mouse experiments

4.2.2.1 Acute and chronic DSS colitis

Mice were fed with 3 % DSS in the drinking water for seven days for induction of an acute DSS colitis. At day 7, DSS was removed and mice received water for two days before they were sacrificed. The endoscopic colitis score was analyzed at day 8 and the blood was drawn with the cell isolation at day 9 of the experiment. Weight loss was analyzed throughout the experiment.

The induction of a chronic DSS colitis was performed in three cycles with 2.5 % DSS. The first two cycles were 5 days long, with 16 days in between the cycles, where the mice recovered from the inflammation. The third cycle lasted for seven days. The endoscopic colitis score was analyzed always one day after removing the DSS. Blood was drawn two days after removing the DSS. The weight loss was analyzed throughout the experiment. Mice were sacrificed two days after the last cycle of DSS.

4.2.2.2 *Citrobacter rodentium* infection

Nalidixic acid-resistant, luciferase-expressing derivative of *Citrobacter rodentium* (ICC180) was grown overnight in Lysogeny broth (LB) medium, containing 50 µg/ml of nalidixic acid, shaking at 37 °C. The suspension of bacteria was washed twice and the concentration was adjusted to 5×10^9 cfu/ml. Mice were infected by oral gavage with 200 µl of *C. rodentium* solution each, containing 1×10^9 cfu. Mice were sacrificed 7 days after infection. Disease severity was analyzed by bacterial load in the stool and caecum content, weight loss, shortening of the colon and histological score. To determine bacterial load, serial dilutions of stool content were plated on LB agar plates supplemented with nalidixic acid and incubated at 37 °C for 24 hours.

4.2.2.3 DDC as a model of chemical induced sclerosing cholangitis

As chemical induced model for sclerosing cholangitis, 3,5-diethoxycarbonyl-1,4-dihydrocollidine (DDC) was used. Wild type mice were fed for 8 days *ad libitum* with 0.1 % DDC diet. For the preparation of the diet, 1 kg of powdered food was mixed with 1 g DDC and approximately 750 ml water. The food was mixed well, spread onto a board and cut into pieces. The food pellets were dried for 3-4 days and were flipped once a day. Dried food pellets were stored in an airtight container at 4 °C in the dark.

4.2.2.4 Fecal microbiome transplantation in germ-free mice

To perform fecal microbiome transplantation (FMT), fresh stool from donor mice or stool from frozen aliquots was used. For the FMT from fresh stool, a donor mouse was sacrificed and the whole colonic stool, including caecum content was put into thioglycolate medium. The stool was smashed through a 70 µm cell strainer and washed with 15 ml BHI medium. Samples were centrifuged 10 minutes, 500 G at 4 °C and the supernatant was discarded. At this point, frozen aliquots could be prepared by resuspending the pellet in 3 ml of 20 % glycerol in PBS. Instead of freezing, the stool could also be used directly, resuspended in 3 ml BHI. Mice are gavaged with 200 µl of stool.

To perform FMT from frozen stool, aliquots were quickly thawed at 37 °C, resuspended in 13 ml of BHI medium and centrifuged 10 minutes, at 500 G at 4 °C. The supernatant was discarded. Pellets were resuspended in 1 ml BHI per 1 ml aliquot. Mice were gavaged with 200 µl of stool. After FMT, the mice were kept for four weeks to establish the new microbiome.

4.2.2.5 *In vivo* depletion of different immune cell subsets

Depletion of Gr-1⁺ cells

For depletion of Gr1⁺ cells, mice were injected with 100 µg of anti-Gr1 mAb i.p. every three days starting at day -1 of the experiment.

Depletion of CD8⁺ T cells

For depletion of CD8⁺ T cells, mice were injected with 250 µg of anti-CD8 mAb i.p. every seven days starting at day -1 of the experiment.

Depletion of CD20⁺ B cells

For depletion of CD20⁺ cells, mice were injected on two consecutive days with 125 µg anti-CD20 mAb i.v. retrobulbar, before the start of the experiment. At day 26 and 27 of the experiment, the two injections were repeated.

DTX mediated depletion of Foxp3⁺ Treg in DERE mice

Mdr2^{-/-}DEREG mice were injected with 250 ng diphtheria toxin (DTX) i.p. every three days, starting at day -1 in order to deplete the Foxp3⁺ Tregs.

4.2.3 Mouse endoscopy

Colitis scoring using endoscopy was performed in a blinded fashion using the Colonview system (125). Mice were anesthetized with isoflurane and colitis scoring was based on the following parameters: stool consistency, granularity of the mucosal surface, vascular pattern, translucency of the colon and fibrin (0-3 points each).

4.2.4 Isolation and preparation of organs and blood samples

On the day of the analysis, mice were first anesthetized with a combination of CO₂/O₂ (80 %/20 %). Afterwards mice were sacrificed by exposure to 100 % CO₂. After cessation of breathing and reflexes, the fur was sprayed with 70 % ethanol and the abdomen and the thorax were opened. A small syringe was used to take blood from the vena cava. Blood was divided in a tube with 3 µl 0.5 M EDTA for plasma collection and a tube for serum collection. Afterwards vena cava was opened and the liver was perfused by injection of 5-8 ml 1xPBS into

the left ventricle. The gallbladder was removed intact and collected. The liver was removed, a piece of the right medial lobe was collected for RNA isolation, and a piece of the right lateral lobe for histology. The rest of the liver was collected for cell isolation. The colon was taken from the anus to the caecum. The fat was removed and length was measured. The proximal part was taken for histology, the next piece for RNA isolation. The rest was opened longitudinally, the content was removed, washed with 1xPBS and collected for cell isolation. If spleen was needed, it was removed, cleared from fat and stored on ice with the liver and the colon for cell isolation. The samples for histology were fixed in 4 % paraformaldehyde (PFA) and the samples for RNA isolation were stored on dry ice and afterwards at -80 °C.

4.2.4.1 Isolation of lymphocytes from the liver

For the isolation of lymphocytes from the liver, it was smashed through a metal strainer and washed with 1xPBS/1 %FBS. Cells were pelleted by centrifugation for 10 minutes at 380 G at 4 °C, washed with 30 ml of 1xPBS/1 %FBS again and centrifuged again. Afterwards, cells were resuspended in 4 ml of 40 % Percoll solution and carefully pipetted on top of 4 ml 67 % Percoll solution. Percoll was diluted with 1xPBS/1 %FBS to dilution. The gradient was centrifuged at room temperature (20 min. at 400 G, ACC:1 DEC:1). The interface was collected in 1 ml and washed with 14 ml 1xPBS/1 %FBS. Cells were pelleted by centrifugation for 7 minutes at 350 G and used for re-stimulation or extracellular staining.

4.2.4.2 Isolation of lymphocytes from the colon

For the isolation of intraepithelial lymphocytes (IELs), the colon was cut into small pieces and was digested in 10 ml DTE solution with freshly added DTT (1.5 mg/10 ml). Samples were incubated for 20 minutes at 37 °C shaking horizontally. Next, the cellular pieces were separated from the solution using a 100 µm cell strainer and washed with 40 ml 1xPBS/1 %FBS. The IELs in the solution were pelleted (7 minutes at 350 G, 4 °C) and kept on ice. The tissue was further digested to isolate the lymphocytes from the lamina propria. Therefore, tissue was cut to a pulp and digested in 4 ml collagenase solution containing collagenase (100 U/ml) and DNase I (1000 U/ml) for 45 min at 37 °C shaking horizontally. Content was smashed through a 100 µm cell strainer and washed with 1xPBS/1 %FBS on top of the pelleted IELs. Pooled lymphocytes from the colon were pelleted again (7 minutes at 350 G, 4 °C). Cells were resuspended in 3 ml of 40 % Percoll solution and carefully pipetted on top of 3 ml 67 % Percoll

solution. The gradient was centrifuged at room temperature (20 min at 400 G, ACC:1 DEC:1). The interface was collected in 1 ml and washed with 14 ml 1xPBS/1 %FBS. Cells were pelleted by centrifugation for 7 minutes at 350 G and used for extracellular staining (4.2.8.2) or re-stimulation (4.2.8.3).

4.2.4.3 Isolation of lymphocytes from the spleen

Spleens were smashed through a 40 µm cell strainer and washed with 1xPBS/1 %FBS followed by centrifugation of the cells for 5 minutes at 350 G at 4 °C. Spleens were further processed for erythrocyte lysis (4.2.4.4).

4.2.4.4 Erythrocyte lysis

For the lysis of erythrocytes, 10x Ammonium-Chloride-Potassium (ACK) buffer was diluted with H₂O to 1x concentration. Pelleted cells or blood were resuspended in 1 ml 1xACK buffer and incubated for 5 minutes at room temperature. Lysis was stopped by addition of 15 ml 1xPBS/1 %FBS buffer. Cells were pelleted for 5 minutes at 350 G, 4 °C.

4.2.4.5 Extraction of blood serum and plasma

Fresh whole blood was transferred into EDTA tubes and stored on ice for the isolation of plasma or in tubes without anything and stored on room temperature for isolation of serum. Tubes were centrifuged at 3000 G for 10 minutes at 4 °C. The upper clear phase was transferred into RNase free 1.5 ml tubes and stored at -20 °C until analysis.

4.2.5 Blood analysis

At the day of the cell isolation, the blood was drawn as described in 4.2.4. During the experiment, blood was drawn retrobulbar with a 100 µl glass capillary and transferred into a tube with 3 µl 0.5 M EDTA. The plasma was isolated as described in 4.2.4.5.

The analysis of the alanine aminotransferase (ALT), aspartate aminotransferase (AST), Bilirubin and alkaline phosphatase (ALP) levels was performed in the Institute for experimental immunology and hepatology (UKE, Hamburg), using an automated procedure (COBAS MIRA; Roche). ALT, AST and Bilirubin levels were measured in the blood plasma, while ALP levels can only be measured in blood serum.

4.2.6 Histology of tissue samples

For histological analysis samples were fixated in 4 % PFA for at least 24 hours. Next, the tissues were kept in 50 % ethanol at room temperature for three hours. This was the first step of an automatically controlled sequence. Samples were transferred into increasing concentrations of ethanol to dehydrate the tissue (60 %, 70 %, 96 %, 100 % EtOH). In the last step, the samples were transferred into xylol and then into paraffin. The whole process took approximately 15 hours. Afterwards, tissue samples were embedded in paraffin.

Tissue paraffin blocks were sectioned into 5 µm cuts using a microtome and transferred onto a glass slide. Slides were dried over night at 37 °C.

4.2.6.1 H&E and Sirius red staining

For histological analysis, samples were stained for haematoxylin/eosin (H&E staining) and Sirius red staining. First, the paraffin was removed in three changes of xylol for 10 minutes each. Next, the tissues were hydrated in three quick changes of ethanol (100 %, 80 %, 70 %). For H&E staining, slides were stained 20 seconds in haematoxylin, washed with H₂O and then stained for eosin for 1 minute. Slides were washed again in H₂O and were ready for dehydration. For Sirius Red staining, the slides were stained for 1 minute in haematoxylin solution, washed in H₂O and stained for 60 minutes in Picro-Sirius Red Stain. Afterwards slides were rinsed in two changes of 0.5 % acetic acid water before they were ready for dehydration. The following steps were again the same for H&E and Sirius red staining. Slides were dehydrated in four quick changes of ethanol (70 %, 80 %, 100 %, 100 %) and three changes of xylol for 10 minutes each. Glass slides were mounted with mounting medium. Inflammation was assessed by a pathologist. Inflammatory activity was scored according to the modified histological activity index (mHAI) and the Fibrosis score (126, 127).

4.2.7 Measurement of bile acids in serum and stool

The analysis of the bile acids from the serum and the stool was performed by the group of Prof. Jörg Heeren from the Institute of biochemistry and molecular cell biology (UKE, Hamburg). Serum samples were collected as described in 4.2.4.5. For the stool analysis the whole caecum was collected. Serum and caecum content was stored at -80 °C upon analysis.

4.2.8 Flow cytometry (FACS)

As wash buffer 1xPBS/1 %FBS was used. Cells were pelleted by centrifugation for 7 minutes, 350 G at 4 °C.

4.2.8.1 Live dead staining

To discriminate dead cells from living cells, isolated cells were washed with 1xPBS and stained with Zombie UV™ Fixable Viability Kit. To that end, cells were incubated with 50 µl zombie dye in 1xPBS (1:200) at room temperature in the dark for 20 minutes. The cell suspension was washed and it was continued with extracellular staining.

4.2.8.2 Extracellular staining

After cell isolation, cells were stained with fluorochrome labeled antibodies diluted in PBS/FBS. Dilutions accordingly to Table 12 were used. Surface staining was performed for 20 minutes at 4 °C in the dark. Cells were washed and centrifuged. Next, cells were either resuspended in 150 µl PBS/FBS or further processed for intracellular staining.

4.2.8.3 Intracellular staining

For intracellular staining, cells were restimulated for 3 hours at 37 °C in RPMI full medium containing PMA (50 ng/ml), ionomycin (1 mM) and Monensin A. After restimulation, cells were washed and centrifuged and the extracellular staining was performed as described in 4.2.8.2. After extracellular staining, cells were fixated with 100 µl fix buffer for 2 minutes at room temperature in the dark. Afterwards cells were washed and centrifuged again. Next, cell membranes were permeabilized for 4 minutes at room temperature in the dark, by resuspending the cells in 100 µl perm buffer. Cells were washed and centrifuged. In a last step, the cells were resuspended in the intracellular antibody cocktail. The dilutions were used according to Table 12. Staining was performed overnight at 4 °C in the dark. The next morning, cells were washed and resuspended in 150 µl PBS/FBS.

Fluorochrome detection was performed on an LSR II flow cytometer using FACS Diva software. For analysis, data were exported from the FACS Diva to FlowJo vX software for windows.

4.2.8.4 Cell counting for FACS

For analyses of the cell number per organ, Sphero™ AccuCount Blank Particles were used. They were diluted in the sample in a ratio of 1:10 and acquired at the FACS. From the number of acquired counting beads was the number of cells calculated, as described in the data sheet.

4.2.9 Fluorescence-activated cell sorting (FACS-sort)

Cells were stained for extracellular surface markers as described in 4.2.8.2 and filtered through a 40 µm cell strainer to prevent clogging of the sorter nozzle. Cells were sorted in a 15 ml tube containing complete medium. Cell sorting was performed on a BD FACS Aria IIIu or AriaFusion.

4.2.10 *In vitro* suppression Assay

To test the suppressive capacity of Treg cells, they were cultured together with CD4⁺ T cells and APCs. The proliferation of the CD4⁺ T cells was analyzed. All the following steps were performed under the clean bench. For each mouse, 300 µl of MACS buffer were used for dilution of antibodies and magnetic beads. Cell pelleting was executed by centrifugation at 350 G for 7 minutes at 4 °C.

4.2.10.1 Isolation of CD4⁺ T cells and APCs using Magnetic activated cell sorting (MACS)

Isolated spleens and lymph nodes were smashed through a 100 µm sterile cell strainer and washed with MACS buffer. Cell suspension was centrifuged. To receive naïve CD4⁺ T cells, CD25⁺ cells and CD44⁺ cells were depleted first. Therefore, cells were incubated with biotinylated antibody against CD25 (1:400) and CD44 (1:200) in MACS buffer for 15 minutes at 4 °C. Cells were then washed with 14 ml of MACS buffer and centrifuged. Next, cells were incubated for 30 minutes at 4 °C with magnetic Streptavidin beads (40 µl/ml MACS buffer), which enabled specific binding to biotinylated primary antibodies. Cell suspension was washed with MACS buffer again. MACS column was placed in a magnet and calibrated with 3 ml MACS buffer. The cell suspension was filtered through a 100 µm sterile cell strainer and transferred into the column. After everything passed through the column, it was washed three times with 3 ml of MACS buffer. The flow through was collected in a 15 ml tube and contained the CD25⁻ CD44⁻ cells. Cells were washed, then centrifuged and incubated with CD4⁺ T cell selecting magnetic beads (1:10) in MACS buffer for 15 minutes at 4 °C. A new MACS column was put in the magnet and calibrated as mentioned above. The column was loaded with the cell

suspension and washed three times as before. The flow through, containing CD4⁻ cells, was collected in a 15 ml tube. In the column were the CD4⁺ cells. The column was removed from the magnet and placed on an empty 15 ml tube. 5 ml MACS buffer was added into the column and quickly pressed through with a stamp. Cells were kept on ice until labeling of the cells with proliferation dye. CD4⁻ cells were incubated with biotinylated primary antibody against CD3 for 15 minutes at 4 °C. Cells were then washed and centrifuged. Next, cells were incubated for 30 minutes at 4 °C with magnetic Streptavidin beads. A MACS column was put in the magnet and was calibrated. The CD3 negative fraction containing APCs was collected with the flow through. To avoid proliferation during *in vitro* culture, APCs were irradiated with 30 Gy and counted using a Neubauer-chamber.

4.2.10.2 Labeling of CD4⁺ T cells with proliferation dye

Isolated CD4⁺ T cells were washed with PBS and centrifuged. During this time, 500 µl 1xPBS were pre-warmed at 37 °C. Next, 1 µl violet dye (5 mM in DMSO) was mixed with warm PBS and added to the CD4⁺ T cells. Cells were stained for 6 minutes at 37 °C. The reaction was stopped by adding 3 ml FBS to the cocktail. Cells were centrifuged and washed again with 3 ml FBS. After another centrifugation step, cell number was determined using a Neubauer-chamber.

4.2.10.3 Isolation of Foxp3⁺ Treg

To isolate the Foxp3⁺ Treg to test the suppressive capacity, spleens and lymph nodes were isolated from mice with a *Foxp3^{mRFP}* reporter gene. They were smashed through a 100 µm sterile cell strainer and washed with MACS buffer. Cell suspension was centrifuged. Afterwards the cell suspension was incubated with CD4⁺ T cell selecting magnetic beads and was proceeded as described in 4.2.10.1 to isolate whole CD4⁺ T cells. Cells were FACS sorted for Foxp3⁺ CD4⁺ T cells as described in 4.2.9.

4.2.10.4 Pipetting scheme of *in vitro* suppression assay

The suppressive capacity of Foxp3⁺ Treg was tested in the ratios 1:2, 1:4, 1:8, 1:16, 1:32 and 1:64 of suppressor to effector cells. A 96 well round bottom plate was used. Per well 1x10⁵ CD4⁺ T cells, 4x10⁵ APCs and the titrated amount of Treg were pipetted in a total volume of 200 µl/well. Additionally, soluble anti-CD3 (2 µg/ml) and soluble anti-CD28 (1 µg/ml) specific antibodies were added to further stimulate the cells. The *in vitro* assay ran for 96 hours at

37 °C and 5 % CO₂. The proliferation of the responder cells was determined via FACS by detecting the intensity of violet dye per cell.

4.2.11 Statistical analysis

Statistical evaluations were performed using GraphPad Prism software. The Mann-Whitney U test, paired t test or one-way ANOVA (Tukey's multiple comparison) were used to calculate statistical significance. A p-value of <0.05 was used to define significance.

5 Results

Primary sclerosing cholangitis (PSC) is a chronic cholestatic inflammation of the intra- and extra-hepatic bile ducts, which progresses to end-stage liver disease (1). The etiology of PSC is still not understood and there is no effective medical treatment available. Several factors are known to impact PSC. Two of these are the co-occurrence of IBD (20) and the presence of genetic predispositions (95). Therefore, the first aim of this study was to understand the strong association of PSC with colitis. The second aim of this study was, to investigate single nucleotide polymorphisms (SNPs) in the *IL2RA* gene, which are known to be associated with PSC and IBD (94, 95, 106). To this end, we used a mouse model recapitulating the rs61839660 *Il2ra* SNP.

5.1 Analysis of the mechanism(s) of how colitis affects PSC

The first aim of this study was to analyze how colitis affects the disease development of PSC. The role of the gut-liver axis might play an important part in the relationship of the two diseases. One hypothesis was that intestinal inflammation and barrier defects promote liver disease because of the influx of bacteria and inflammatory cells to the liver. Indeed it was shown that induction of DSS and T-cell transfer colitis resulted in bacterial translocation and immune cell migration from the gut to the liver. Furthermore, colitis induction, in the absence of Foxp3⁺ Treg, resulted in a pathological condition of the liver (35). However, it was shown that the liver is able to clear commensals from the systemic vasculature independently of the spleen. Therefore, the liver can function as a vascular firewall mediating the mutualism between the host and its gut commensal microbiota (28).

5.1.1 Induction of colitis in an experimental mouse model of PSC, leads to reduced liver pathology

On the basis of the above-mentioned data, the role of colitis on PSC development was investigated using mouse models. To that end, a chronic DSS colitis was induced into *Mdr2*-deficient mice. *Mdr2*-deficient mice present a liver pathology directly after birth, which is characterized by acute, hepatitis-like inflammation. The mice transition into the chronic phase of disease, characterized by fibrosis, between 12-14 weeks of age (111, 112). A chronic time point of disease was investigated. Previously, it was shown by our group that DSS colitis

protects young *Mdr2*-deficient mice regarding PSC development (123). However, the impact at later stages of the disease was unclear. Therefore, 24-week-old *Mdr2*-deficient mice were used and a chronic DSS colitis was induced in these mice.

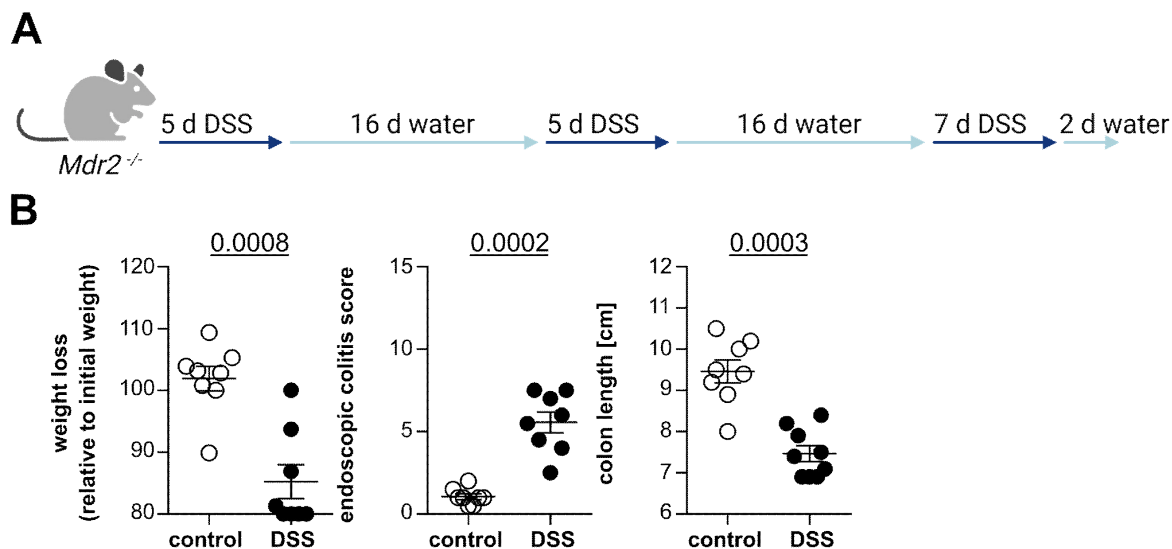


Figure 1: Induction of a chronic DSS colitis in *Mdr2*-deficient mice.

A) A chronic 2.5% DSS colitis was induced in 24 week old *Mdr2*-deficient mice. **B)** To determine the inflammation of the colon, the weight loss (d51), endoscopic colitis score (d50) and the colon length (day 51) were analyzed. Shown are the data of two independent experiments. Control n=9 DSS n=9. For statistical analysis, Mann-Whitney *U* test was performed ($p \leq 0.05$). Lines indicate mean \pm SEM.

The *Mdr2*-deficient mice received three cycles of DSS, the first 2 cycles for 5 days, and the 3rd cycle for 7 days with 16 days of remission in between, as shown in Figure 1A. To determine successful colitis development, the endoscopic colitis score was analyzed one day before the mice were sacrificed, on day 50 of the experiment. On day 51, when the mice were sacrificed, the weight loss and the colon length were analyzed (Figure 1B).

As markers for liver pathology, ALT, AST, bilirubin and ALP levels were measured in the blood serum on day 51 of the experiment (Figure 2A). In line with previous experiments (using 12-14 week old mice (123)), significantly decreased ALT and ALP levels were found in the mice that had developed DSS colitis compared to *Mdr2*-deficient control mice. The AST and bilirubin levels showed a tendency to lower levels.

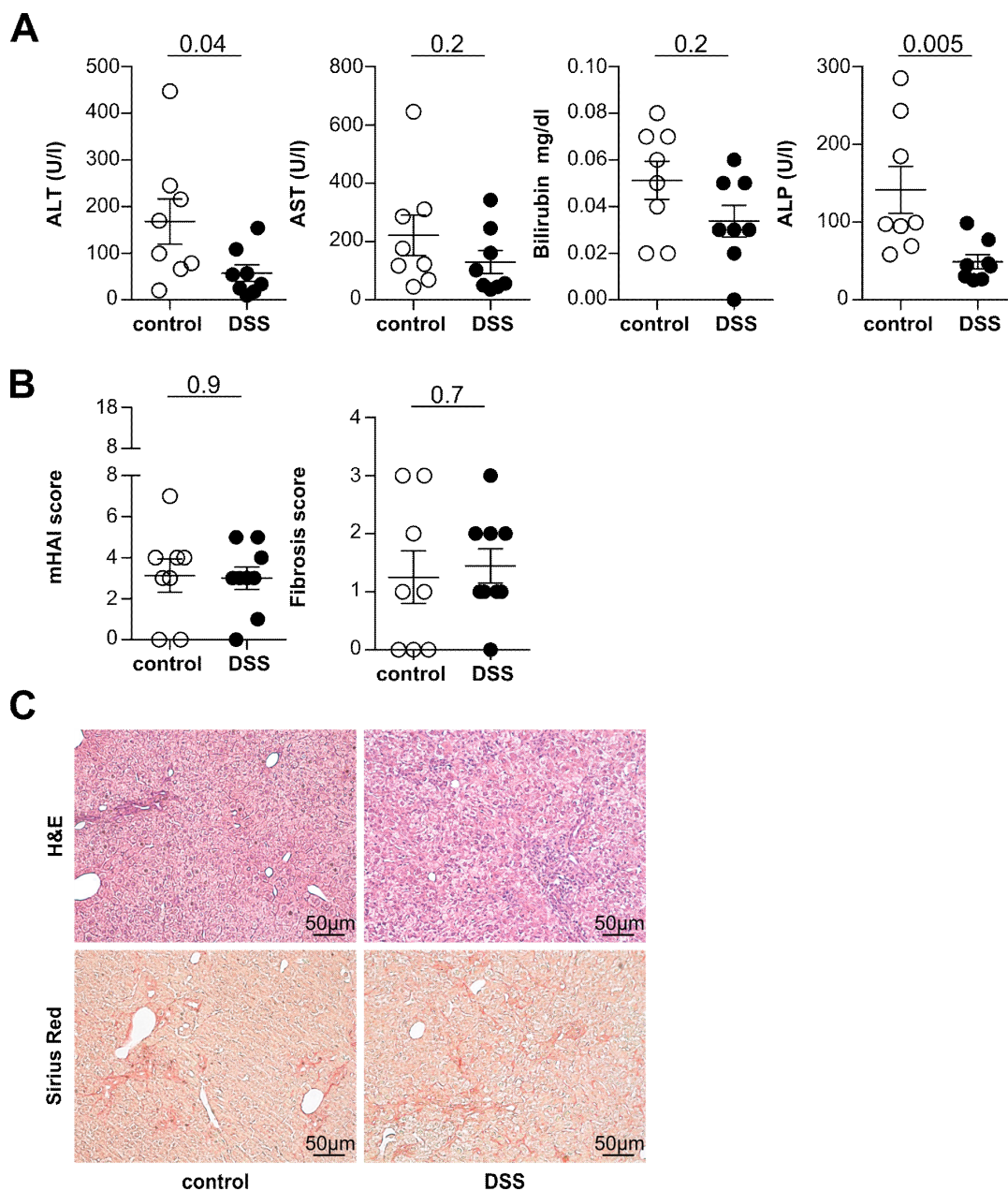


Figure 2: Induction of chronic DSS colitis in 24 week old *Mdr2*-deficient mice.

A) To determine the pathology of the liver, the ALT, AST, bilirubin and ALP levels were measured at day 51. **B)** Liver sections were stained for H&E and Sirius red to analyze the mHAI and Fibrosis score of the livers. **C)** Representative histological liver sections are shown. Shown are the data of two independent experiments. Control n=9 DSS n=9. For statistical analysis, Mann-Whitney *U* test was performed ($p \leq 0.05$). Lines indicate mean \pm SEM.

Liver sections were stained for H&E and Sirius red staining and mHAI and Fibrosis score of the liver were analyzed. No differences in the liver histology were detected, as shown in Figure 2B and the representative pictures in Figure 2C. Taken together, induction of chronic DSS colitis in 24-week-old *Mdr2*-deficient mice resulted in reduced ALT, AST, bilirubin and ALP levels as markers of liver pathology.

Next, it was investigated whether the observed protection might be dependent on the *Mdr2*-deficient mouse model. Therefore, an alternative mouse model for sclerosing cholangitis was tested, the 3,5-diethoxycarbonyl-1,4-dihydrocollidine (DDC) induced liver pathology (113).

C57BL/6J wild type mice were fed for eight days with 0.1 % DDC diet to induce sclerosing cholangitis. Three days later, the mice were split into two groups, one received drinking water with DSS for 7 days to induce an acute colitis, and a control group received pure drinking water. Nine days after colitis induction, the mice were sacrificed (Figure 3A). Induction of colitis was verified by comparing endoscopic colitis score one day after removing the DSS, and weight loss, as well as shortening of the colon were analyzed at the end of the experiment. Induction of DSS colitis, led to significantly more weight loss compared to controls. They also showed an increased endoscopic colitis score and shortening of the colon at the end of the experiment, as shown in Figure 3B, displaying that the colitis induction was successful. As markers of liver pathology, ALT and AST levels were analyzed in the blood serum at the end of the experiment. As shown in Figure 3C, the ALT and AST levels were significantly decreased in the group which received DDC+DSS compared to the DDC group without colitis. The mice showed no differences in liver histology measured by mHAI and Fibrosis score, as shown in Figure 3D. Figure 3D also shows that feeding of DDC for eight days led to very mild fibrosis development in the liver overall. Representative histological liver sections for H&E and Sirius red are shown in Figure 3E. Thus, induction of acute DSS colitis in a mouse model of DDC induced liver pathology results in reduced liver pathology measured by ALT and AST levels.

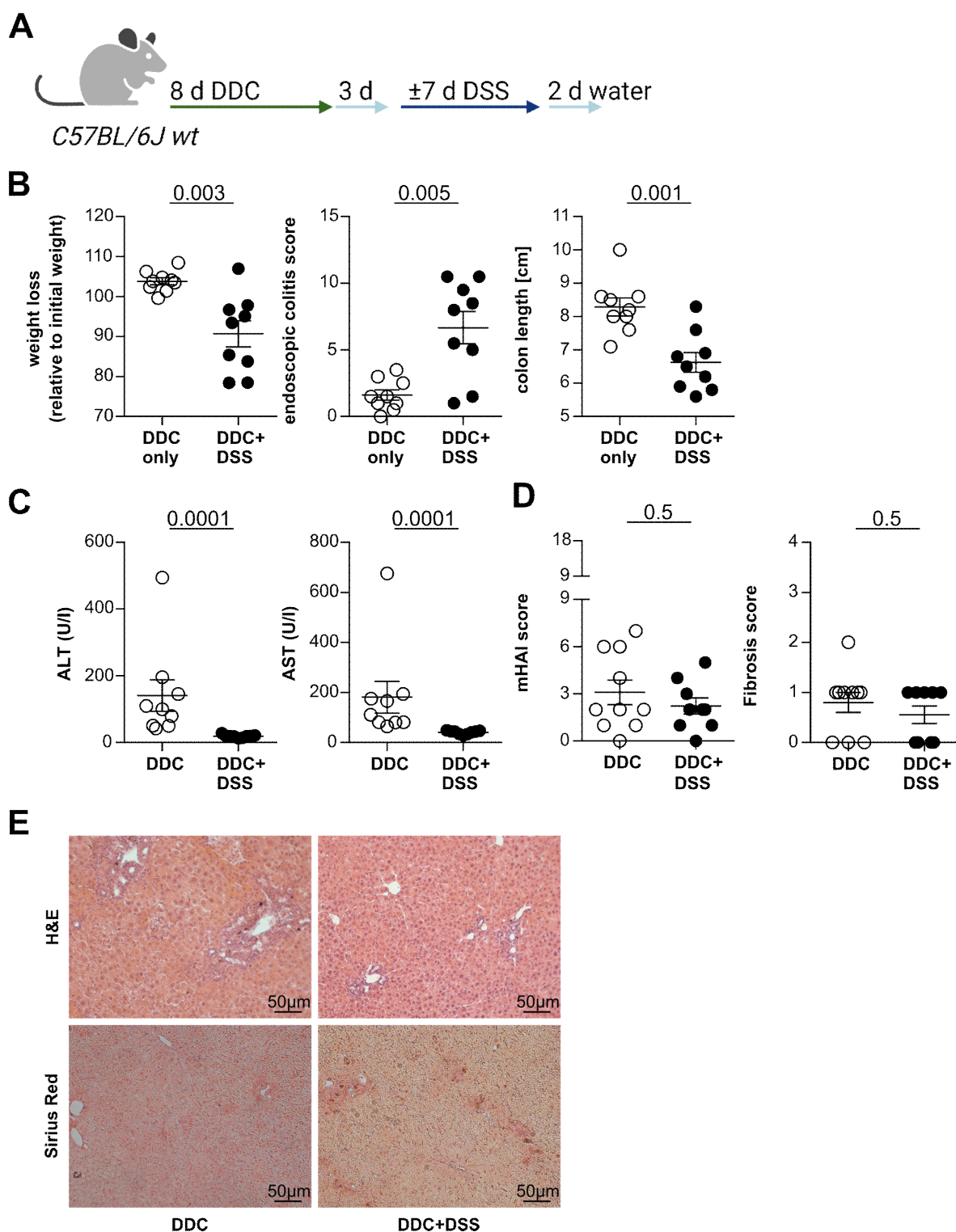


Figure 3: Induction of DSS colitis in DDC fed mice led to a reduced liver pathology.

A) To confirm the generated data in a second mouse model for PSC, the 0.1% DDC induced liver pathology was used and a 3% DSS colitis was induced afterwards. **B)** As disease readout for colitis development, the weight loss, endoscopic colitis score and colon length were analyzed. **C)** To determine the pathology of the liver, the ALT and AST levels were measured. **D)** Liver sections were stained for H&E and Sirius red to analyze the mHAI and Fibrosis score of the livers. **E)** Representative histological liver sections are shown. Shown are the data of two independent experiments. DDC n=9 DDC+DSS n=9. For statistical analysis, Mann-Whitney U test was performed ($p \leq 0.05$). Lines indicate mean \pm SEM.

To test, if the protection is a general consequence of colitis development, an alternative model for the DSS colitis was tested with the infection model of *Citrobacter rodentium* (122). Therefore, *Mdr2*-deficient mice were infected with the mouse pathogen *C. rodentium* for seven days (Figure 4A).

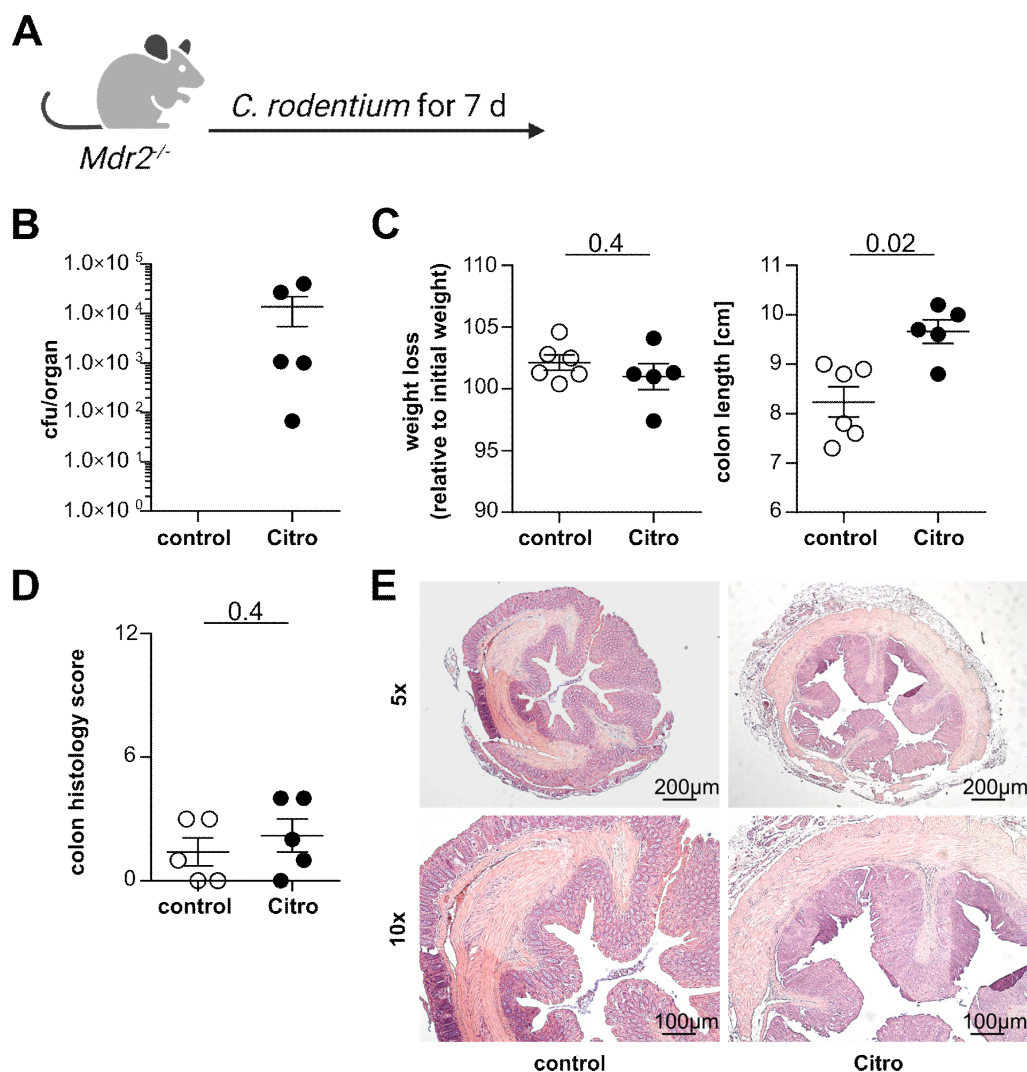


Figure 4: *Citrobacter rodentium* infection of *Mdr2*-deficient mice.

A) To analyze a second colitis model, *Mdr2*-deficient mice were infected with *C. rodentium* for seven days. **B)** The colony forming unit (CFU) was assessed from the caecum content. **C)** To determine the severity of the colitis the weight loss and the colon length were measured. **D)** The proximal colon was sectioned and stained for H&E to analyze the histology score. Shown are the data of one experiment. Control n=6 Citro n=5. For statistical analysis, Mann-Whitney *U* test was performed ($p \leq 0.05$). Lines indicate mean \pm SEM.

The colony forming unit (CFU) was assessed from the caecum content of the mice to confirm successful infection. *C. rodentium* was detectable in the caecum content of infected mice but not in control mice (Figure 4B). The severity of the colitis induction was measured by weight loss, colon length and histology of the proximal colon. As shown in Figure 4C, the mice did not lose weight, and also no shortening of the colon was detectable. Additionally, the histology of

the proximal part of the colon did not show significantly more inflammation in comparison to the controls. However, CFU assessment of the caecum content indicated successful *C. rodentium* infection. The ALT and AST levels were measured in the blood serum as markers of liver pathology. As shown in Figure 5A, the *C. rodentium* infected mice showed a significant decrease in the ALT and AST levels. Liver sections were stained for H&E and Sirius red and the inflammation and fibrosis of the liver was determined. No changes in the histologic mHAI and Fibrosis score were observed (Figure 5B). This was also shown in the representative pictures in Figure 5C.

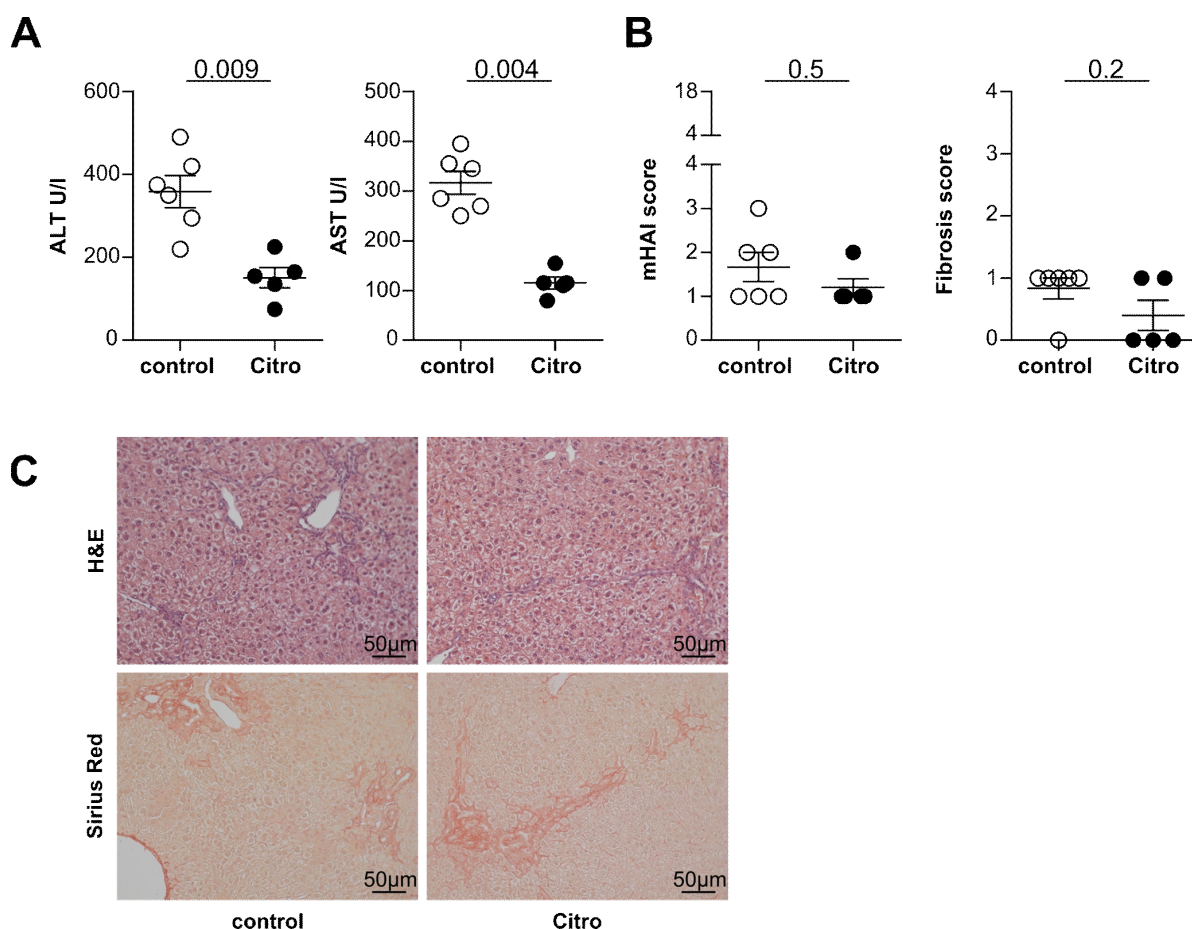


Figure 5: Infection with *Citrobacter rodentium* of *Mdr2*-deficient mice led to a reduced liver pathology.

A) The liver pathology was analyzed measuring ALT and AST levels. **B)** Liver sections were stained for H&E and Sirius red to analyze the mHAI and Fibrosis score of the livers. **C)** Representative histological liver sections are shown. Shown are the data of one experiment. Control n=6 Citro n=5. For statistical analysis, Mann-Whitney *U* test was performed ($p < 0.05$). Lines indicate mean \pm SEM.

In summary, a decrease in ALT and AST levels as markers of liver pathology, also after intestinal infection with *C. rodentium*, was found.

Taken together analyses of liver pathology in two experimental models of PSC, namely *Mdr2*-deficient mice and DDC feeding in wild type mice, after induction of intestinal inflammation by DSS and *C. rodentium* showed a protective effect of intestinal inflammation on liver pathology as assessed by serum liver transaminases. However, no impact on histological score of inflammation and fibrosis in the liver was found. On the basis of these data, we decided to use in the subsequent experiments 12-14-week-old *Mdr2*-deficient mice, as these show reduction of serum transaminases and histological sign of inflammation and fibrosis upon colitis induction (123).

5.1.2 Role of the microbiota in the protective effect of colitis on PSC development

PSC and IBD are both strongly associated with a change in the fecal microbiota, marked by reduced bacterial diversity (37, 42, 128, 129). A possible role of the microbiota in the disease development of PSC has been proposed for a long time. The general 'leaky gut' hypothesis describes that gut microbes and their metabolites can pass the gut barrier due to inflammation, and are transferred via the portal vein to the liver, where they trigger inflammation (32-34). A bacterial translocation and an influx of inflammatory cells from the gut to the liver was shown in mice during colitis induction (35). Additionally it was shown, that the liver is able to clear commensals from the systemic vasculature independently of the spleen through the livers own arterial supply. It is possible that changes in the gut microbiota due to IBD development result in a reduced severity of PSC. Therefore, a possible role of the fecal microbiota in the protective effect of colitis on PSC development in mouse models of PSC and colitis was further investigated.

5.1.2.1 The protective effect of colitis on the liver pathology was not transferable via fecal microbiota transplantation

As described above, the microbiota could be a very important player in the protection of colitis on PSC development. Subsequently, it was investigated whether the protective effect was transferable via the stool microbiota. Therefore, a fecal microbiota transplantation (FMT) was performed. Stool from mice which had only received the DDC diet to induce sclerosing cholangitis, or stool from mice that had first received the DDC diet and afterward a DSS colitis was used. The FMT was performed in 6-week-old, germ-free wild type mice. After four weeks of reconstitution, sclerosing cholangitis was induced in both groups using the DDC diet. The

experimental plan is shown in Figure 6A. To investigate, if the different microbiota had a colitogenic potential, the endoscopic colitis score and the colon length were analyzed. As shown in Figure 6B the mice did not develop signs of colitis as indicated by endoscopic colitis score and colon shortening.

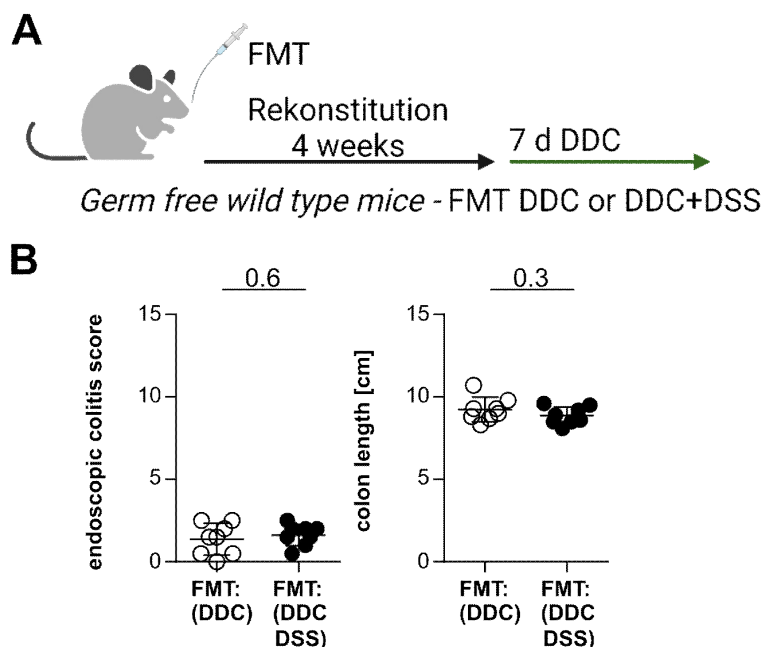


Figure 6: FMT with stool from DDC fed mice, or DDC+DSS fed mice into germ-free wild type mice, did not lead to colitis development.

A) Germ-free wild type mice received a FMT with stool from DDC alone or DDC+DSS fed mice with 6 weeks of age. After 4 weeks reconstitution, sclerosing cholangitis was induced by feeding them 0.1% DDC for 7 days. **B)** To analyze if the mice developed an inflammation in the colon due to the FMT, the endoscopic colitis score and colon length were examined. Shown are the data of one experiment. FMT: (DDC) n=8, FMT: (DDC+DSS) n=8. For statistical analysis, Mann-Whitney *U* test was performed ($p \leq 0.05$). Lines indicate mean \pm SEM.

The impact of the microbiota originating from mice with or without DSS colitis on DDC mediated liver pathology was analyzed by measurement of the ALT, AST, bilirubin, and ALP levels in the blood serum, as markers of liver pathology. Surprisingly, as shown in Figure 7A, an increase in ALT levels and a significant increase in AST levels was found in the group, which received the FMT with the stool of the DDC+DSS treated mice. Also, significantly increased bilirubin levels and a trend in ALP levels were found (Figure 7B). Liver sections were taken and stained for H&E and Sirius red to analyze the liver histologically. No differences in the mHAI and Fibrosis score of the liver were detected, as shown in Figure 7C and the representative pictures in Figure 7D.

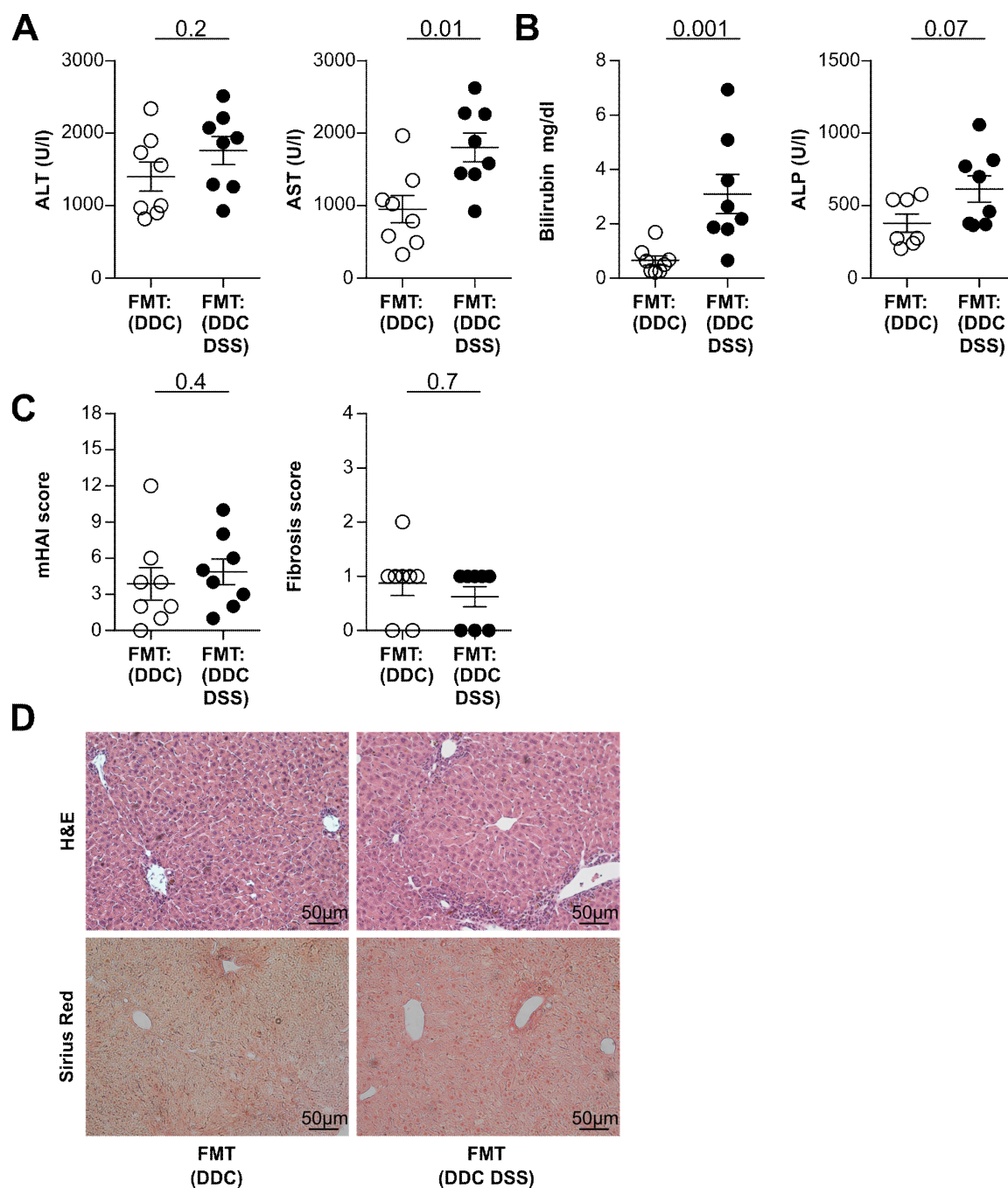


Figure 7: FMT with stool from mice received DDC and DSS led to a stronger DDC induced sclerosing cholestasis compared to a FMT with stool from mice received DDC only.

ALT and AST levels (**A**) as well as bilirubin and ALP levels (**B**) were measured to determine the pathology of the liver. **C**) Liver sections were stained for H&E and Sirius red to analyze the mHAI and Fibrosis score of the livers. **D**) Representative histological liver sections are shown. Shown are the data of one experiment. FMT: (DDC) n=8, FMT: (DDC+DSS) n=8. For statistical analysis, Mann-Whitney U test was performed ($p \leq 0.05$). Lines indicate mean \pm SEM.

Taken together, increased DDC mediated liver pathology after FMT of DDC+DSS stool was found compared to the FMT of DDC stool. These changes were detectable by measurement of ALT and AST levels as markers of liver pathology in the blood serum. Histologically, no differences were found in liver pathology. Thus, the protective effect of colitis on PSC

development described in section 3.1.1 does not seem to be mediated via changes of the intestinal microbiota. These data suggest that the DSS colitis induced microbiota, if anything, promotes liver pathology upon DDC feeding

5.1.3 Role of bile acids in the protective effect of colitis on PSC development

The gut-liver axis plays a critical role in bile acid metabolism (130). Hepatocytes synthesize the primary bile acids, cholic acid (CA) and chenodeoxycholic acid (CDCA) from cholesterol, which are conjugated with taurine or glycine to make them soluble in water. They are secreted into the bile and stored in the gallbladder (45). During meal intake, bile acids are released into the gastrointestinal tract. In the terminal ileum, 90-95 % of the primary bile acids are actively absorbed, enter the enterohepatic circulation, and are transported back to the liver. Around 5-10 % of the primary bile acids reach the colon where the gut microbiota deconjugates the bile acids and converts CA and CDCA into the secondary bile acids lithocholic acid (LCA) and deoxycholic acid (DCA). Some of these secondary bile acids cross the colonic epithelium by passive diffusion and enter the enterohepatic circulation (130). Thus, it was hypothesized that colitis induced microbial dysbiosis, which impacts the composition of the bile acids that re-enter the enterohepatic circulation, resulted in the observed protective effect of colitis on PSC development.

5.1.3.1 Unconjugated bile acids were reduced in the gut microbiota of *Mdr2*-deficient mice with DSS colitis

To investigate the role of the bile acid metabolism on the protective effect of colitis on PSC development, the composition of bile acids in the stool and the serum of *Mdr2*-deficient mice with and without DSS colitis was compared. To this end a chronic DSS colitis was induced in *Mdr2*-deficient mice, and the blood serum as well as the whole caecum content were taken at the end of the experiment. The bile acids were measured at this time point (Figure 8A). After comparing all bile acids, no differences were found in the blood serum in conjugated or unconjugated bile acids (Figure 8B). In the caecum content, no differences were found in conjugated bile acids, but a significant decrease in unconjugated bile acids, in the group which received a DSS colitis, was detected (Figure 8C). Since a significant decrease in this group was found, the unconjugated bile acids and its metabolites were further examined. There were

twelve unconjugated bile acids found in the caecal content which were significantly decreased, as shown in Figure 8D.

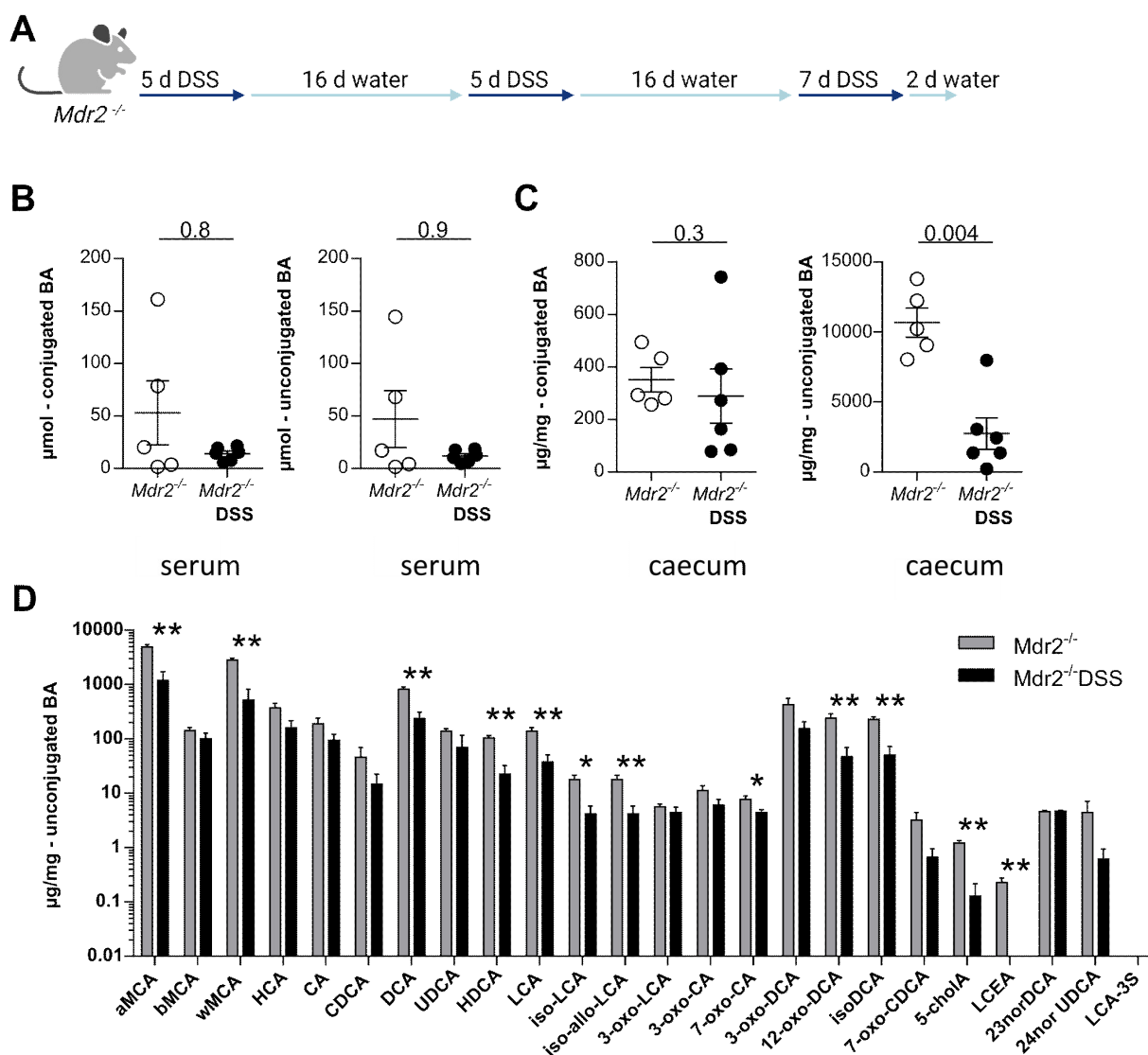


Figure 8: Unconjugated bile acids were overall reduced in the stool microbiota of *Mdr2*-deficient mice with DSS colitis.

A) A chronic 2.5% DSS colitis was induced in 12 week old *Mdr2*-deficient mice. The caecal content as well as the blood serum were collected for the bile acid analysis. Conjugated and unconjugated bile acids were analyzed in the blood serum (**B**) and in the content of the caecum (**C**). **D)** Twenty four unconjugated bile acids and its metabolites were further analyzed from the caecum content. Shown are the data of one experiment. *Mdr2*^{-/-} n=5, *Mdr2*^{-/-}DSS n=6. For statistical analysis, Mann-Whitney *U* test was performed ($p \leq 0.05$, * ≤ 0.05 , ** ≤ 0.001). Lines indicate mean \pm SEM.

Overall, a significant decrease of unconjugated bile acids was found in the content of the caecum.

5.1.4 The innate immune system was not the major driver of the observed reduction in liver pathology in the presence of colitis

It has been proposed that bacteria translocate from the inflamed gut to the liver, which leads to an influx of inflammatory cells in the liver (35). Therefore, it is likely that the pathogenesis of PSC involves activation of the innate immune system by bacterial components delivered to the liver via the portal vein (9). The exaggerated immune response may contribute to PSC progression, as has been postulated for the associated IBD (77, 131, 132). Therefore, it was hypothesized that innate immune cells might promote the protective effect of colitis observed in the experimental mouse models of PSC. To this end, the role of macrophages, neutrophils and granulocytes was investigated after induction of DSS colitis in experimental mouse models of DDC- and *Mdr2*^{-/-} mediated PSC. In addition, a mouse model without T- and B- cells was used, to investigate if the observed protective effect was really mediated by the innate immune system.

5.1.4.1 Impairment of the phagocytosis during PSC-associated colitis still resulted in reduced liver pathology

Guicciardi *et al.* were able to show that macrophages contribute to the pathogenesis of sclerosing cholangitis in mice (74). Their results implicate a role of macrophages in PSC and PSC-like diseases in mice. More importantly, they found that pharmacological inhibition of macrophage recruitment to the liver reduces PSC-like liver injury in mice. It was hypothesized that this reduction of macrophage-function in the liver can also be due to associated inflammation in the colon. To test the functional role of macrophages in the protective effect observed in liver pathology in PSC-associated colitis, a DDC mediated liver pathology was induced in *AM*^{ff}/*Csf1r*^{Cre} deficient mice, which have an impaired phagocytosis capacity, prior to acute DSS colitis induction (Figure 9A). Mice without DSS colitis, as well as *AM*^{+/+}/*Csf1r*^{Cre} mice served as controls. The severity of the induced colitis was monitored by the weight loss, endoscopic colitis score and shortening of the colon, shown in Figure 9B. Depicted is the endoscopic colitis score one day after removing the DSS and the weight loss and the colon length two days after removing the DSS when the mice were sacrificed. The DSS treated mice showed a strong weight loss, significantly increased endoscopic colitis score and shortening of

the colon, confirming that the induction of the DSS colitis was successful and similar between the groups.

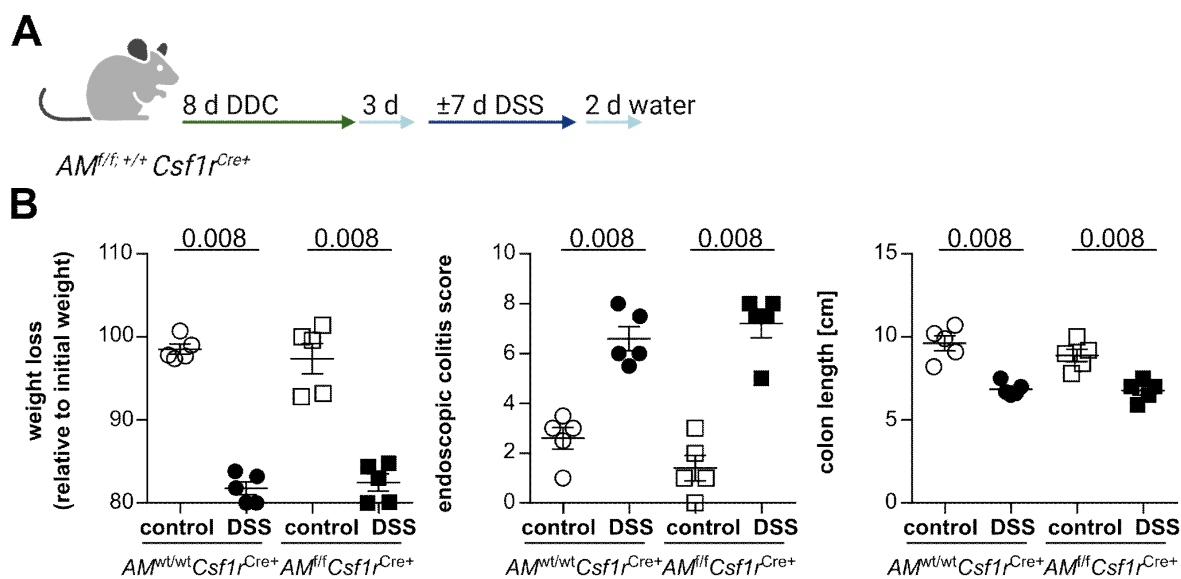


Figure 9: Induction of DSS colitis in $AM^{fl/fl}Csf1^{Cre}$ mice with DDC mediated liver pathology.

A) $AM^{fl/fl}Csf1^{Cre}$ and $AM^{+/+}Csf1^{Cre}$ mice were fed with 0.1% DDC diet for 8 days to induce sclerosing cholangitis. After 3 days remission, an acute 3 % DSS colitis was induced in two groups. **B)** As disease readout for colitis development, the weight loss, endoscopic colitis score and colon length were analyzed. Shown are the data of one experiments. $AM^{wt/wt}Csf1^{Cre+}$ control n=5, $AM^{wt/wt}Csf1^{Cre+}$ DSS n=5, $AM^{fl/fl}Csf1^{Cre+}$ control n=5, $AM^{fl/fl}Csf1^{Cre+}$ DSS n=5. For statistical analysis, Mann-Whitney *U* test was performed ($p \leq 0.05$). Lines indicate mean \pm SEM.

The blood serum was analyzed for ALT, AST, bilirubin and ALP levels (Figure 10A-B), as markers to determine the pathology of the liver. The ALT levels were reduced in the groups that had received the DSS colitis. These changes were only a trend and not significant. The AST and bilirubin levels were not changed. The serum levels for ALP were significantly decreased in both, the $AM^{+/+}Csf1^{Cre}$ and the $AM^{fl/fl}Csf1^{Cre}$ mice, with DSS colitis compared to the controls without colitis. Overall the ALT, AST, bilirubin and ALP levels were rather low, suggesting that the induced liver pathology was only mild. This was also shown in the liver histology in Figure 10C. The mHAI score was very low and no fibrosis was detectable in any of the groups. Representative histological liver sections are shown in Figure 10D.

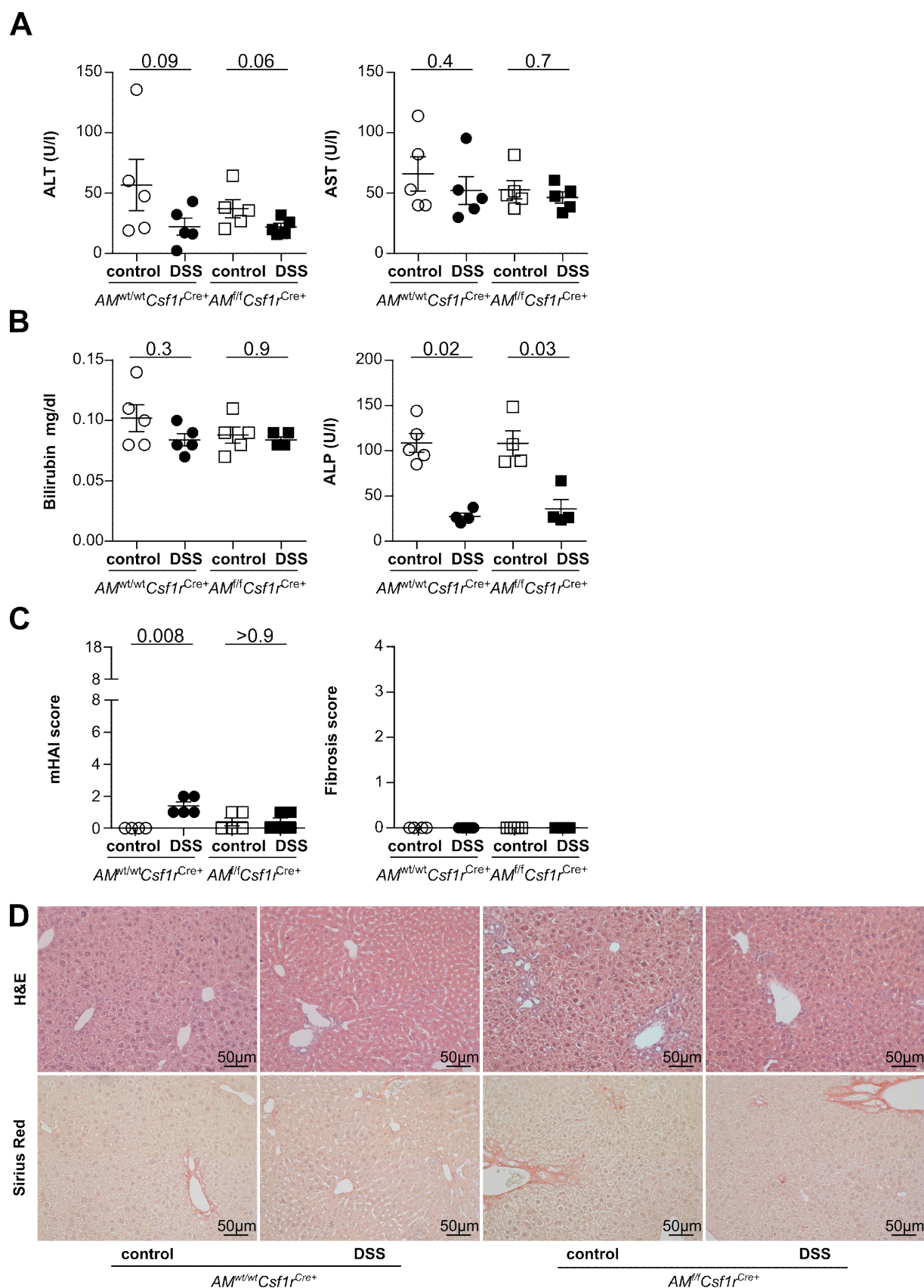


Figure 10: Severity of liver pathology after induction of DSS colitis in $AM^{fl/fl}Csf1^{rCre}$ mice and $AM^{+/+}Csf1^{rCre}$ littermates with DDC mediated liver pathology.

To determine the pathology of the liver, the ALT and AST levels (**A**) as well as bilirubin and ALP (**B**) were measured. **C**) Liver sections were stained for H&E and Sirius red to analyze the mHAI and Fibrosis score of the livers. **D**)

Representative histological liver sections are shown. Shown are the data of one experiments. *AM^{wt/wt}Csf1^{Cre+}* control n=5, *AM^{wt/wt}Csf1^{Cre+}* DSS n=5, *AM^{fl/fl}Csf1^{Cre+}* control n=5, *AM^{fl/fl}Csf1^{Cre+}* DSS n=5. For statistical analysis, Mann-Whitney *U* test was performed ($p \leq 0.05$). Lines indicate mean \pm SEM.

Taken together, although the DDC induced liver pathology was very low, ALT levels were decreased by trend, and moreover, ALP levels were significantly reduced in both groups after DSS colitis induction. Therefore, these data suggest no major role of macrophages in the protection of colitis on PSC development.

5.1.4.2 The reduced liver pathology during colitis was not dependent on neutrophils and granulocytes

A recent publication showed that PSC is associated with massive cellular infiltration and with a distinct presence of neutrophils, which are otherwise rarely observed in non-PSC control bile ducts (68). Therefore, in a next step the role of CD11b⁺Ly6G⁺ neutrophils and granulocytes was analyzed. To this end, neutrophils and granulocytes were depleted in *Mdr2*-deficient mice during the course of acute DSS colitis using an anti-Gr1 antibody (Figure 11A). At day 9 of the experiment, lymphocytes were isolated from the liver and the colon and analyzed for CD11b⁺Ly6G⁺ neutrophils and granulocytes (Figure 11B). The inflammation of the colon was measured by weight loss, endoscopic colitis score and colon length as shown in Figure 11C.

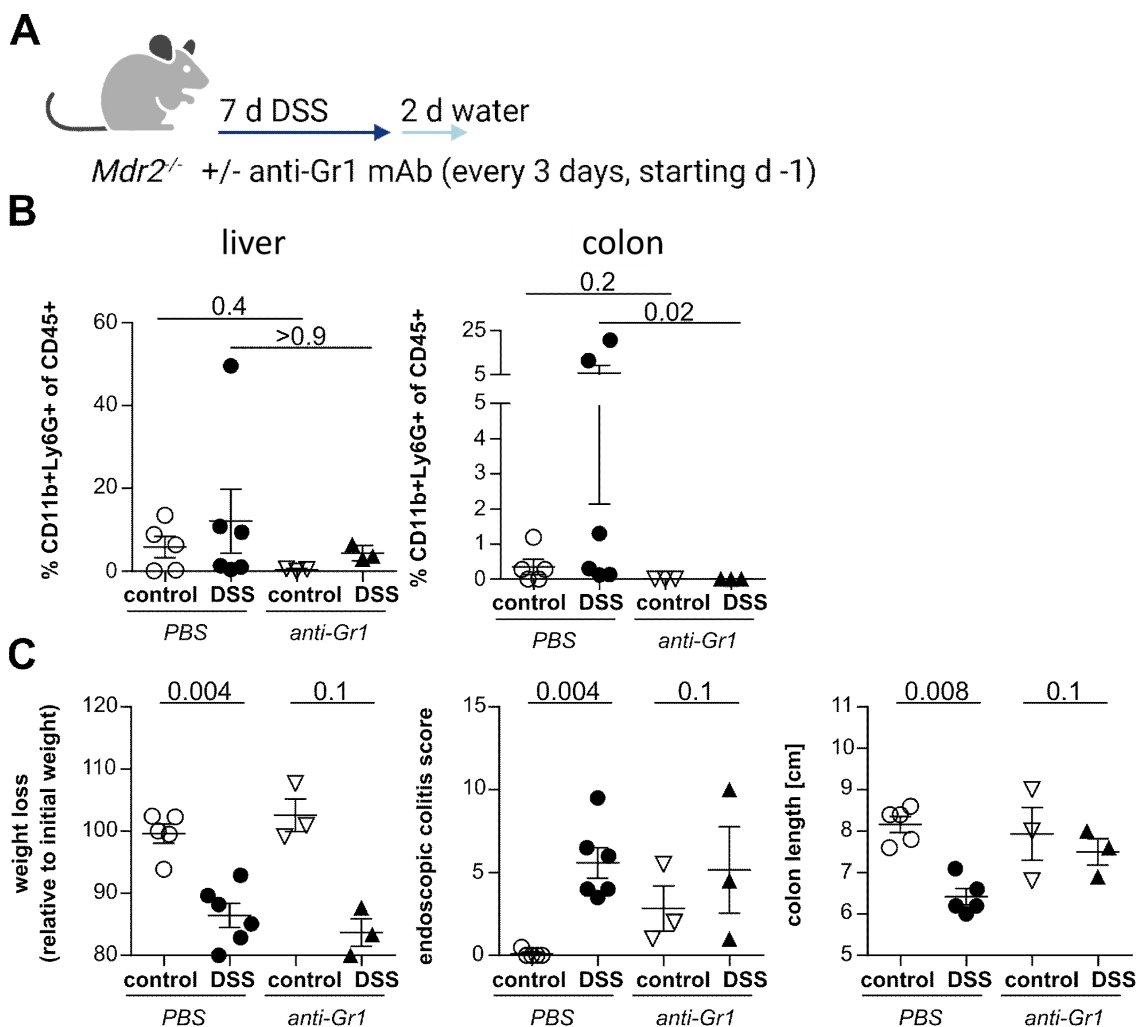


Figure 11: Depletion of Ly6G⁺ cells during PSC-associated colitis.

A) Ly6G⁺ cells were depleted in *Mdr2*-deficient mice during induction of acute 3% DSS colitis. **B)** At day 9 the frequency of CD11b⁺Ly6G⁺ cells was analyzed in the liver and colon tissue. **C)** As disease readout for colitis development the weight loss, endoscopic colitis score and colon length were analyzed. Shown are the data of two independent experiments. PBS control n=5, PBS DSS n=6, anti-Gr1 control n=3, anti-Gr1 DSS n=3. Four mice were excluded, due to insufficient depletion of Ly6G⁺ cells. For statistical analysis, Mann-Whitney *U* test was performed ($p \leq 0.05$). Lines indicate mean \pm SEM.

The two groups, which received the anti-Gr1 antibody showed reduced frequencies of CD11b⁺Ly6G⁺ neutrophils and granulocytes in the liver and the colon (Figure 11B). The groups with DSS colitis lost significantly more weight than the control groups. Shown is the weight loss at day 9 relative to the initial weight. An increased endoscopic colitis score at day 8 and shortening of the colon at day 9 was shown, confirming that the colitis induction worked well (Figure 11C). The liver pathology was analyzed by measurement of ALT and AST levels in the blood serum at day 9 of the experiment and liver sections were stained for histological analysis. The DSS treated groups showed a strong decrease in the ALT and AST levels compared to the control groups without DSS (Figure 12A). This tendency was also visible in the liver

histology but the changes were not significant (Figure 12B). This is also shown in the representative histological liver sections in Figure 12C.

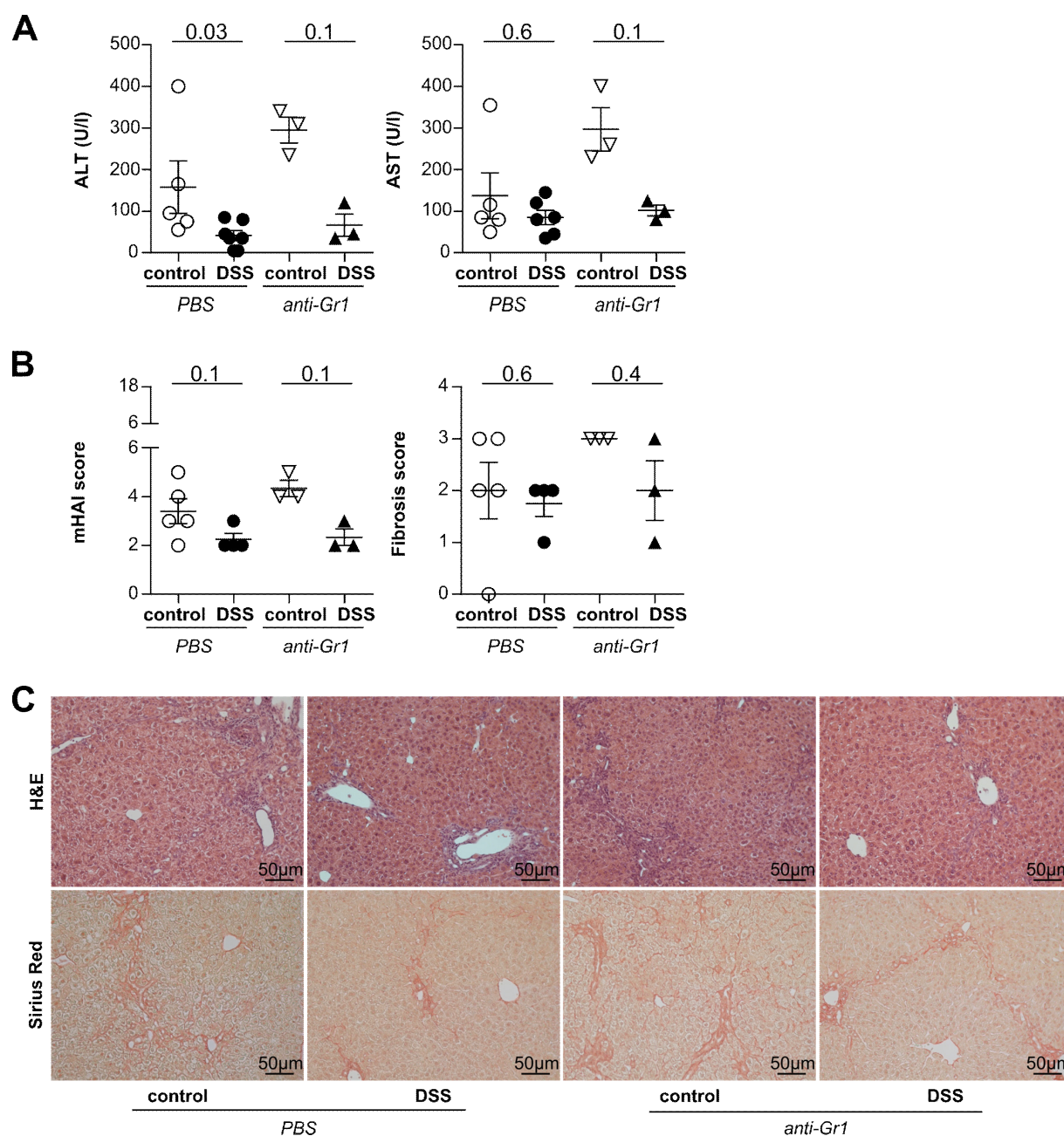


Figure 12: Depletion of Ly6G⁺ cells during PSC-associated colitis using an anti-Gr1 antibody.

A) To determine the pathology of the liver, the transaminases were measured. **B)** Liver sections were stained for H&E and Sirius red to analyze the mHAI and Fibrosis score of the livers. **C)** Representative histological liver sections are shown. Shown are the data of two independent experiments. PBS control n=5, PBS DSS n=6, anti-Gr1 control n=3, anti-Gr1 DSS n=3. For statistical analysis, Mann-Whitney *U* test was performed ($p \leq 0.05$). Lines indicate mean \pm SEM.

Taken together these data showed the protective effect of colitis on PSC development, both in the presence and absence of Ly6G⁺ neutrophils and granulocytes, suggesting that neutrophils and granulocytes were not the major driver of the observed protection.

5.1.4.3 A mouse model without T and B cells suggested a non-essential role of the innate immune system in the protective effect

The previous generated data suggest that the phagocytic function of macrophages, as well as neutrophils and granulocytes, did not promote the protection of colitis on PSC development. But since the data were not completely conclusive, another mouse model without T and B cells was used to confirm the results obtained in the previous experiments. Therefore, the impact of chronic DSS colitis on liver pathology in *Rag1* x *Mdr2*-deficient mice, that are deficient of T and B cells, was assessed and additionally compared to T and B cell proficient *Mdr2*-deficient mice (Figure 13A). The colitis induction was controlled by weight loss, endoscopic colitis score and shortening of the colon as shown in Figure 13B. The colitis was successfully induced in both, *Mdr2*-deficient and *Rag1* x *Mdr2*-deficient mice. This was shown by increased endoscopic colitis score on day 50, shortening of the colon and reduced weight loss both at day 51 after colitis induction, although *Rag1* x *Mdr2*-deficient mice showed a stronger weight loss (Figure 13B).

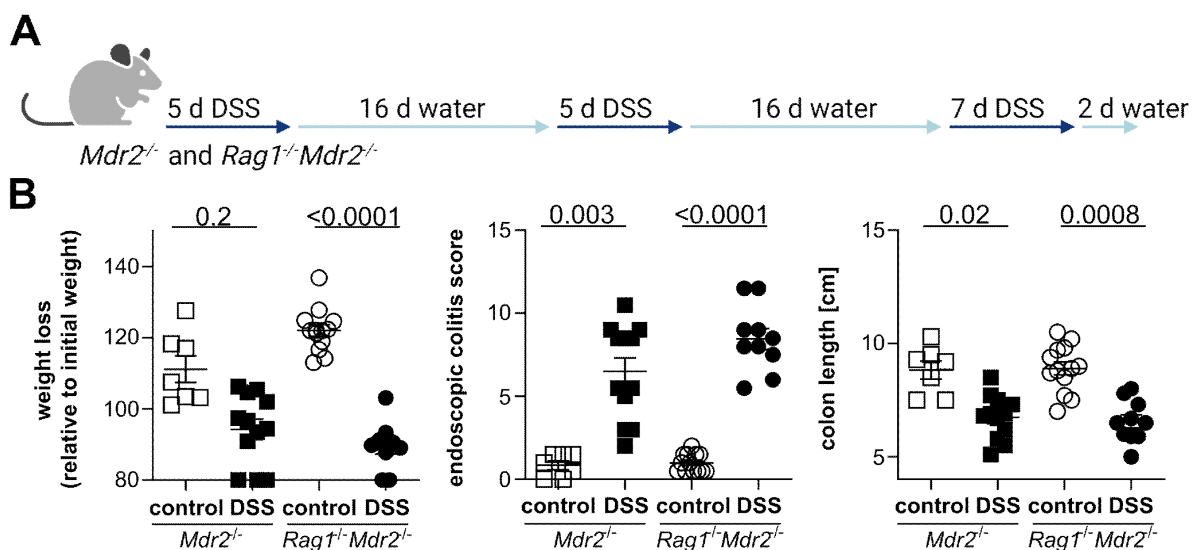


Figure 13: Induction of PSC-associated colitis in a mouse model without T and B cells.

A) A chronic 2.5% DSS colitis was induced in *Mdr2*-deficient mice and *Rag1* x *Mdr2*-deficient mice. **B)** As disease readout for colitis development the weight loss, the endoscopic colitis score and the colon length were analyzed. Shown are the data of two independent experiments. *Mdr2*^{-/-} control n=7, *Mdr2*^{-/-} DSS n=12, *Rag1*^{-/-}*Mdr2*^{-/-} control n=13, *Rag1*^{-/-}*Mdr2*^{-/-} DSS n=10. For statistical analysis, Mann-Whitney *U* test was performed ($p \leq 0.05$). Lines indicate mean \pm SEM.

Next, the pathology of the liver was analyzed by measurement of the ALT and AST levels in the blood serum, as well as by liver histology. The ALT and AST levels of day 51, as markers for liver inflammation are shown in Figure 14A.

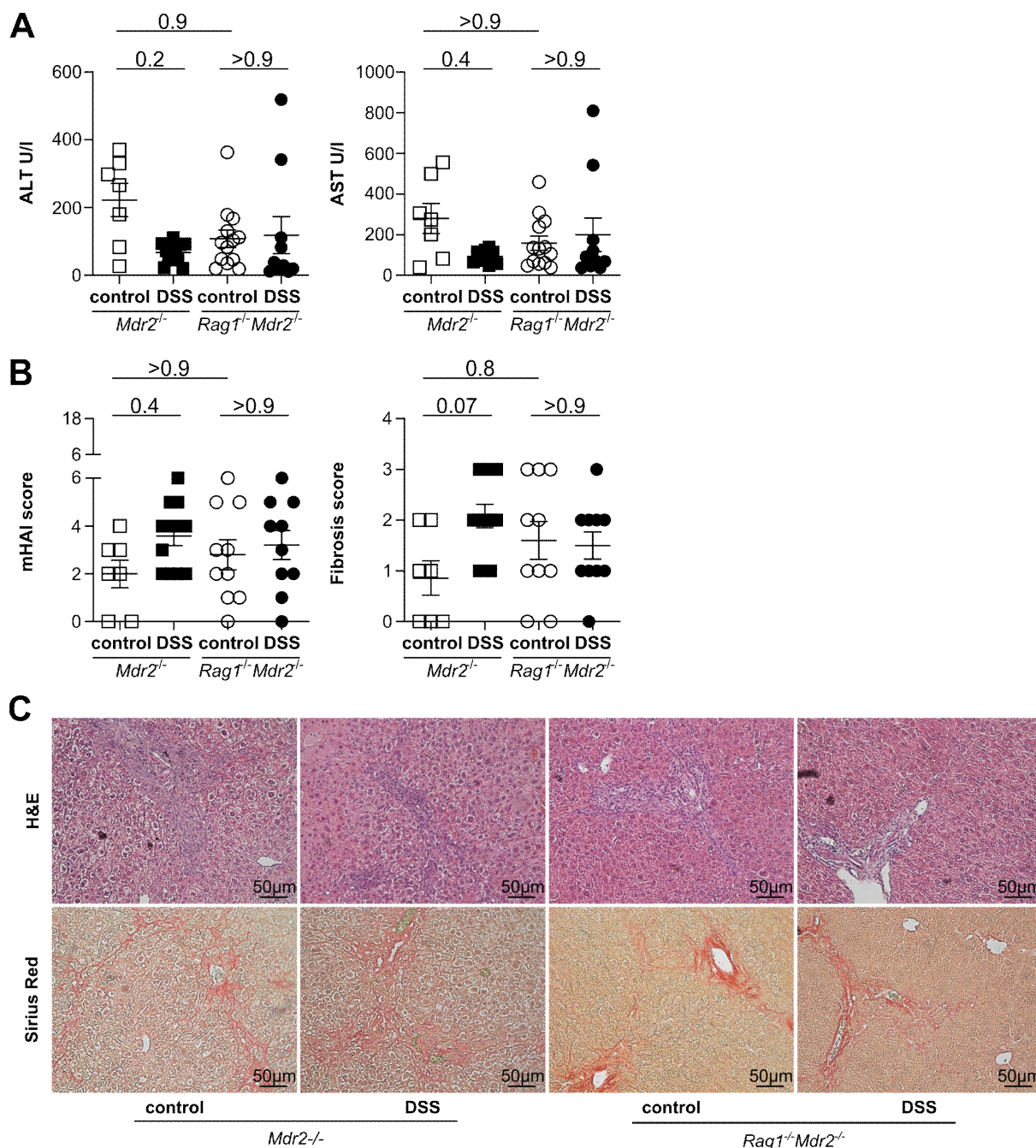


Figure 14: Induction of PSC-associated IBD in a mouse model without T and B cells.

A) To determine the pathology of the liver, the ALT and AST levels were measured in the blood serum. **B)** Liver sections were stained for H&E and Sirius red to analyze the mHAI and Fibrosis score of the livers. **C)** Representative histological liver sections are shown. Shown are the data of two independent experiments. *Mdr2*^{-/-} control n=7, *Mdr2*^{-/-} DSS n=12, *Rag1*^{-/-}*Mdr2*^{-/-} control n=13, *Rag1*^{-/-}*Mdr2*^{-/-} DSS n=10. For statistical analysis, Kruskal-Wallis test was performed ($p < 0.05$). Lines indicate mean \pm SEM.

The reduction of ALT and AST levels in the DSS treated *Mdr2*^{-/-} deficient control mice was reduced similarly to the experiments shown in paragraph one of this work. But in this experiment the difference was not statistically significantly different due to the limited number of mice, and thus needs to be repeated (Figure 14B). Of note, *Rag1* x *Mdr2*-deficient mice show no difference between the control group and the DSS colitis group in ALT and AST

levels. Also in the liver histology no differences in the mHAI and Fibrosis score were found. In Figure 14C representative histological liver sections are shown.

Taken together these data showed, that DSS colitis in *Rag1 x Mdr2*-deficient mice, in contrast to *Mdr2*-deficient mice, did not reduce liver pathology. ALT and AST levels as well as liver histology were comparable between the control group and the DSS colitis group. The conclusion from this experiment was that the innate immune system is not the major driver of the observed protection, but rather that the loss of T and B cells leads to the absence of the protective effect of colitis on PSC development.

5.1.5 Role of T and B cells in the protection

The protection of colitis on PSC development was not mediated by the innate immune system as described above. Moreover, previous experiment using *Rag1 x Mdr2*-deficient mice suggested that rather T and/or B cells promoted the colitis-mediated protective effect. Therefore, in the following experiments, the role of different T-cell subsets and B cells was further analyzed.

5.1.5.1 CD8⁺ T cells were not the major driver of the observed protection of colitis in *Mdr2*-deficient mice

Next, the impact of CD8⁺ T cells in the protective effect of colitis on PSC development was studied. Different publications described a role of CD8⁺ T cells in the disease development of PSC (82, 133). In 2019 it was shown that IFN- γ changed the phenotype of hepatic CD8⁺ T cells towards increased cytotoxicity and its absence attenuated liver fibrosis in chronic sclerosing cholangitis in mice (82).

To decipher a possible role of CD8⁺ T cells in the protective effect of colitis on PSC development, CD8⁺ T cells were depleted in *Mdr2*-deficient mice upon induction of chronic DSS colitis. Therefore, anti-CD8 mAb was injected every seven days, starting at day -1, as shown in Figure 15A. The control mice were injected with PBS. To confirm the depletion of CD8⁺ T cells, blood samples were taken on day 28 and day 51, and lymphocytes were isolated from the liver and colon of the mice on day 51 to stain for CD8⁺ T cells. On day 28, a reduction of circulating CD8⁺ T cells was found in the blood. However, on day 51, blood circulating CD8⁺ T cells were no longer reduced (Figure 15B). Likewise, the levels of CD8⁺ T cells in the liver and

the colon were similar in between the groups. However, CD8⁺ T-cell levels were overall low with 3-4 % of all CD45⁺ cells in the liver, and a maximum of 1 % of all CD45⁺ cells in the colon (Figure 15C).

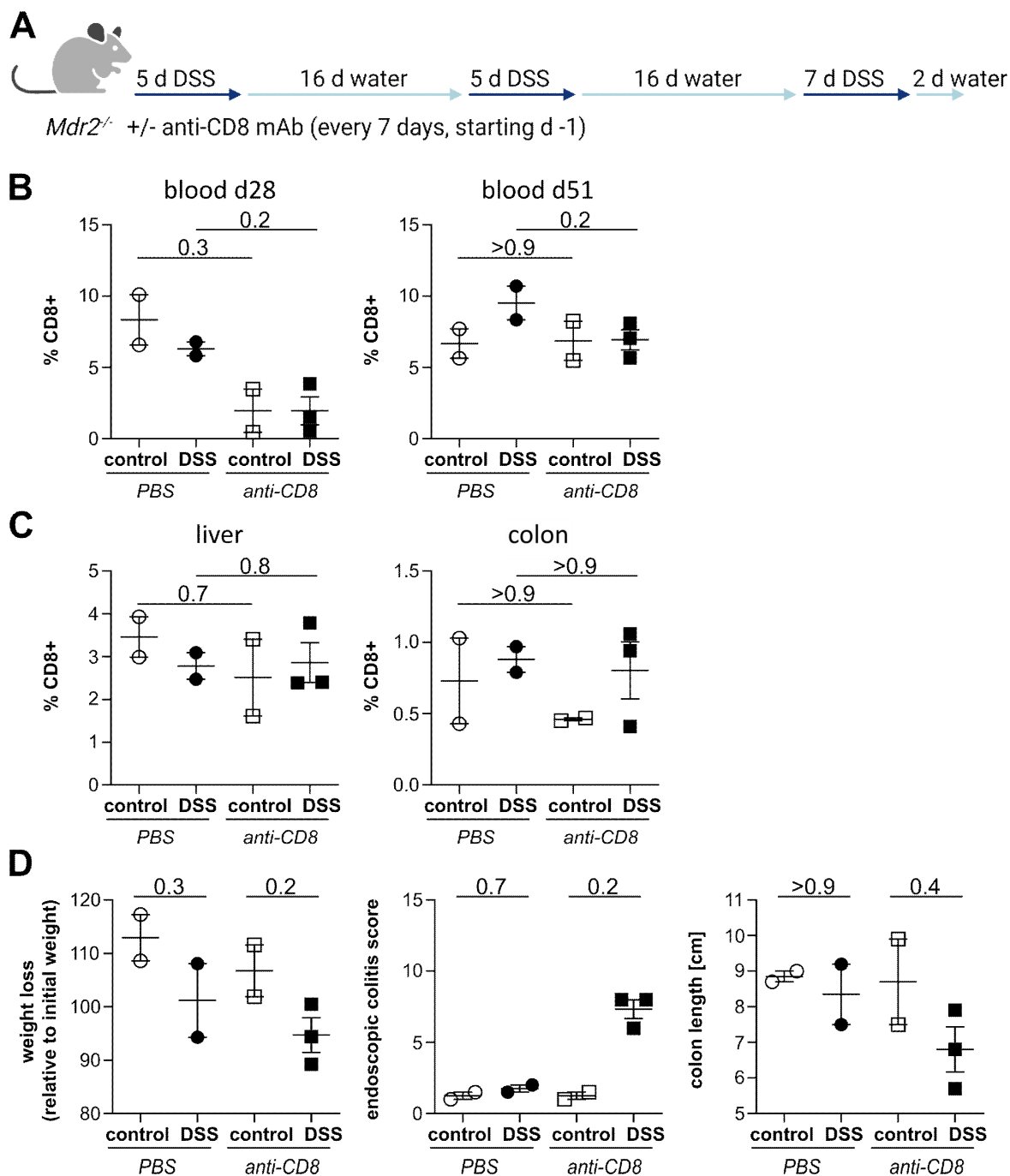


Figure 15: Depletion of CD8⁺ T cells in *Mdr2*-deficient mice during chronic colitis induction.

A) A chronic DSS colitis was induced in *Mdr2*-deficient mice and CD8⁺ T cells were depleted using an *in vivo* anti-CD8 antibody. **B)** The frequency of CD8⁺ T cells in the blood was analyzed at day 28 and day 51 of the experiment. **C)** At day 51 the frequency of CD8⁺ T cells was analyzed in the liver and colon tissue. **D)** As disease readout for colitis development the weight loss, endoscopic colitis score and colon length were analyzed. Shown are the data of one experiment. PBS control n=2, PBS DSS n=2, anti-CD8 control n=2, anti-CD8 DSS n=3. For statistical analysis, Mann-Whitney *U* test was performed ($p \leq 0.05$). Lines indicate mean \pm SEM.

To confirm the colitis induction, the weight loss, endoscopic colitis score and colon length were measured. As shown in Figure 15D, the mice developed no or mild colitis after DSS treatment, as shown by weight loss and colon shortening on day 51 and endoscopic score on day 50. Overall, in this experiment, only *Mdr2*-deficient mice in which CD8⁺ T cells had been depleted, developed signs of colitis.

Next, the liver pathology was analyzed via measurements of ALT, AST, bilirubin and ALP levels in the blood serum. A reduction of the ALT, AST, and ALP levels was found in the DSS treated mice in the absence of CD8⁺ T cells on day 51. Bilirubin levels were not changed overall (Figure 16A-B). Due to the absence of colitis development, *Mdr2*-deficient mice, showed no reduced liver pathology with respect to ALT, AST, ALP and bilirubin upon DSS colitis induction (Figure 16A-B). Histological determination of liver pathology and fibrosis by H&E and Sirius red staining revealed no detectable changes in the mHAI or Fibrosis score (Figure 16C and the representative liver sections in Figure 16D).

Taken together, no major role of CD8⁺ T cells was observed in the protective effect of colitis on PSC development. A decrease of ALT, AST, and ALP levels as markers of liver pathology was found in the group with depleted CD8⁺ T cells and DSS colitis. Even if the depletion of CD8⁺ T cells was not as strong as suspected on day 51 of the experiment, the CD8⁺ T cells were still depleted on day 28 after the second cycle of DSS. No changes in the histology of the liver were detectable. The n-value of this experiment was very low. The experiment has to be repeated to finally exclude a possible role of CD8⁺ T cells in the protective effect of colitis on PSC development.

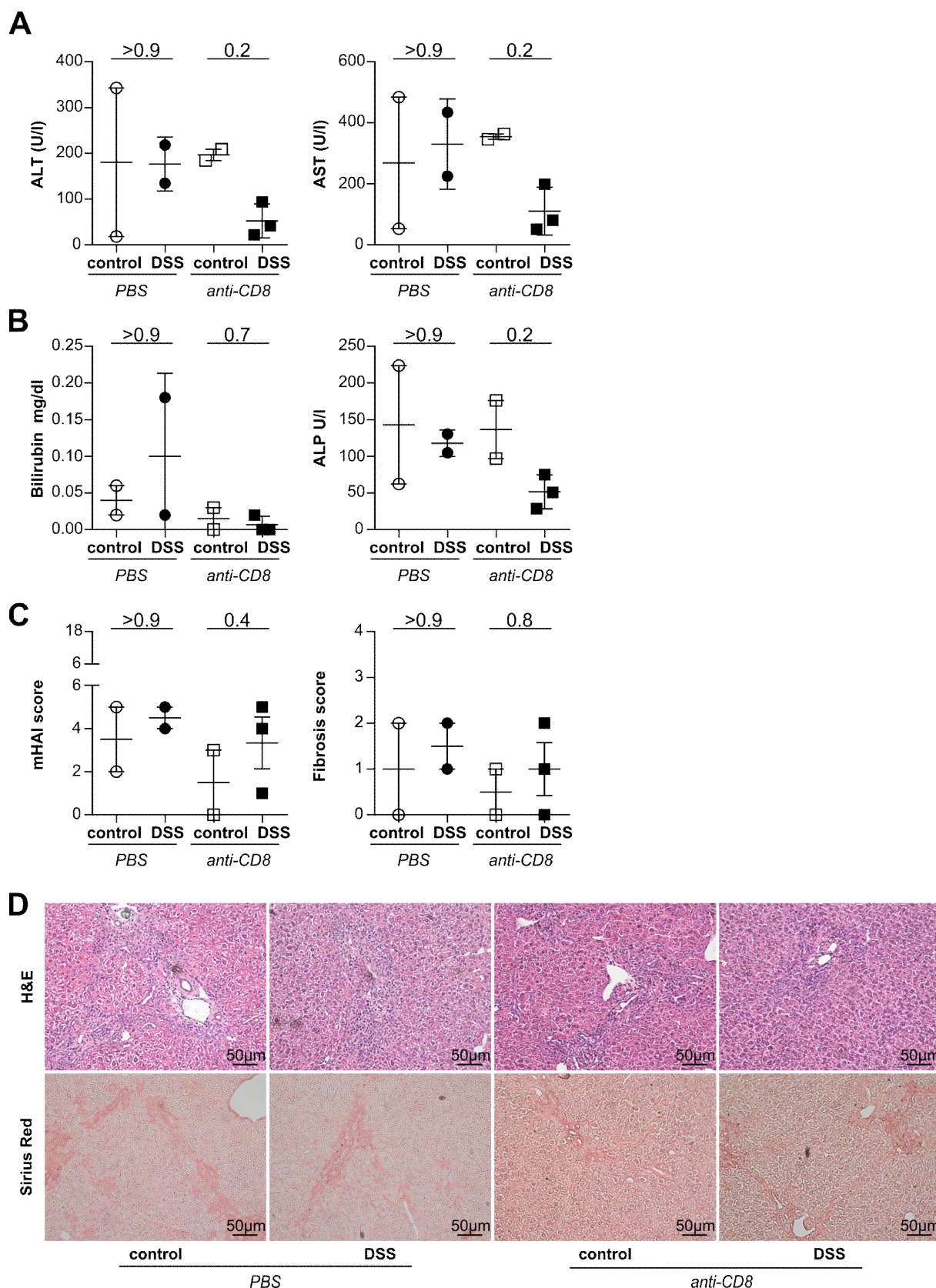


Figure 16: Depletion of CD8⁺ T cells in *Mdr2*-deficient mice during colitis induction results in reduced pathology of the liver.

A) To determine the inflammation of the liver, the ALT and AST levels as well as **(B)** bilirubin and ALP levels were measured. **(C)** Liver sections were stained for H&E and Sirius red to analyze the mHAI and Fibrosis score of the livers. **(D)** Representative histological liver sections are shown. Shown are the data of one experiment. PBS control

n=2, PBS DSS n=2, anti-CD8 control n=2, anti-CD8 DSS n=3. For statistical analysis, Mann-Whitney U test was performed ($p \leq 0.05$). Lines indicate mean \pm SEM.

5.1.5.2 Role of CD4⁺Foxp3⁺ regulatory T cells in the protective effect

Previous experiments from our lab had already shown that general CD4⁺ T-cell depletion did not reduce experimental PSC severity upon DSS colitis induction in *Mdr2*-deficient mice (123). Although Treg were also depleted, it might be still possible that Treg are involved via CD8⁺ T-cell suppression (134, 135), innate immune cell maturation (136-138), antigen presentation (139) and suppression of B cells (140, 141), and this effect may be mitigated by the absence of effector CD4⁺ T cells upon CD4⁺ T-cell depletion.

Thus, to test selectively the role of Foxp3⁺ Treg in the protective effect of colitis on PSC development, *DEREG* mice were used, a mouse model in which Foxp3⁺ Treg can be depleted by injection of diphtheria toxin (DTX) (142). These mice were crossed with *Mdr2*-deficient mice. An acute DSS colitis was induced in these mice and the Treg were depleted by i.p. injection of DTX every three days starting at day -1, as shown in Figure 17A.

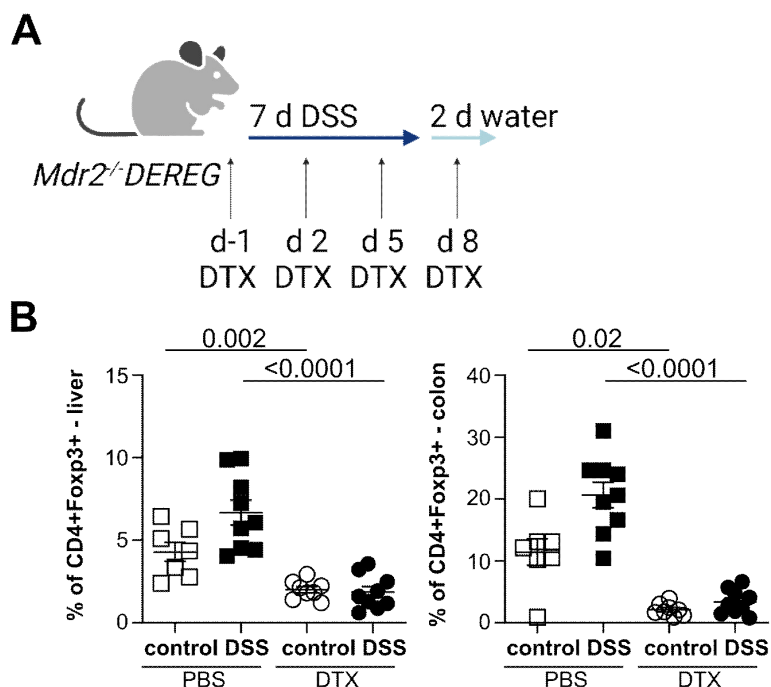


Figure 17: Depletion of Foxp3⁺ Treg in *Mdr2*^{-/-}*DEREG* mice during acute DSS colitis.

A) An acute 3% DSS colitis was induced in *Mdr2*^{-/-}*DEREG* mice and Foxp3⁺ Treg were depleted by injection of diphtheria toxin (DTX). **B)** CD4⁺Foxp3⁺ Treg cells were analyzed in the liver and colon to confirm sufficient depletion of these cells. Shown are the data of seven independent experiments. PBS control n=5, PBS DSS n=12, DTX control n=5, DTX DSS n=13. For statistical analysis, Mann-Whitney U test was performed ($p \leq 0.05$). Lines indicate mean \pm SEM.

Lymphocytes were isolated from the liver and the colon to confirm the successful depletion of Foxp3⁺ Treg. As shown in Figure 17B, a significant depletion was shown in the liver in both DTX treated groups. Only a tendency of reduction of Foxp3⁺ Treg was detectable in the colon in the DTX treated group. A significant decrease was found for Foxp3⁺ Treg in the colon of DSS+DTX treated mice in comparison to the DSS group. To check the severity of colitis induction, the weight loss of day 9 relative to the initial weight, the endoscopic colitis score of day 8, and the colon length of day 9 were determined (Figure 18A). Significant changes in both DSS treated groups were found in comparison to the controls without colitis. The mice lost more weight relative to the initial weight, developed a higher endoscopic colitis score and displayed shortening of the colon, confirming a successful colitis induction.

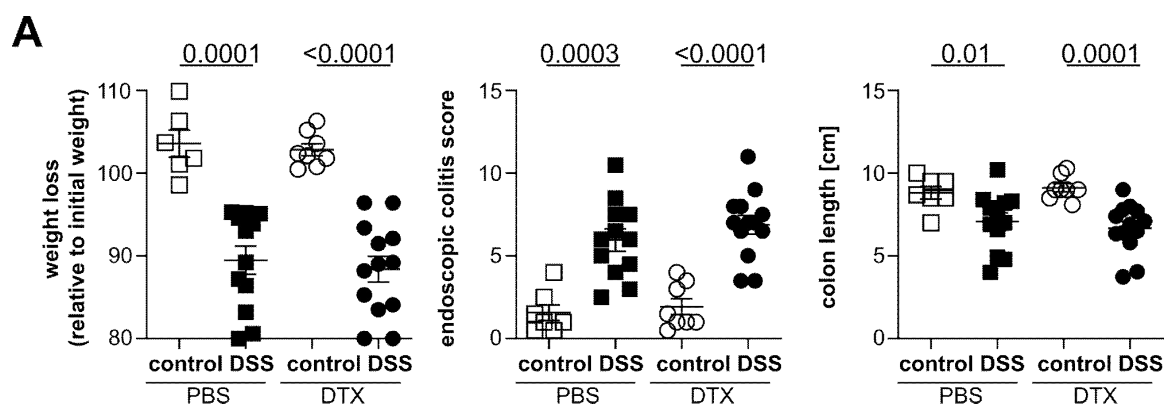


Figure 18: Induction of acute DSS colitis in *Mdr2*^{-/-}DEREG mice.

A) As disease readout for colitis development the weight loss, endoscopic colitis score and colon length were analyzed. Shown are the data of seven independent experiments. PBS control n=5, PBS DSS n=12, DTX control n=5, DTX DSS n=13. For statistical analysis, Mann-Whitney *U* test was performed ($p \leq 0.05$). Lines indicate mean \pm SEM.

Next, concomitant liver pathology was assessed in these mice. Therefore, the blood serum was analyzed for ALT, AST, bilirubin and ALP levels as markers to determine the pathology in the liver. As shown in Figure 19A, significant decreased ALT and AST levels were found in the two DSS treated groups compared to the two control groups without DSS. The reduction in bilirubin levels was only significant in the DSS+DTX group compared to the DTX group (Figure 19B). The levels of bilirubin in the control and DSS treated group were similar. A significant decrease of ALP levels in the DSS treated groups compared to the control groups were also seen (Figure 19B).

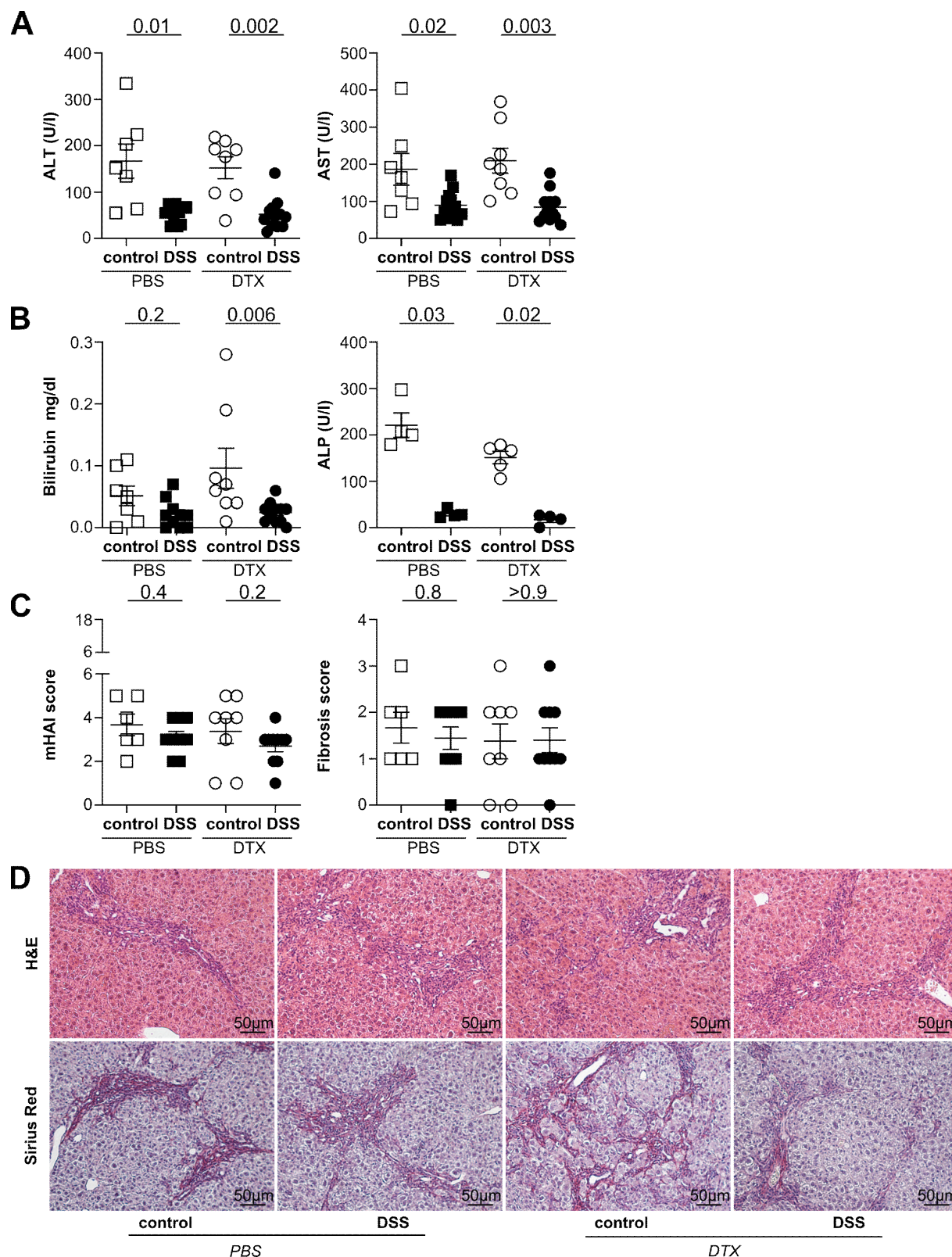


Figure 19: Depletion of Foxp3⁺ Treg in *Mdr2*-deficient mice did not change the observed protective effect after induction of acute DSS colitis.

A) To determine the pathology of the liver the ALT, AST **(B)** bilirubin and ALP levels were measured. **C)** Liver sections were stained for H&E and Sirius red to analyze the mHAI and Fibrosis score of the livers. **D)** Representative histological liver sections are shown. Shown are the data of seven independent experiments. PBS control n=5, PBS DSS n=12, DTX control n=5, DTX DSS n=13. For statistical analysis, Mann-Whitney *U* test was performed ($p \leq 0.05$). Lines indicate mean \pm SEM.

In order to histologically analyze liver pathology, sections of the liver were stained with H&E and Sirius red staining to define the mHAI and Fibrosis score. As shown in Figure 19C and the representative liver sections in Figure 19D, no significant changes were detectable in the liver histology in between the groups.

In summary, no significant impact of Foxp3⁺ Treg was detected in the protective effect of colitis on PSC development in the *Mdr2*^{-/-}*DEREG* mouse model. After depletion of Foxp3⁺ Treg and induction of DSS colitis, the protective effect in the liver pathology was still detectable as assessed by measurement of ALT, AST, bilirubin and ALP levels. In conclusion these data showed, that Foxp3⁺ Treg do not mediate the protective effect of colitis on PSC development.

5.1.5.3 B cells might be one major player in the protection of colitis on liver pathology

It was published in 2018 that gut and liver B cells of a common clonal origin were found in the gut and liver of patients with PSC- associated IBD (87). This finding supports the concept that lymphocytes of same antigen specificities circulate within the gut-liver axis. Therefore, B cells could be an important player in the observed protection of IBD on PSC development.

To test the role of B cells in the protective effect, B cells were depleted using an anti-CD20 antibody in *Mdr2*-deficient mice and a chronic DSS colitis was induced in these mice. The experimental plan is shown in Figure 20A. The mice were injected with anti-CD20 mAb or IgG control on two consecutive days before the induction of chronic DSS colitis. On day 26 and day 27 of chronic DSS colitis, the mice were injected again with anti-CD20 mAb or IgG control. Lymphocytes were isolated from the spleen, the liver and the colon to check the depletion of B cells in the tissue. Therefore, CD19⁺B220⁺ B cells were stained. As shown in Figure 20B, a reduction of B cells in the spleen, liver and colon was found. The induction of the DSS colitis was verified by weight loss on day 51, the endoscopic colitis score on day 50 and the shortening of the colon on day 51 of the experiment, as shown in Figure 20C. Even if the mice did not lose weight, the colitis development was confirmed by endoscopic colitis score and shortening of the colon.

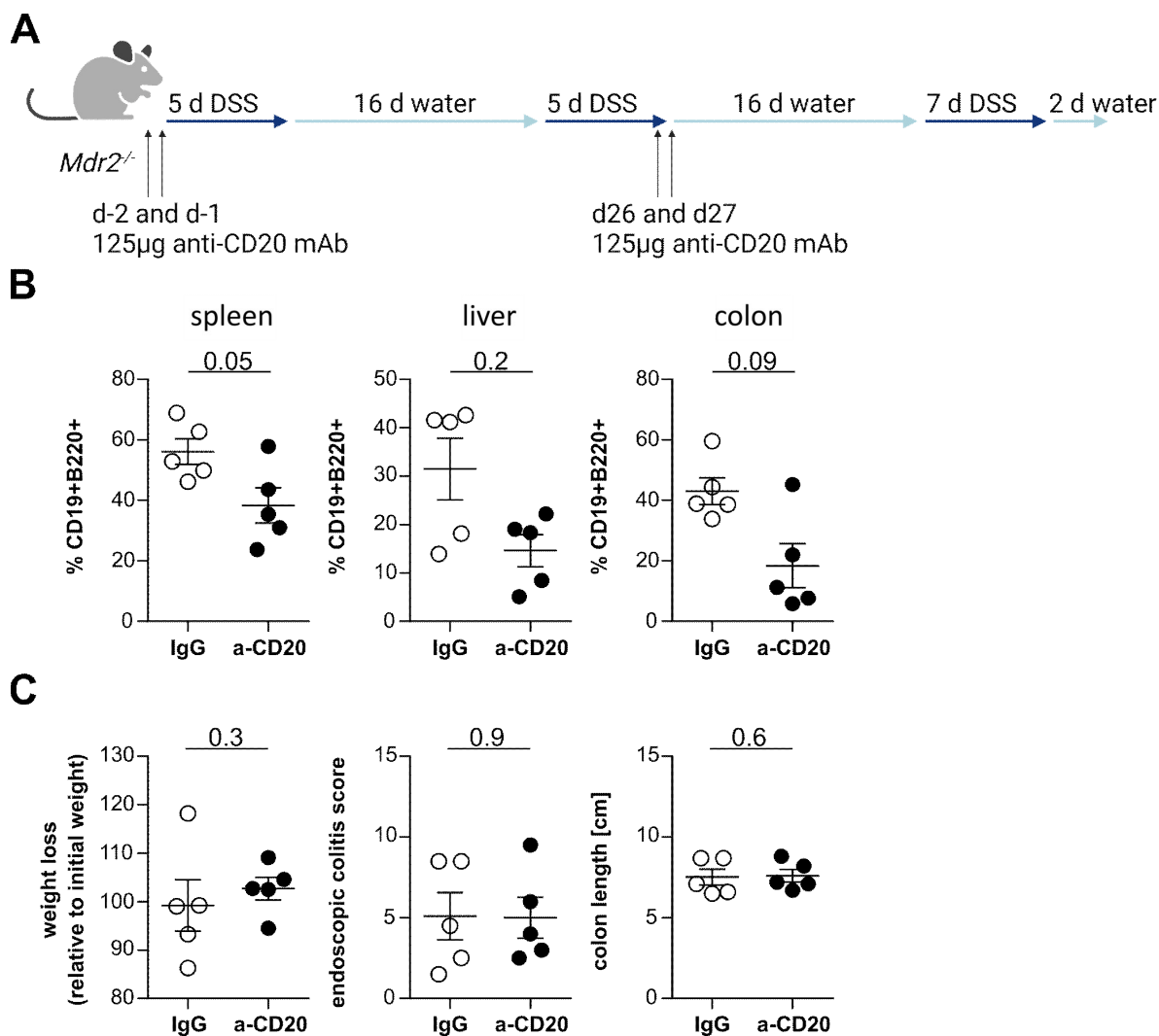


Figure 20: Depletion of B cells using an anti-CD20 antibody in *Mdr2*-deficient mice during chronic DSS colitis. **A)** B cells were depleted in 12 week old *Mdr2*-deficient mice using an anti-CD20 antibody. At day -1 and day 0 of the DSS colitis 125µg antibody were injected i.v., controls were injected with IgG control. At day 26 and 27 of the DSS colitis the injections were repeated. A chronic 2.5% DSS colitis was induced in the mice. **B)** Lymphocytes were isolated from the spleen, liver and colon to analyze the frequency of CD19⁺B220⁺ B cells. **C)** To verify the colitis severity the weight loss, endoscopic colitis score and colon length were analyzed. Shown are the data of two independent experiments. IgG n=5, anti-CD20 n=5. For statistical analysis, Mann-Whitney *U* test was performed ($p < 0.05$). Lines indicate mean \pm SEM.

Next, the pathology of the liver was determined. It was analyzed by measurement of the ALT, AST, bilirubin, and ALP levels in the blood serum, as well as liver histology. A strong increase in liver pathology by ALT, AST and ALP levels was found, in the group with depleted B cells (Figure 21A). To further investigate the pathology of the liver, histological liver sections were stained for H&E and Sirius red staining to determine the mHAI and Fibrosis histology score. As shown in Figure 21B, the mHAI score was comparable between the control group and the group with depleted B cells, while a mild increase in Fibrosis is detectable in the mice with

depleted B cells compared to controls. This is also shown in the representative histological liver sections in Figure 21C.

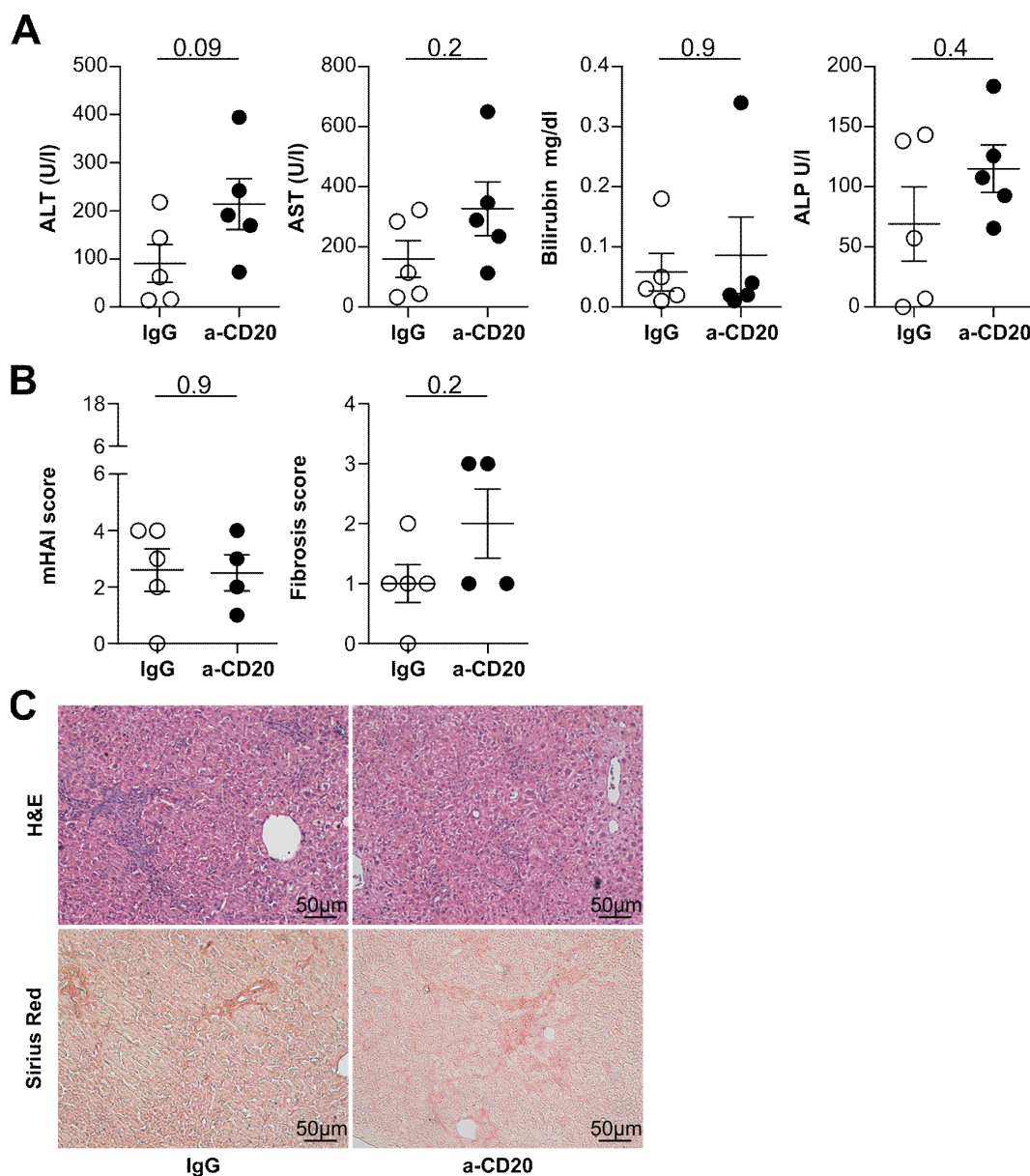


Figure 21: Depletion of B cells in *Mdr2*-deficient mice impairs the protection in liver pathology during DSS colitis.

A) Blood serum was analyzed for ALT, AST, bilirubin, and ALP levels to determine the pathology of the liver. **B)** Liver sections were stained for H&E and Sirius red to analyze the mHAI and Fibrosis score of the livers. **C)** Representative histological liver sections are shown. Shown are the data of two independent experiments. IgG n=5, anti-CD20 n=5. For statistical analysis, Mann-Whitney *U* test was performed ($p < 0.05$). Lines indicate mean \pm SEM

Overall no protection was found in the liver pathology after induction of colitis in an experimental mouse model for PSC when B cells were depleted. These data suggested an important role of B cells in the protective effect of colitis on PSC development in a mouse model.

5.2 Role of an *Il2ra*^{SNP} in disease development of PSC

Genetic factors are another risk factor of developing PSC, as siblings of PSC patients have an enhanced risk of developing PSC (91). Different genome wide association studies (GWAS) found single nucleotide polymorphisms (SNPs) in the *IL2RA* gene to be associated with PSC and IBD (94, 95, 106). Therefore, the second aim of this project was to investigate the role of the rs61839660 SNP in the *IL2RA* gene, known from human patients, in a mouse model of sclerosing cholangitis. This SNP is one of the most common ones and has an analog in the mouse.

5.2.1 Generation of *Il2ra*^{SNP} mice

To investigate the role of the rs61839660 SNP, an *Il2ra*^{SNP} mouse model was generated using CRISPR-Cas9 technology. The SNP, known from human to be associated with PSC and IBD, was inserted into the genome of *Mdr2*-deficient mice, as shown in Figure 22A. The *Mdr2*^{-/-}*Il2ra*^{SNP} (here called *Mdr2*^{-/-}*Il2ra*^{SNP_HH}) mouse line was generated by Irm Hermans-Borgmeyer (Transgenic mouse core facility, UKE). At the same time, Simeonov *et al.* described a discovery platform that could identify stimulus-responsive enhancers for a target gene, independent of stimulus exposure. Therefore, they focused on two key autoimmunity risk loci, one of which was the *IL2RA*. They used their own engineered mouse model of the same SNP, the *Il2ra*^{SNP} (here called *Il2ra*^{SNP_Mson}), and found that sequence perturbation of the disease-associated *Il2ra* enhancer did not entirely block *Il2ra* expression, but rather delayed the timing of gene activation in response to specific extracellular signals (109). Professor Marson's group generously provided us with the mice. For the purpose of experimentation, they were crossed to the *Mdr2*-deficient background.

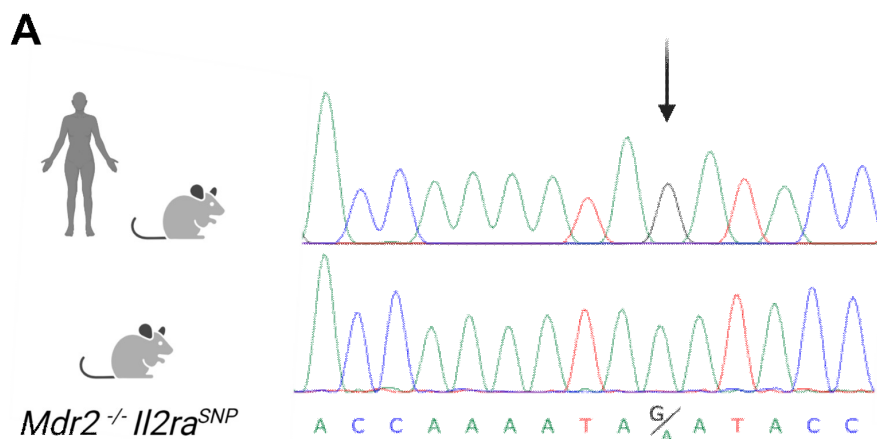


Figure 22: Generation of a mouse model with an *Il2ra*^{SNP}.

A) The rs61839660 SNP is located in the first intron of the *IL2RA* gene. This area is homologous between the human and the mouse. Therefore, it was possible to modify the known SNP from human into the mouse genome (marked with the black arrow). The SNP was generated using CRISPR-Cas9 technology, directly into the *Mdr2*^{-/-} background, to generate the *Mdr2*^{-/-} *Il2ra*^{SNP} mouse line.

5.2.2 *Il2ra*^{SNP} ex vivo Treg show a reduced suppressive capacity *in vitro*

Signaling through the IL-2R contributes to T-cell tolerance by controlling three important aspects of Treg. IL-2 is essential for thymic Treg development and regulates Treg homeostasis and suppressive function (143). Therefore, to investigate if the *Il2ra*^{SNP} impairs the suppressive capacity of the Foxp3⁺ Treg, an *in vitro* suppression assay was performed. The *Il2ra*^{SNP-HH} mice were crossed with the *Foxp3*^{mRFP} *Il10*^{eGFP} *IFNg*^{Katuschka} reporter mouse. Foxp3⁺ Treg were isolated from this mouse and the suppressive capacity was tested in a T-cell proliferation model. For this purpose, CD4⁺ T cells were activated to proliferate with addition of APCs and anti-CD3/28 mAb to the culture. *Il2ra*^{wt} or *Il2ra*^{SNP} Treg were added to the culture and the capacity to suppress the proliferation of the T cells was measured.

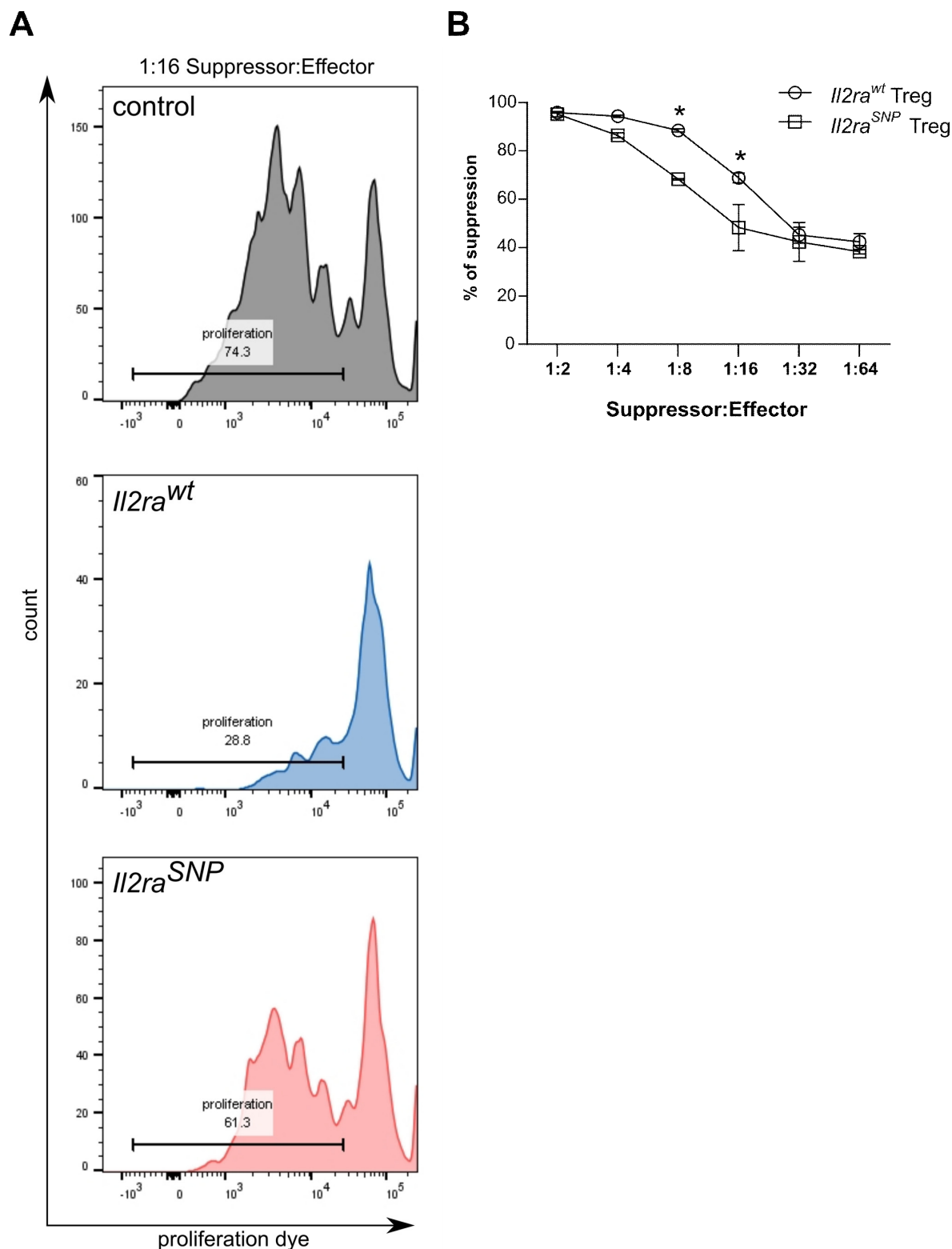


Figure 23: *Il2ra^{SNP}* ex vivo isolated Treg show a reduced suppressive capacity in vitro.

An *in vitro* suppression assay was performed comparing the suppressive capacity of *Il2ra^{SNP}* and *Il2ra^{wt}* Treg. **A)** Representative histograms for the three conditions: control, without Treg, *Il2ra^{wt}* Treg and *Il2ra^{SNP}* Treg. **B)** The frequency of suppression is depicted. Shown are the data of one experiment with technical duplicates. The same trend was repeated in a second experiment. For statistical analysis a multiple t test was performed ($*\leq 0.05$). Lines indicate mean \pm SEM. The frequency of proliferated cells was measured using the violet proliferation dye. With the percentage of proliferated cells, the frequency of suppressed cells was calculated.

Depicted in Figure 23A are representative histograms of the proliferation of the different conditions. The proliferation of CD4⁺ T cells without Foxp3⁺ Treg, CD4⁺ T cells with *Il2ra*^{wt} Treg and CD4⁺ T cells with *Il2ra*^{SNP} Treg were analyzed. The control CD4⁺ T cells without Treg proliferated most. The addition of *Il2ra*^{wt} Treg to the culture resulted in a strong suppression and the CD4⁺ T cell proliferation. In comparison to the *Il2ra*^{wt} culture, a higher proliferation was shown in the culture where *Il2ra*^{SNP} Treg were added, showing a reduced suppressive capacity of the *Il2ra*^{SNP} Treg. In Figure 23B, the frequency of suppression for the *Il2ra*^{wt} in comparison to the *Il2ra*^{SNP} Treg is shown. The *Il2ra*^{SNP} Treg showed a significantly reduced suppressive capacity in the 1:8 and 1:16 ratios to the effector cells. In summary, a significant decreased suppressive capacity of *Il2ra*^{SNP} Treg in comparison to *Il2ra*^{wt} Treg was found.

5.2.3 Characterization of *Il2ra*^{SNP} mice (comparison HH vs. Marson)

The *Mdr2*^{-/-}*Il2ra*^{SNP_HH} and *Mdr2*^{-/-}*Il2ra*^{SNP_Mson} mice were compared *in vivo* starting at 6 weeks of age, until 12 weeks of age, with respect to pathology in the liver. The mice were examined endoscopically between 8-12 weeks to analyze the inflammation in the colon. Shown on the left side of Figure 24, in red, are the *Mdr2*^{-/-}*Il2ra*^{SNP_HH} mice, and on the right side of the Figure 24, in yellow, are the *Mdr2*^{-/-}*Il2ra*^{SNP_Mson} mice (Figure 24A). The endoscopic score of the mice was determined starting with 8 weeks of age to investigate a possible role of the *Il2ra*^{SNP} on spontaneous inflammation in the colon. As shown in Figure 24B and C, neither the *Mdr2*^{-/-}*Il2ra*^{SNP_HH} mice nor the *Mdr2*^{-/-}*Il2ra*^{SNP_Mson} mice develop spontaneous colitis between 8 and 12 weeks of age. Blood was drawn from the mice once a week, starting at 6 weeks of age until 12 weeks of age, to measure liver transaminases and determine the pathology of the liver. Overall, the ALT and AST levels were quite variable between 6 and 12 weeks of age between the mice (Figure 24D-G). No significant differences in ALT levels, were detectable between the *Mdr2*^{-/-}*Il2ra*^{SNP} and the *Mdr2*^{-/-}*Il2ra*^{wt} mice for the HH mice as well as the Marson mice (Figure 24D-E). The same was found for the AST levels as shown in Figure 24F-G.

In summary no impact of the *Il2ra*^{SNP} in the early disease development of *Mdr2*-deficient mice was found. The ALT and AST levels, as markers of liver pathology, were similar over time. There were also no detectable changes between the two different mouse models for the *Il2ra*^{SNP} found.

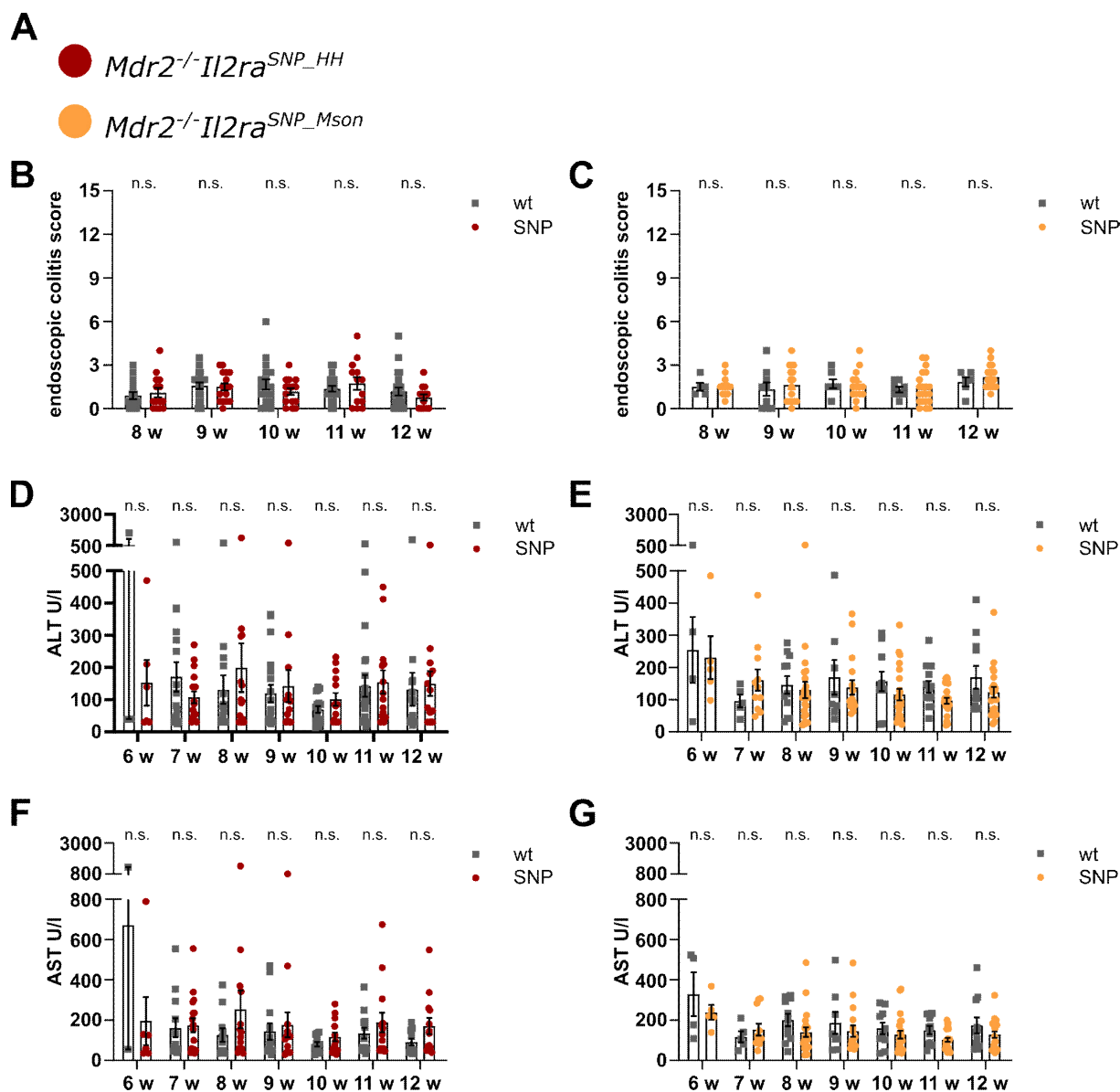


Figure 24: Characterization of the *Mdr2*^{-/-}*Il2ra*^{SNP_HH} mice in comparison to the *Mdr2*^{-/-}*Il2ra*^{SNP_Mson} mice.

A) In red and on the left side of the figure is the steady state characterization of the *Mdr2*^{-/-}*Il2ra*^{SNP_HH} mice shown, compared to the *Mdr2*^{-/-}*Il2ra*^{SNP_Mson} mice in yellow on the right side. **B-C)** To determine any inflammation of the colon of the mice, endoscopy of the colon was performed once a week. To investigate the pathology of the liver the ALT (**D-E**) and AST (**F-G**) blood serum levels were measured. *Mdr2*^{-/-}*Il2ra*^{wt_HH} 6w n=3, 7w n=18, 8w n=15, 9w n=19, 10w n=17, 11w n=22, 12w n=18, *Mdr2*^{-/-}*Il2ra*^{SNP_HH} 6w n=6, 7w n=17, 8w n=14, 9w n=13, 10w n=14, 11w n=14, 12w n=13. *Mdr2*^{-/-}*Il2ra*^{wt_Mson} 6w n=4, 7w n=5, 8w n=11, 9w n=8, 10w n=10, 11w n=13, 12w n=11, *Mdr2*^{-/-}*Il2ra*^{SNP_Mson} 6w n=5, 7w n=11, 8w n=21, 9w n=17, 10w n=22, 11w n=24, 12w n=23. For statistical analysis, Mann-Whitney *U* test was performed ($p \leq 0.05$). Lines indicate mean \pm SEM.

5.2.4 *Il2ra*^{SNP} mice develop more severe sclerosing cholangitis compared to *Il2ra*^{wt} mice in a chronic state of disease

No differences in the disease development of sclerosing cholangitis, with and without the *Il2ra*^{SNP} between 6 and 12 weeks of age, were detectable in *Mdr2*-deficient mice. But an impairment of the suppressive capacity of *Il2ra*^{SNP} Foxp3⁺ Treg *in vitro* was found. *Mdr2*-deficient mice develop an acute liver pathology from birth on, which transitions into a chronic disease around 12 weeks of age (111, 112). Therefore, a more chronic time point was analyzed. The *Mdr2*^{-/-}*Il2ra*^{SNP-HH} mice were sacrificed with 14 weeks of age and the pathology of the colon and the liver were analyzed. Immune cells were isolated from the liver and stained for T-cell subsets.

As shown in Figure 25A, no sign of inflammation was detectable in the colon of 14-week-old *Mdr2*^{-/-}*Il2ra*^{SNP-HH} mice. The inflammation in the colon was measured by endoscopic colitis score and shortening of the colon length. The pathology in the liver was measured by ALT and AST levels in the blood serum and liver histology. As shown in Figure 25B, at 14 weeks of age, a significant increase in ALT and AST levels in the *Mdr2*^{-/-}*Il2ra*^{SNP} mice was found in comparison to *Mdr2*^{-/-}*Il2ra*^{wt} littermates. Liver sections were taken and stained for H&E and Sirius Red to analyze the mHAI and Fibrosis score of the liver, to investigate the liver histologically. An increased mHAI and Fibrosis score in the livers of *Mdr2*^{-/-}*Il2ra*^{SNP-HH} mice compared to the *Mdr2*^{-/-}*Il2ra*^{wt} littermates was detected by trend (Figure 25C). The differences are also shown in the representative pictures in Figure 25D.

Binding of IL-2 to the IL-2R is crucial for the functionality of activated CD4⁺ T cells and Foxp3⁺ Treg cells. Therefore, lymphocytes were isolated from the livers of the mice and the frequency and number of Th1, Th17 and Treg cells were analyzed. Therefore, cells were stained for IFN γ ⁺ Th1 cells, IL-17A⁺ Th17 cells and Foxp3⁺ Treg. As shown in Figure 26, no significant changes were found in frequency or number for IFN γ ⁺ Th1 cells (Figure 26A), IL-17A⁺ Th17 cells (Figure 26B) or Foxp3⁺ Treg cells in the *Mdr2*^{-/-}*Il2ra*^{SNP-HH} compared to *Mdr2*^{-/-}*Il2ra*^{wt} mice at 14 weeks of age.

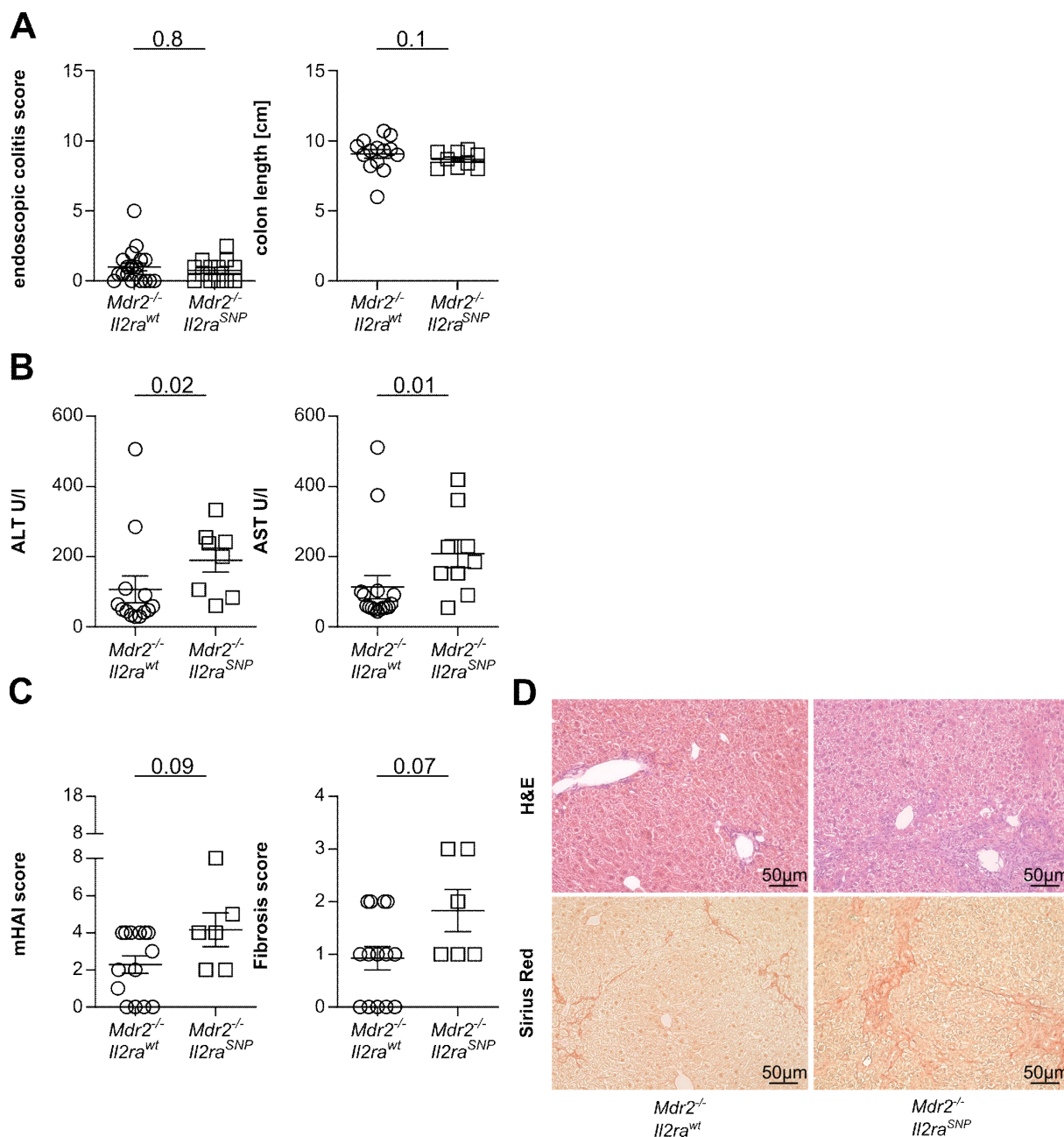


Figure 25: *Il2ra*^{SNP} mice developed more severe sclerosing cholangitis compared to *Il2ra*^{wt} mice with 14 weeks of age.

Mdr2^{-/-}*Il2ra*^{SNP_{HH}} mice and *Mdr2*^{-/-}*Il2ra*^{wt} littermates were analyzed. **A)** As disease readout for colitis development the endoscopic colitis score and the shortening of the colon were analyzed. **B)** The ALT and AST levels were analyzed with 14 weeks of age. **C)** Liver sections were stained for H&E and Sirius red to analyze the mHAI and Fibrosis score of the liver. **D)** Representative histological liver sections are shown. Shown are the data of three independent experiments. *Mdr2*^{-/-}*Il2ra*^{wt} n=13, *Mdr2*^{-/-}*Il2ra*^{SNP} n=8. For statistical analysis, Mann-Whitney *U* test was performed ($p < 0.05$). Lines indicate mean \pm SEM.

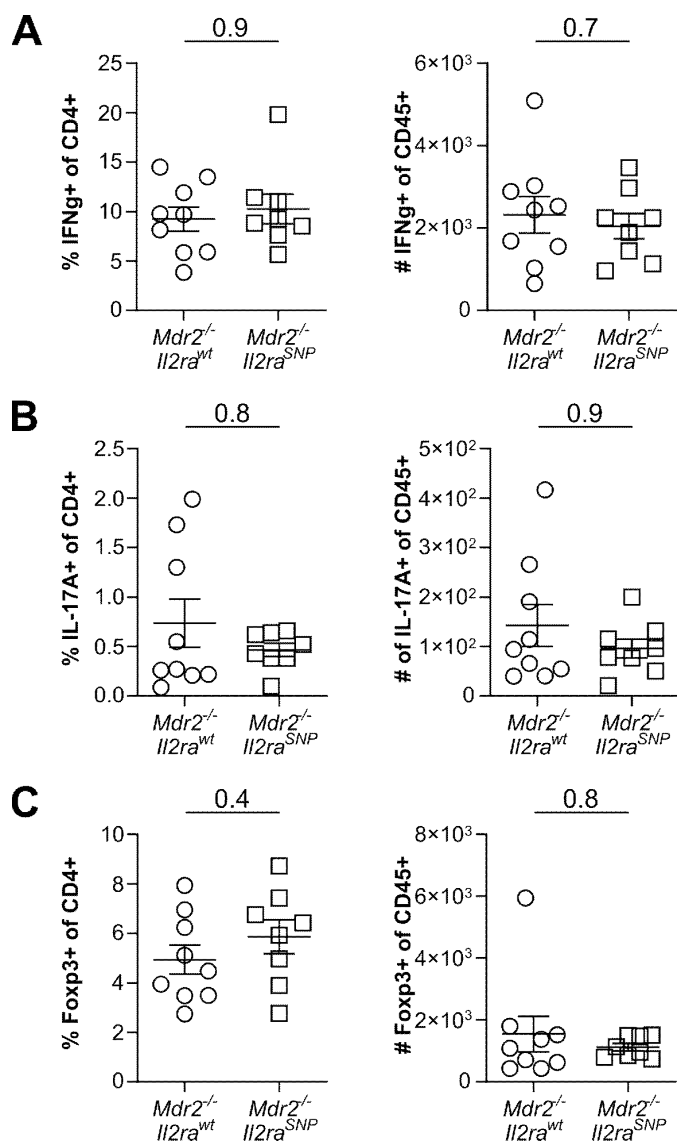


Figure 26: Analysis of CD4⁺ T cells in the livers of *Mdr2*^{-/-}/*Il2ra*^{SNP} mice.

Lymphocytes were isolated from the liver and stained for CD4⁺, IFNγ⁺, IL-17A⁺ and Foxp3⁺ T cells. **A)** The frequencies and numbers of IFNγ⁺ Th1 cells, **B)** the frequencies and numbers of IL-17A⁺ Th17 cells, and **C)** the frequencies and numbers of Foxp3⁺ Treg cells are shown. Shown are the data of three independent experiments. *Mdr2*^{-/-}/*Il2ra*^{wt} n=9, *Mdr2*^{-/-}/*Il2ra*^{SNP} n=8. For statistical analysis, Mann-Whitney *U* test was performed ($p \leq 0.05$). Lines indicate mean \pm SEM.

Taken together an increased disease development of sclerosing cholangitis measured by increased ALT and AST levels and increased liver histopathology was found in *Mdr2*^{-/-}/*Il2ra*^{SNP-HH} mice at 14 weeks of age compared to control. No changes in the frequency or number of Th1, Th17 or Treg cells in the liver of these mice were observed.

5.2.5 The *Il2ra*^{SNP} has no impact on the protective effect of colitis on PSC development in the model of acute DSS colitis

Since it was found that colitis has a protective effect on PSC development, the role of the *Il2ra*^{SNP} was investigated on this protective effect. Therefore, 12 week old *Mdr2*^{-/-}*Il2ra*^{SNP_HH} mice and *Mdr2*^{-/-}*Il2ra*^{wt} littermates were used. They were split into two groups and an acute DSS colitis was induced in one of the groups. The induction of colitis was measured by weight lost, endoscopic colitis score and colon length (Figure 27A). The groups that had received the DSS colitis lost significantly more weight, had an increased endoscopic colitis score and showed shortening of the colon compared to control groups, suggesting that the colitis induction was successful. Next, the liver pathology was analyzed through measurement of ALT and AST levels in the blood serum. When comparing the control groups, increased ALT and AST levels in *Mdr2*^{-/-}*Il2ra*^{SNP_HH} mice were found, as described in 5.2.4 The *Mdr2*^{-/-}*Il2ra*^{wt} group showed the protection between the control and the DSS treated group in ALT and AST levels as markers of liver pathology only in a very mild trend (Figure 27B). In the *Mdr2*^{-/-}*Il2ra*^{SNP} mice, a significant decrease in the ALT levels was seen and a trend was visible in the AST levels (Figure 27B). To further investigate the protective effect, liver sections were taken and stained for H&E and Sirius Red. The mHAI and Fibrosis score of the livers were analyzed. No differences in the liver pathology were found by mHAI or Fibrosis score in all four groups (Figure 27C-D).

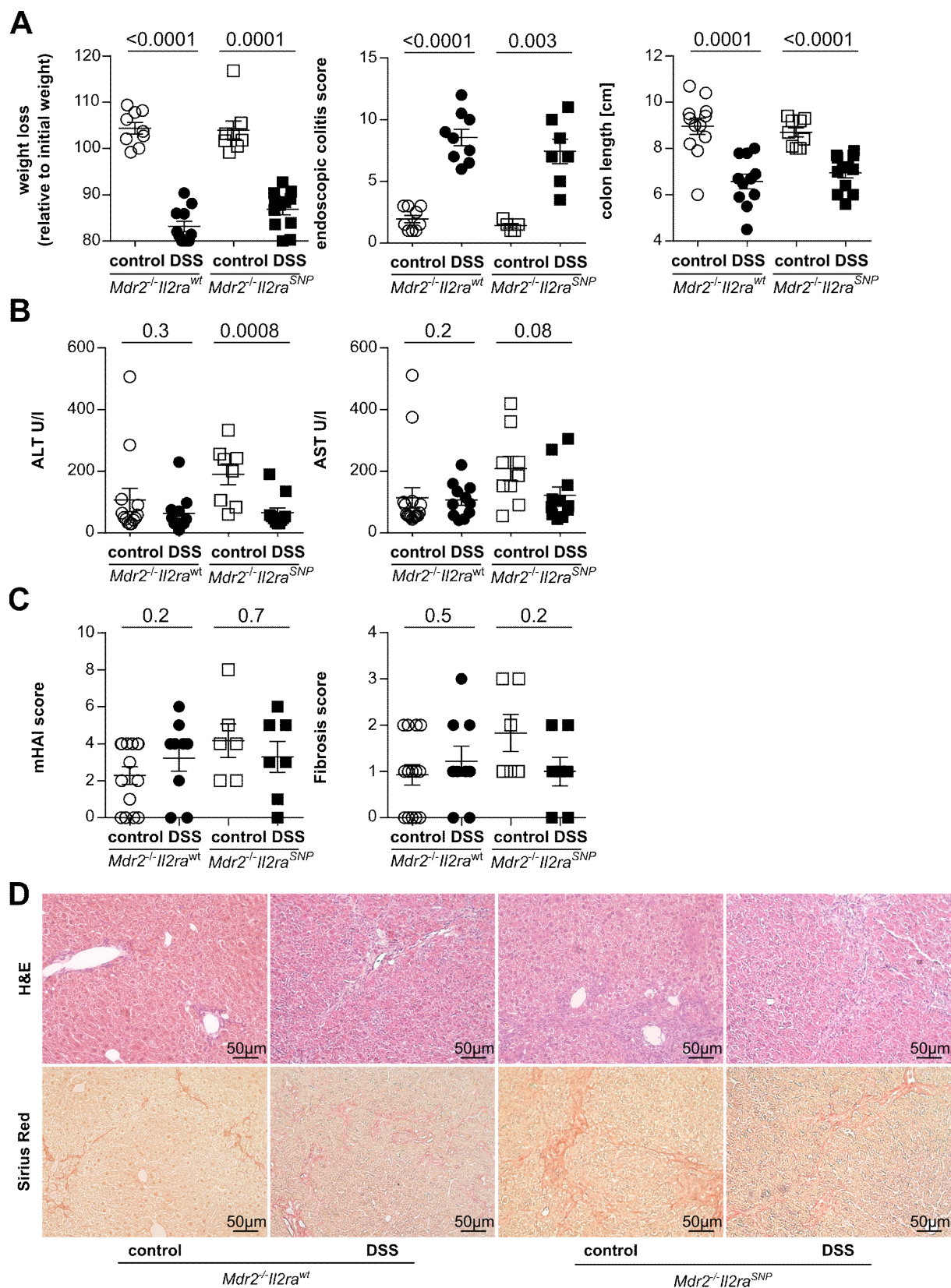


Figure 27: Induction of acute DSS colitis in $Mdr2^{-/-}Il2ra^{SNP}$ mice and $Mdr2^{-/-}Il2ra^{wt}$ littermates.

A) As disease readout for colitis development the weight loss, endoscopic colitis score and colon length were analyzed. **B)** To determine the pathology of the liver the ALT and AST levels were measured. **C)** Liver sections were stained for H&E and Sirius red to analyze the mHAI and Fibrosis score of the livers. **D)** Representative histological liver sections are shown. Shown are the data of five independent experiments. $Mdr2^{-/-}Il2ra^{wt}$

control=13, *Mdr2*^{-/-}*Il2ra*^{wt} DSS=11, *Mdr2*^{-/-}*Il2ra*^{SNP} control=8, *Mdr2*^{-/-}*Il2ra*^{SNP} DSS=11. For statistical analysis, Mann-Whitney *U* test was performed ($p \leq 0.05$). Lines indicate mean \pm SEM.

Taken together, no evidence was found, indicating that the *Il2ra*^{SNP} played a role in the protective effect of colitis on PSC development. Even with the *Il2ra*^{SNP} resulting in an increased disease severity of sclerosing cholangitis, the protection in PSC development during colitis was still observable.

6 Discussion

Primary sclerosing cholangitis (PSC) is a chronic cholestatic disease of the intra- and extra-hepatic bile ducts, which commonly leads to end-stage liver disease (144). The pathogenesis of PSC is not fully understood and liver transplantation is the only curative treatment option, whereas at least 25 % of patients develop recurrent disease afterwards (8). Two potential factors impacting PSC are concomitant inflammatory bowel disease (IBD) and genetic polymorphisms.

The first aim of this study was to understand the strong association of PSC development with colitis. To this end, two mouse models of sclerosing cholangitis (*Mdr2*^{-/-}, DDC) and two models of colitis induction (DSS, *Citrobacter rodentium* infection) were analyzed. Furthermore, attempts were made to identify the mechanism underlying the protective effect of colitis on PSC development. A possible role of the intestinal microbiota, the bile acid composition and different immune cell subsets, was investigated. All three of these were suggested to play an important role in the disease development of PSC (9, 29, 145), as well as IBD (66, 129). A possible interaction of these subsets was also described (45, 52, 80, 131, 132).

The second goal of this project focused on the role of single nucleotide polymorphisms (SNPs) in the *IL2RA* gene. Genome wide association studies (GWAS) found SNPs in the *IL2RA* gene to be associated with PSC and IBD (94, 95, 106). The role of the rs61839660 *Il2ra* SNP was investigated in the disease development of PSC in an experimental mouse model. In addition, changes in the interaction of colitis and PSC were investigated in the presence of the *Il2ra* SNP in mice.

6.1 Colitis protects against PSC in different experimental mouse models

PSC and IBD are highly associated. Around 50-80 % of PSC patients have a concomitant IBD (21). Until now it is still not understood, how these two diseases affect each other. The first aim of the study was to investigate the effects of colitis on PSC development. Therefore, two different models of colitis were investigated in two different models of sclerosing cholangitis in mice.

The *Mdr2*^{-/-} (*Abcb4*) mouse model is a well-established experimental mouse model for PSC. The knock-out of the *Mdr2* gene leads to a defect in phosphoflippase, which actively transports phospholipid from the liver into the bile ducts. Impairment leads to insufficient solution of the bile acids. High concentrations of bile acids induce a toxic effect on the bile duct epithelium, resulting in chronic inflammation around the bile ducts, resembling the PSC phenotype. The liver pathology starts with birth and is characterized in the first weeks of life by acute hepatitis-like inflammation. The disease develops between 12-14 weeks of age into a chronic inflammation characterized by fibrosis (61, 111, 112). As a second model for sclerosing cholangitis, the chemical 3,5-diethoxycarbonyl-1,4-dihydrocollidine (DDC)-induced liver pathology was tested. DDC is a porphyrinogenic hepatotoxin. Feeding it to mice leads to the formation of porphyrin crystals in the hepatocytes and porphyrin plugs in the bile ducts, leading to increased concentrations of bile acids and chronic inflammation similar to what is seen in PSC patients (113-115).

Dextran sulfate sodium (DSS) is a chemically induced model for acute or chronic colitis in mice. Damage to the epithelial cells in the large intestine allows the dissemination of bacteria and their metabolites into underlying tissue, resulting in an inflammatory response (116, 118). As a second model for colitis induction, the *Citrobacter rodentium* infection model was used. Infection with the mouse-restricted pathogen results in crypt hyperplasia, loss of goblet cells, and an accumulation of undifferentiated colonocytes at the luminal surface, leading to inflammation (119, 121, 122).

In line with previous work carried out in our lab (123), a protective effect of colitis on sclerosing cholangitis was detected in different experiments. Indeed, preliminary data from our lab showed, that induction of DSS colitis in 6-8 week old mice decreased transaminases in the blood serum, but no differences in the liver histology were detectable. In 12-14 week old *Mdr2*-deficient mice decreased transaminases in the blood serum, and also decreased liver histology and fibrosis were found (123). I further tested this protective effect of colitis on sclerosing cholangitis in two different mouse models of PSC and colitis. Furthermore, the mechanism mediating this effect was not previously identified, therefore, I aimed to study this as a part of this project.

By induction of chronic DSS colitis in 24-week-old *Mdr2*-deficient mice, I tested whether this protective effect was further increased in the chronic phase of disease. The results showed decreased transaminases compared to controls without colitis, but no differences in liver histology were detectable.

Together with previous data (123), my data suggests that the protective effect of colitis on PSC development could be age-dependent in *Mdr2*-deficient mice. Since the liver pathology in *Mdr2*-deficient mice changes with age, it is likely that the severity and stage of the sclerosing cholangitis is important in the protective effect seen. *Mdr2*-deficient mice already develop liver pathology directly after birth. In the first weeks of life, it is characterized by acute, hepatitis-like inflammation. Between 12-14 weeks of age, the mice transition into a chronic phase of disease, characterized by fibrosis (111, 112). The previous generated data suggested, that in the early phase of disease, in 6-8 week old *Mdr2*-deficient mice, the protective effect was observed mainly in the serum markers for liver pathology, also due to minor liver histopathology (123). Apart from this, I showed that in 24 week old *Mdr2*-deficient mice with advanced liver pathology and fibrosis, the protective effect did not affect the histology and fibrosis of the liver, but was only observable in serum markers for liver pathology. The biggest protective effect of colitis on sclerosing cholangitis development was detectable at the beginning of the chronic phase, before the liver fibrosis was too advanced already. Here, it was found that the induction of colitis reduced not only the transaminases but also the development of fibrosis (123, 146).

The same concept relates to the data of the DDC-induced liver pathology. DDC is a very acute model of liver pathology, and would be comparable to the 6-8 week old *Mdr2*-deficient mice. Accordingly, I showed here that induction of DDC-mediated sclerosing cholangitis upon DSS colitis, led to decreased liver transaminases in the group with colitis, compared to mice without colitis. No changes in the liver histology were detectable. The latter might be due to the overall low liver fibrosis in this model. The DDC was only fed for eight days, which led to an increased mHAI score, but this model was too short to induce fibrosis in the liver. To observe if the fibrosis can also be reduced in the DDC model, it would be interesting to induce the DDC-mediated liver pathology in a more chronic setting.

Next, the role of colitis was further evaluated using a second experimental model of intestinal inflammation, the infection with *C. rodentium*. In the data previously shown, the most protective effect was found in 12-14 week old *Mdr2*-deficient mice. Therefore, 12-14 week old *Mdr2*-deficient mice were infected with *C. rodentium*. A significant decrease in transaminases was found after *C. rodentium*-dependent colitis induction, but no changes in the liver histology or fibrosis were detectable. The infection with *C. rodentium* induced a very mild inflammation in the colon. In addition, the model was very short, compared to the chronic DSS colitis. It would be possible, that due to the short time of the inflammation in the colon, the colitis was not strong enough to have an impact on the liver histology and fibrosis, but only on the transaminases.

Taken together, these data suggest that colitis protects against liver pathology, as assessed by measurement of ALT and AST levels and through histological means. This could be dependent on the stage of liver pathology, since the protective effect was most effective in the beginning of the chronic phase and less so in young and aged *Mdr2*-deficient mice, and in mice with an acute DDC-induced liver pathology. It also might be dependent on the duration and intensity of the colitis. These data go hand-in-hand with preliminary human data collected in our lab. Fibroscan data, a liver stiffness measurement to quantify fibrosis, of PSC and PSC-IBD patients were analyzed. It was found that PSC-IBD patients have significant reduced liver fibrosis compared to PSC patients. The fibrosis was even further reduced in patients with active IBD, compared to patients with IBD in remission (*unpublished data*). These data represent the same trend found in the mouse data. Also in human patients, colitis reduced the severity of liver pathology in sclerosing cholangitis patients, and the protective effect was dependent on active inflammation in the colon.

6.2 An indirect effect of the microbiota by a change in the fecal bile acid composition, could play a role in the protection of colitis on PSC development

The frequent coexistence of PSC and IBD points to a potential role of the gut-liver axis in the protective effect of IBD on PSC development. Around 50-80 % of PSC patients have a concomitant IBD (21), suggesting that a damaged barrier integrity of the gut might play a role in PSC, yet its underlying mechanism remains unknown.

It was further characterized that if gut-derived bacteria which infiltrate the liver after colitis induction, ameliorate PSC development. Therefore, fecal microbiota transfer (FMT) of stool from mice fed with DDC upon DSS induction, or stool from mice only fed with DDC, was performed in germ-free wild type (wt) mice. After reconstitution, a DDC-mediated liver pathology was induced to test the protective capacity of the transferred microbiota. Mice with a DDC+DSS FMT developed a stronger liver pathology upon DDC induction, compared to the mice received a FMT with DDC fecal microbiota. This observation was verified by FMT from *Mdr2*-deficient mice with and without DSS colitis into germ-free wild type mice, and subsequent induction of a DDC-mediated liver pathology. Overall, these data show, that FMT of the different microbiota had an effect on the severity of the DDC-induced liver pathology. However, the protective effect of colitis on PSC development was not transferable via the fecal microbiota. In fact, the germ-free mice receiving a FMT from mice treated with DDC+DSS, were even more susceptible to DDC-induced liver pathology, compared to germ-free mice engrafted with fecal microbiota from DDC treated mice.

In line with these data, Nakamoto *et al.* found, that gnotobiotic mice with PSC/UC patient microbiota were more susceptible to DDC induced hepatobiliary damage, compared to gnotobiotic mice with fecal microbiota from healthy controls and germ-free mice. This process was, at least in part, mediated by *Klebsiella pneumoniae*, identified in the patients stool samples. *K. pneumoniae* disrupted the epithelial barrier to initiate bacterial translocation and liver inflammatory responses (29). Thus, the PSC/UC microbiota seems to promote PSC development and progression compared to healthy microbiota and germ-free mice. One caveat of this study was the missing comparison of the PSC microbiota.

In contrast to the data of Nakamoto *et al.*, a study by Tabibian *et al.*, who originally characterized germ-free *Mdr2*-deficient mice, demonstrated the importance of the commensal microbiota and associated metabolites in protecting against biliary injury. Primary bile acids (BAs) were similar, whereas secondary BAs were absent in germ-free mice compared to conventionally housed controls. Germ-free *Mdr2*-deficient mice showed exacerbated biochemical and histological features of PSC and increased cholangiocyte senescence, a characteristic and potential mediator of progressive biliary disease. Interestingly, cholangiocyte senescence was abrogated *in vitro* by ursodeoxycholic acid (UDCA) treatment

(147). These data support the notion that interaction between the microbiota and secondary bile acids (BAs) maybe involved in PSC pathology.

The function of BAs is closely associated with the fecal microbiota. Primary BAs metabolized in the liver are conjugated to taurine or glycine before they are transported into the bile ducts and secreted into the duodenum. For reabsorption in the terminal ileum, the BAs must be conjugated to taurine or glycine. Around 90-95 % of BAs are reabsorbed in the terminal ileum. The conjugation to taurine or glycine has a toxic effect on the fecal microbiota. Therefore, the bacteria have the capacity to deconjugate the 5-10 % of BAs which reach the colon, where they are metabolized into secondary bile acids by the fecal microbiota. Therefore, the microbiota can have an impact on changes in the bile acid metabolism.

Since it could not be excluded that BAs play a possible role in the protective effect of colitis on PSC development, BAs were measured in the serum and the caecum content of *Mdr2*-deficient mice, after induction of DSS colitis. Overall, significantly decreased unconjugated BAs were found in the caecum content of these mice. In total, twelve unconjugated BAs and associated metabolites were found to be significantly reduced after colitis. These included α - and ω MCA, DCA, HDCA and LCA, as well as the metabolites iso-LCA, iso-allo-LCA, 7-oxo-LCA, 12-oxo-DCA, isoDCA, 5-choIA and LCEA.

Interestingly, DCA, HDCA and LCA were also found in a recent publication that investigated the BA profiles in PSC patients and their ability to predict hepatic decompensation. Plasma BA profiling of PSC patients and healthy controls was performed. When comparing plasma BA composition of PSC patients with comorbid IBD relative to PSC patients without history or evidence of IBD, they found that patients with ulcerative colitis (UC) had significantly decreased fractions of DCA, HDCA and LCA. Whereas, patients with Crohn's Disease (CD) and intermediate IBD had an increased fraction of CDCA, relative to the no-IBD patients (145).

In addition, BAs have been shown to play a role in immune cell differentiation. Iso-allo-LCA a derivate of LCA, which was also significantly reduced after colitis induction in *Mdr2*-deficient mice, was recently described to increase the differentiation of Treg cells *in vitro* and *in vivo* through the production of mitochondrial reactive oxygen species (mitoROS), which led to increased expression of FOXP3 (80). The reduction of iso-allo-LCA in *Mdr2*-deficient mice with DSS colitis and reduced liver pathology suggested a pathogenic role of the iso-allo-LCA. The

data from Hang *et al.* showed that iso-allo-LCA leads to increased levels of Foxp3⁺ Treg, suggesting a more anti-inflammatory role of this metabolite.

In conclusion, the protective effect of colitis on PSC development observed in murine studies was not transferable via FMT into germ-free mice. In fact, the mice receiving a FMT with microbiota of mice with PSC and colitis developed an even more severe sclerosing cholangitis upon DCC-treatment.

One caveat of these experiments is that the fecal microbiota composition will change during reconstitution in parallel to the reduction of toxic BAs in germ-free wild type mice. To overcome this caveat, the FMT could be performed in germ-free *Mdr2*-deficient mice. This way the bile acid composition remains stable. Additionally, the mice could be observed starting from the acute phase, until they transition into the chronic phase of disease. These experiments will be performed soon, as germ-free *Mdr2*-deficient mice are now available in the lab.

Another factor that could mediate the protective effect of colitis on PSC development, and was not investigated in this study until now, is the biliary microbiota. It was recently discovered that the bile fluid of PSC patients harbors a diverse microbiota that was distinct from the oral cavity, the duodenal fluid, and duodenal mucosa communities, compared to healthy controls. A concomitant IBD was detected in 67 % of the evaluated patients, but it was not distinguished whether this was between PSC patients with or without IBD (148). Therefore, it might be very interesting to investigate the differences in the biliary microbiota of PSC patients and PSC-IBD patients, and thereby also examine the role of the biliary microbiota in the protective effect of colitis on PSC development.

6.3 The major driver of the observed protection is not the innate immune system

The strong association of PSC and IBD suggests a potential role of the gut-liver axis (38, 69). Under physiological conditions, the liver is continuously exposed to gut-derived antigens through the portal vein. Moreover, bacterial degradation of metabolites reach the liver and influence its innate and adaptive immune responses (9, 149). Also, cells of the immune system can leave the 'leaky gut' during inflammation and migrate via the portal vein to the liver,

where they can induce inflammation. Therefore, the role of the two major subsets of the innate immune system, macrophages and neutrophils were investigated in the protective effect of colitis on PSC development.

First, the role of macrophages was tested in the protective effect of colitis on PSC development. Macrophages represent a key cellular component of the liver, essential for maintaining tissue homeostasis and ensuring rapid responses to hepatic injury (150). Macrophages are a very heterogeneous population dependent on their developmental origin (resident or infiltrating macrophages) and their polarization (inflammatory or anti-inflammatory) regulated by microenvironmental cues, such as danger signals and cellular debris taken up by phagocytosis (151). Liver macrophages consist of ontogenetically distinct populations, referred to as kupffer cells and infiltrating monocyte-derived macrophages (152).

Balmer *et al.* showed that the liver can act as a firewall mediating the mutualism between the host and its gut commensal microbiota. They showed that kupffer cells clear commensals through their own arterial supply. Damage to the liver firewall in mice impairs functional clearance of commensals, and results in spontaneous priming of non-mucosal immune responses through increased systemic exposure to gut commensals (28). Taniki *et al.* found, that IL-10 producing CD11b⁺ macrophages contribute to immune tolerance in the inflamed liver during intestinal inflammation with diminished intestinal barrier function. This protective effect was canceled out by gut sterilization, suggesting that immune balance in the liver is potentially regulated by gut microbiota and metabolites (153). These data show, that the macrophages could play a role in immune tolerance in the liver. Therefore, they were an important target to check in the protective effect of colitis on liver pathology.

The *AM^{f/f}Csf1r^{Cre}* mouse line was used to analyze the role of macrophages in the protective effect of colitis on PSC development. This mouse model has an impairment in the AM receptors of the TAM receptors (Tyro3, Axl and MerTK) on all *Csf1r*⁺ cells. They have a functional defect in the phagocytosis of macrophages. *AM^{f/f}Csf1r^{Cre}* deficient mice were fed the DDC diet to induce liver pathology upon induction of DSS colitis. Significantly reduced ALP levels and a strong trend in decreased ALT levels were detected in the mice, receiving DSS colitis compared to controls. Overall, the pathology in the liver was very low, resulting in low mHAI and Fibrosis scores. Nevertheless, the strong decrease of ALP and ALT levels suggested

that macrophages were not the major driver of the observed protection of colitis on PSC severity.

Therefore, the role of neutrophils and granulocytes, the second major subset of the innate immune system, was analyzed in the protective effect of colitis on PSC development. Neutrophils capture and destroy invading microorganisms through phagocytosis, intracellular degradation, release of granules, and the formation of neutrophil extracellular traps after detecting pathogens (72). To this end, neutrophils and granulocytes were depleted in *Mdr2*-deficient mice during the course of acute DSS colitis using an anti-Gr1 antibody. A significant reduction in transaminases, and a decrease of the mHAI histology score by trend, were detected in the mice with DSS colitis compared to controls without colitis. Since the protection was still observable in mice with depleted Ly6G⁺ neutrophils, it was concluded that neutrophils and granulocytes were also not the major driver of the observed protection.

In line with these data, Zimmer *et al.* found a massive infiltration of neutrophils in the bile ducts of PSC patients compared to patients without PSC. In this study, 86 % of the PSC patients had a concurrent IBD. A similar increase in neutrophils was also noted in colonic biopsies in patients with PSC-IBD compared to healthy controls. However elevated bile duct neutrophil counts in patients with PSC were independent of concurrent intestinal inflammation (68). These data additionally confirmed that the neutrophils seem to play an important role in the disease development and progression of PSC. But since there were no differences between the groups with or without concomitant IBD, this also suggested that the neutrophils were not the major driver of the observed protective effect of colitis on PSC development.

6.4 The cells of the adaptive immune system are involved in the protective effect of IBD on PSC development

The important role of the gut-liver axis is also promoting the adaptive immune response. Gut-derived bacteria and bacterial metabolites activate the innate immune cells, which further induce adaptive immune responses. It was shown, that activated cells of the adaptive immune system can migrate from the inflamed gut to the liver and mediate the inflammation in the target organ (35). Memory T cells of common clonal origin were detected in paired gut and liver samples of patients with PSC-IBD. These data demonstrated that a proportion of the T

cells in the gut and the liver are derived from the same origin, and therefore react to similar triggers. This proportion is particularly high in patients with PSC and IBD (154). Also, for B cells it was shown that a proportion of gut and liver B cells originate from a common clonal origin (i.e., likely to recognize the same antigen) in patients with PSC-associated IBD (87). This suggests that T- and B-cell antigens are shared across the gut-liver axis.

To investigate if T and B cells play a role in the protective effect of colitis on PSC development, *Rag1 x Mdr2*-deficient mice, an experimental system without T and B cells, was used. Therefore, a chronic DSS colitis was induced in *Rag1 x Mdr2*-deficient mice. Strikingly, no differences in the transaminases of *Rag1 x Mdr2*-deficient mice with or without colitis were observed. Also, the liver histology score remained unchanged in the group with or without colitis. The absence of the protective effect in *Rag1 x Mdr2*-deficient mice strongly suggests a role of T and B cells in the protection of colitis on PSC development, since they were absent in this model. Therefore, the role of T and B cells was further investigated.

6.4.1 Depletion of T cells does not ameliorate the protective effect of IBD on PSC development

It is well known that an imbalance of the TH17 – Treg cell axis is associated with PSC (35). Foxp3⁺ Treg are a regulatory T-cell subset of CD4⁺ T cells. They are critical in maintaining immune tolerance and homeostasis of the immune system by regulating immune responses to self-antigens, allergens, and commensal microbiota as well as to infectious agents and tumors (155). Foxp3⁺ Treg are reduced in the livers of PSC patients. Although it is suggested that concomitant colitis is independent of this reduction (78), it was also published that colitis promotes a pathological condition of the liver in the absence of Foxp3⁺ Treg (35).

Previous experiments from our lab have already shown that the depletion of CD4⁺ T cells did not change the protection of colitis on PSC development (123). However, since Treg were also depleted, it might still be possible that Treg are involved via suppression of CD8⁺ T cells (134, 135), innate immune cell maturation (136-138), antigen presentation (139) and B cell suppression (140, 141). Therefore, the specific role of Foxp3⁺ Treg in the protection of colitis on PSC development was analyzed.

To this end, an acute DSS colitis was induced in *Mdr2*-deficient DERE mice upon depletion of Foxp3⁺ Treg by injection of diphtheria toxin (142). Significantly decreased transaminases, bilirubin and ALP levels were detected in mice without Foxp3⁺ Treg and DSS colitis, compared to controls with depleted Foxp3⁺ Treg and without colitis. The protective effect was comparable to the controls with Foxp3⁺ Treg and colitis. In conclusion, these data showed that Foxp3⁺ Treg do not mediate the protective effect of colitis on PSC development. One caveat of this experiment was that it was only tested in the acute model of DSS colitis. However, the depletion of Foxp3⁺ Treg during chronic DSS colitis was not possible. It was shown that repeated long-term DTX application induces a neutralizing anti-DTX antibody response (156). One possibility would be the transfer of DERE T cells into *Rag1* × *Mdr2*-deficient mice and to induce chronic DSS colitis and Treg depletion. However, our data indicate a possible role of the B cells in the protective effect of colitis on PSC development. Of note, B cells would be absent in this approach, which would bias the experiment.

CD8⁺ T cells have been shown to migrate to the gut and to the liver, enabling them to induce inflammation (157). Mechanistically, it was shown that IFN- γ can change the phenotype of hepatic CD8⁺ T cells towards increased cytotoxicity, and its absence attenuates liver fibrosis in chronic sclerosing cholangitis in mice (82). On the other hand, a regulatory role of CD8⁺ T cells is known by the production of IL-10. It was shown that these regulatory CD8⁺ T cells can block the activation of naïve or effector T cells and suppress IgG/IgE antibody responses by B cells (158). In addition, IL-17 produced by antigen specific CD8⁺ T cells protected against CD8⁺ T-cell mediated cholangitis (159). Therefore, another interesting target is CD8⁺ T cells.

The role of CD8⁺ T cells on the protective effect of colitis on PSC development was tested by induction of a chronic DSS colitis in *Mdr2*-deficient mice upon depletion of CD8⁺ T cells, using an anti-CD8 antibody. Analysis of liver pathology showed a strong trend in reduced transaminases and ALP levels in the group with colitis and depleted CD8⁺ T cells compared to the control. However, two problems were observed in this experiment. First, the experimental group with depleted CD8⁺ T cells developed severe colitis, whereas the CD8⁺ T-cell proficient group did not. Second, depletion of the CD8⁺ T cells was not sufficient throughout the whole experiment. Due to the long experiment of 51 days, it is possible that B cells produce antibodies against the anti-CD8 depleting antibody, and thereby may have impaired sufficient depletion. Yet, the reduced transaminases and ALP levels after CD8⁺ T-cell depletion indicated

that CD8⁺ T cells were not involved in the protective effect of colitis in PSC development. However, a repetition of this experiment is required for further conclusions. Alternatively, the use of a transfer model in which CD4⁺ T cells are transferred with or without CD8⁺ T cells into *Rag1 x Mdr2*-deficient mice could be helpful to overcome the possible production of neutralizing antibodies by B cells.

Taken together, our experiments and those that were previously performed by colleagues suggest that Foxp3⁺ Treg, CD4⁺ and CD8⁺ T cells do not play a role in the protective effect observed in the disease severity of liver pathology upon colitis induction.

6.4.2 B cells are an important player in the observed protection

The induction of chronic DSS colitis in *Rag1 x Mdr2*-deficient mice suggested an important role of T and/or B cells in the protective effect of colitis on PSC development. After exclusion of T cells in this process, the role of B cells in the protective effect of colitis on PSC development was assessed next. It is known that a proportion of gut and liver B cells originate from a common clonal origin in patients with PSC-associated IBD, which suggests that B-cell antigens are shared across the gut-liver axis (87). Furthermore, activated and differentiated B cells in the intestine produce secretory immunoglobulin A (IgA), which binds commensals to preserve a healthy microbial ecosystem (89). Thus, B cells could be a key player that promote the protective effect of colitis on PSC development. To this end, a chronic DSS colitis was induced in *Mdr2*-deficient mice after depletion of B cells using an anti-CD20 mAb. An increase in transaminases was found in the mice with depleted B cells, compared to the mice injected with IgG control. These data highly suggest that B cells play an important role in the protective effect of colitis on PSC development.

Interestingly, Thapa *et al.* described a pathogenic role of intrahepatic B cells in the fibrosis development of *Mdr2*-deficient mice. Depletion of B cells by anti-CD20 mAb reduced the hepatic fibrosis (160). These findings suggest that the concomitant colitis plays an important role, as the mice in the study of Thapa *et al.* did not have colitis. These findings shine a light on two important points to consider. First, the origin of the B cells might play an important role in the inflammatory or anti-inflammatory nature of the B cells. Second, the concomitant colitis influences the activity of the B cells.

Indeed, preliminary data from our group indicated that the induction of a chronic DSS colitis leads to a strong infiltration of B cells from the colon to the liver of *Mdr2*-deficient mice that were reconstituted with bone marrow from *Kaede* mice (123). Immune cells in these chimeric mice expressed a green fluorescence protein, that was photoconverted into a red fluorescent signal upon exposure of the colon to UV-light, and therefore allowed tracking of the migration of these cells (161).

One mechanism by which colonic B cells could reduce the progression of liver pathology in *Mdr2*-deficient mice could be IgA production. IgA-coating of bacteria in the microbiota identifies inflammatory commensals that preferentially drive intestinal disease (90). It was already shown that IgA producing plasma cells which had originated in the gut, can migrate to the central nervous system (CNS) during experimental autoimmune encephalomyelitis (EAE), and play an important role in suppressing neuroinflammation (162). In line with these observations, it is tempting to speculate that IgA-producing plasma cells might migrate from the inflamed intestine to the liver, where these cells neutralize inflammatory commensals, leading to a reduced liver pathology.

Besides the production of antibodies, B cells also produce cytokines, such as IL-10, which is a marker cytokine of regulatory B cells (Breg). These cells have the capacity to suppress autoimmune inflammation, and furthermore, certain gut resident bacteria have been shown to induce production of IL-10 in B cells with anti-inflammatory activity (86, 163). Thus, another possible mechanism of how B cells might promote the observed protective effect of colitis on PSC progression, is the induction or conversion of colonic Bregs, which induce anti-inflammatory signals in the liver during sclerosing cholangitis.

It remains unknown if one of these proposed mechanisms is involved in the observed protection. Further analysis is needed to investigate the B-cell derived suppressive mechanisms in the liver, such as measurement of IgA production and single cell sequencing of colonic-derived B cells isolated from the liver.

6.5 Role of an *IL2ra* SNP on the disease severity of PSC and PSC-associated IBD, as well as the protective effect of IBD on PSC development

The *IL2RA* encodes a subunit of the high-affinity interleukin-2 (IL-2) receptor (also known as CD25). IL-2 receptor signaling is crucial for the suppressive capacity of Foxp3⁺ Treg, and for activation and survival of activated CD4⁺ T cells. Naïve CD4⁺ T effector cells (Teff) express only the IL-2R β and γ chains that bind IL-2 with a low affinity. Upon activation, the IL-2R α subunit is upregulated on Teff cells allowing high affinity binding of IL-2 to its receptor, which promotes survival and IL-2 production via a positive feedback, favoring continued IL-2-dependent activation. In contrast to this, Foxp3⁺ Treg are characterized by their constitutive high-affinity IL-2R (IL-2R $\alpha\beta\gamma$) expression. In contrast to Teff cells, Treg do not produce, but consume IL-2. Therefore, one hypothesis is that T cells may die by neglect, because the available IL-2 is consumed by Foxp3⁺ Treg (104, 164).

In line with the importance of the IL-2 signaling, Genome wide association studies (GWAS) identified non-coding SNPs in the *IL2RA* gene to be associated with PSC and IBD and other autoimmune disorders. Therefore, it was the aim of the second part of this project to investigate the effect of single nucleotide polymorphisms (SNPs) in the *IL2RA* gene on PSC severity and on the protective effect of IBD on PSC development.

6.5.1 *IL2ra*^{SNP} mice have impaired Treg function and develop more liver pathology in a mouse model of sclerosing cholangitis

GWAS identified the rs61839660 *IL2RA* SNP, located in the first intron of the *IL2RA* gene, to be associated with IBD and PSC (94, 95, 106). This area of the gene is highly conserved and has an orthologue in mice, which has made it possible to modify that exact SNP in the mouse genome. A mouse model with the *IL2ra*^{SNP} on the background of *Mdr2*-deficient mice was generated using CRISPR/Cas9 technology.

Simeonov *et al.* investigated stimulation-responsive immune enhancers, and focused on the rs61839660 *IL2RA* SNP as a described autoimmune risk variant being associated with PSC, IBD, and also type 1 diabetes (94, 95, 106, 109). Sequence perturbation of the disease associated *IL2RA* enhancer did not entirely block *IL2RA* expression, but rather delayed the timing of gene activation in response to specific extracellular signals (109). It was also described that multiple

nucleotide polymorphisms in the first intron of the *IL2RA* gene affect transcription factor binding and enhancer activity (108). For the rs61839660 SNP, reduced activity of the according enhancer was shown to be due to disrupted binding of transcription factors. These data show already that a non-coding SNP can result in impaired functionality. In line with these data, a reduced suppressive capacity of the *Il2ra*^{SNP} Treg *in vitro* compared to *Il2ra*^{wt} Treg was found in this study.

To test the role of rs61839660 *IL2RA* SNP *in vivo*, two different mouse models were characterized. The *Il2ra*^{SNP-HH} mice were generated in Hamburg by Irm Hermans-Borgmeyer (Transgenic mouse core facility, UKE), and the *Il2ra*^{SNP-Mson} mice were provided by the group of Professor Marson (109). It was shown that *in vivo* phenotyping of the *Il2ra*^{SNP-Mson} mouse revealed no evidence of overt immune dysregulation. T-cell development was normal, with no differences in thymic cellularity or developmental stages. Furthermore, the enhancer did not appear to be required for IL-2R α expression in Treg at steady state, as SNP Treg cells had normal surface expression (109). These mice were crossed to *Mdr2*-deficient mice, the experimental mouse model for sclerosing cholangitis, and disease development was analyzed together with *Mdr2*^{-/-}*Il2ra*^{SNP-HH} mice. In the first 12 weeks of age, no differences in liver pathology were detectable and the mice did not develop spontaneous colitis. At 14 weeks, when the inflammation transitioned into a more chronic phase of disease development, a significant increase in transaminases, as well as a strong trend in increased liver histology, was detectable in the *Mdr2*^{-/-}*Il2ra*^{SNP-HH} mice compared to the controls.

These data showed that the SNP in the *Il2ra* gene had an effect on the disease development of sclerosing cholangitis in mice, which might be associated with reduced suppressive capacity of Foxp3⁺ Treg cells. However, the mechanism of how the *Il2ra*^{SNP} affects the immune system, and therefore, disease development, is not yet understood. A possible role of the SNP on Foxp3⁺ Tregs and CD4⁺ Teff cells should be investigated, since the expression of the IL-2R α is not limited to Foxp3⁺ Treg.

6.5.2 The protective effect of IBD on PSC development is not impaired due to the *Il2ra*^{SNP} in a mouse model of DSS colitis

PSC and IBD are highly associated in patients. As described in the first part of this work, a protective effect of colitis on PSC development was found. Furthermore, data from our group

also described a protective effect of PSC on the development of colitis (*unpublished data*). These findings suggest that these two diseases should not appear together. But, since they are highly associated, it was hypothesized that genetic predispositions, like the SNP in the *IL2RA* gene, can drive PSC and colitis development and thereby overcome the protective effect. Especially since the rs61839660 *IL2RA* SNP is described to be associated with the disease development of UC, CD and PSC (94, 106).

To analyze the protective effect of colitis on PSC development with regards to the *Il2ra*^{SNP}, *Mdr2*^{-/-}*Il2ra*^{SNP} mice were used upon induction of acute DSS colitis. No differences in the disease development of PSC-associated colitis were found, and the protective effect of colitis on PSC development, measured by the reduction of transaminases, was still detectable. The *Il2ra*^{SNP} did not influence the protective effect of colitis on PSC development.

One caveat could be the severity of the colitis model. To observe the effect of the colitis development in a more chronic phase of disease, a chronic DSS colitis could be induced in *Mdr2*^{-/-}*Il2ra*^{SNP} mice. This might rather be the time point where the increased inflammation could overcome the protection of colitis on PSC development. The increased development of sclerosing cholangitis described above was also only detectable in the chronic phase of disease.

A recent publication from Goldberg *et al.* analyzed the role of the rs61839660 *IL2RA* SNP in patient with Crohn's disease (CD). They showed that the SNP enhances IL-2 signaling in CD4⁺ T effector cells from CD patients by upregulating the expression of the IL-2R α . Effector T cells from *IL2RA* SNP patients displayed the ability to respond to doses of IL-2, which normally only activated Treg cells show (164). These findings are in contrast to the work of Simeonov *et al.*, where transcript data collected from stimulated CD4⁺ T cells from people with or without the SNP were analyzed. These data depict that the SNP is altering the transcriptional response to stimulation. This resulted in reduced levels of *IL2RA* transcript in stimulated T cells, confirming the functional effect of the *IL2RA* SNP on human T-cell gene regulation (109). The data from Simeonov *et al.* also supported the data generated in this project, where decreased suppressive capacity of *Il2ra*^{SNP} Treg cells, as well as increased susceptibility to PSC development in *Mdr2*-deficient mice was found. But the data from Goldberg *et al.* elucidate that the focus should not only be laid on the Foxp3⁺ Treg, but also on CD4⁺ effector T cells.

Overall, these data show an important role of an intronic SNP in the *Ii2ra* gene on the disease development of sclerosing cholangitis in mice. Further studies will be critical to decipher the underlying mechanisms. Since PSC is associated with SNPs in several other genes, this study highlights the importance of investigating them further. Generating mouse models with SNPs known from human patients is a great way to study the effect of genetic predispositions in diseases with unknown etiology.

7 Conclusion and Outlook

Primary sclerosing cholangitis (PSC) is characterized by chronic bile duct obstruction leading to end stage liver disease. The etiology of PSC is still unknown. However, two known factors impacting PSC are concomitant inflammatory bowel disease (IBD) and genetic predispositions, which were investigated in this study.

Overall, the findings presented in this study demonstrated that colitis reduced the disease severity of sclerosing cholangitis in mouse models. Furthermore, our data indicate a crucial role of B cells in mediating this effect, while involvement of T cells and innate immune cells does not seem to play a critical function. Furthermore, the protective effect of the colitis was not transferrable via fecal microbiota transplantation arguing against a key role of the intestinal microbiota. Finally, the bile acid composition was changed after colitis induction in a mouse model of sclerosing cholangitis, but the significance of this effect could not be addressed in this study. Thus, B cells seem to mediate the protective effect of colitis on PSC development. However, the exact mechanism is not yet known and requires further work.

In the second part of this study, it was found that SNPs in the *Il2ra* gene, which are known to be associated with PSC patients, increased the disease development of sclerosing cholangitis in an experimental mouse model. These findings underline the importance of IL-2R signaling in PSC. However, further studies are needed to decipher the involvement of Treg and T effector cells in mediating this effect. Finally, the protective effect of colitis on PSC development was not abrogated by the presence of the SNP, providing evidence that Tregs do not mediate the protective effect induced by the presence of colitis.

Together both parts of this study provide a better understanding of PSC pathology, which may build the basis for new therapeutic options, either targeting Tregs in patients with *IL2RA* gene polymorphisms or B cells in PSC patients without concomitant IBD.

8 Appendix

8.1 References

1. G. M. Hirschfield, T. H. Karlsen, K. D. Lindor, D. H. Adams, Primary sclerosing cholangitis. *Lancet* **382**, 1587-1599 (2013).
2. R. Chapman *et al.*, Diagnosis and management of primary sclerosing cholangitis. *Hepatology* **51**, 660-678 (2010).
3. J. H. Ngu, R. B. Gearry, C. M. Frampton, C. A. Stedman, Mortality and the risk of malignancy in autoimmune liver diseases: a population-based study in Canterbury, New Zealand. *Hepatology* **55**, 522-529 (2012).
4. EASL, EASL Clinical Practice Guidelines: management of cholestatic liver diseases. *J Hepatol* **51**, 237-267 (2009).
5. E. Aadland *et al.*, Primary sclerosing cholangitis: a long-term follow-up study. *Scand J Gastroenterol* **22**, 655-664 (1987).
6. T. Hildebrand *et al.*, Biliary strictures and recurrence after liver transplantation for primary sclerosing cholangitis: A retrospective multicenter analysis. *Liver Transpl* **22**, 42-52 (2016).
7. T. J. Weismüller *et al.*, Patient Age, Sex, and Inflammatory Bowel Disease Phenotype Associate With Course of Primary Sclerosing Cholangitis. *Gastroenterology* **152**, 1975-1984.e1978 (2017).
8. Y. Ueda *et al.*, Long-term Prognosis and Recurrence of Primary Sclerosing Cholangitis After Liver Transplantation: A Single-Center Experience. *Transplant Direct* **3**, e334 (2017).
9. J. H. Aron, C. L. Bowlus, The immunobiology of primary sclerosing cholangitis. *Semin Immunopathol* **31**, 383-397 (2009).
10. R. E. Rossi, D. Conte, S. Massironi, Primary sclerosing cholangitis associated with inflammatory bowel disease: an update. *Eur J Gastroenterol Hepatol* **28**, 123-131 (2016).
11. K. Bambha *et al.*, Incidence, clinical spectrum, and outcomes of primary sclerosing cholangitis in a United States community. *Gastroenterology* **125**, 1364-1369 (2003).
12. R. H. Wiesner *et al.*, Primary sclerosing cholangitis: natural history, prognostic factors and survival analysis. *Hepatology* **10**, 430-436 (1989).
13. T. H. Karlsen, T. Folseraas, D. Thorburn, M. Vesterhus, Primary sclerosing cholangitis - a comprehensive review. *J Hepatol* **67**, 1298-1323 (2017).
14. B. Lindkvist, M. Benito de Valle, B. Gullberg, E. Björnsson, Incidence and prevalence of primary sclerosing cholangitis in a defined adult population in Sweden. *Hepatology* **52**, 571-577 (2010).
15. K. Boonstra, U. Beuers, C. Y. Ponsioen, Epidemiology of primary sclerosing cholangitis and primary biliary cirrhosis: a systematic review. *J Hepatol* **56**, 1181-1188 (2012).
16. N. A. Molodecky *et al.*, Incidence of primary sclerosing cholangitis: a systematic review and meta-analysis. *Hepatology* **53**, 1590-1599 (2011).
17. K. Boonstra *et al.*, Population-based epidemiology, malignancy risk, and outcome of primary sclerosing cholangitis. *Hepatology* **58**, 2045-2055 (2013).
18. D. C. Baumgart, W. J. Sandborn, Inflammatory bowel disease: clinical aspects and established and evolving therapies. *Lancet* **369**, 1641-1657 (2007).
19. K. Boonstra *et al.*, Primary sclerosing cholangitis is associated with a distinct phenotype of inflammatory bowel disease. *Inflamm Bowel Dis* **18**, 2270-2276 (2012).
20. A. Ricciuto, B. M. Kamath, A. M. Griffiths, The IBD and PSC Phenotypes of PSC-IBD. *Curr Gastroenterol Rep* **20**, 16 (2018).
21. R. K. Weersma, K. D. Lindor, Shifting Paradigms: What Is the True Prevalence and Clinical Course of Primary Sclerosing Cholangitis? *Gastroenterology* **151**, 590-593 (2016).
22. H. H. Rasmussen *et al.*, Hepatobiliary dysfunction and primary sclerosing cholangitis in patients with Crohn's disease. *Scand J Gastroenterol* **32**, 604-610 (1997).
23. E. V. Loftus, W. J. Sandborn, K. D. Lindor, N. F. Larusso, Interactions between chronic liver disease and inflammatory bowel disease. *Inflamm Bowel Dis* **3**, 288-302 (1997).
24. E. V. Loftus *et al.*, PSC-IBD: a unique form of inflammatory bowel disease associated with primary sclerosing cholangitis. *Gut* **54**, 91-96 (2005).
25. L. Marelli *et al.*, Does the severity of primary sclerosing cholangitis influence the clinical course of associated ulcerative colitis? *Gut* **60**, 1224-1228 (2011).
26. C. Palmela, F. Peerani, D. Castaneda, J. Torres, S. H. Itzkowitz, Inflammatory Bowel Disease and Primary Sclerosing Cholangitis: A Review of the Phenotype and Associated Specific Features. *Gut Liver* **12**, 17-29 (2018).
27. E. Liaskou *et al.*, Loss of CD28 expression by liver-infiltrating T cells contributes to pathogenesis of primary sclerosing cholangitis. *Gastroenterology* **147**, 221-232.e227 (2014).
28. M. L. Balmer *et al.*, The liver may act as a firewall mediating mutualism between the host and its gut commensal microbiota. *Sci Transl Med* **6**, 237ra266 (2014).
29. N. Nakamoto *et al.*, Gut pathobionts underlie intestinal barrier dysfunction and liver T helper 17 cell immune response in primary sclerosing cholangitis. *Nat Microbiol* **4**, 492-503 (2019).

30. P. J. Turnbaugh *et al.*, The human microbiome project. *Nature* **449**, 804-810 (2007).
31. S. Tuddenham, C. L. Sears, The intestinal microbiome and health. *Curr Opin Infect Dis* **28**, 464-470 (2015).
32. J. H. Tabibian, A. H. Ali, K. D. Lindor, Primary Sclerosing Cholangitis, Part 1: Epidemiology, Etiopathogenesis, Clinical Features, and Treatment. *Gastroenterol Hepatol (N Y)* **14**, 293-304 (2018).
33. S. P. O'Hara, J. H. Tabibian, P. L. Splinter, N. F. LaRusso, The dynamic biliary epithelia: molecules, pathways, and disease. *J Hepatol* **58**, 575-582 (2013).
34. A. Shah, G. A. Macdonald, M. Morrison, G. Holtmann, Targeting the Gut Microbiome as a Treatment for Primary Sclerosing Cholangitis: A Conceptual Framework. *Am J Gastroenterol* **115**, 814-822 (2020).
35. F. Mathies *et al.*, Colitis Promotes a Pathological Condition of the Liver in the Absence of Foxp3. *J Immunol* **201**, 3558-3568 (2018).
36. L. Bajer *et al.*, Distinct gut microbiota profiles in patients with primary sclerosing cholangitis and ulcerative colitis. *World J Gastroenterol* **23**, 4548-4558 (2017).
37. M. Kummen *et al.*, The gut microbial profile in patients with primary sclerosing cholangitis is distinct from patients with ulcerative colitis without biliary disease and healthy controls. *Gut* **66**, 611-619 (2017).
38. R. Little, E. Wine, B. M. Kamath, A. M. Griffiths, A. Ricciuto, Gut microbiome in primary sclerosing cholangitis: A review. *World J Gastroenterol* **26**, 2768-2780 (2020).
39. R. Wiest, M. Lawson, M. Geuking, Pathological bacterial translocation in liver cirrhosis. *J Hepatol* **60**, 197-209 (2014).
40. R. Tang *et al.*, Gut microbial profile is altered in primary biliary cholangitis and partially restored after UDCA therapy. *Gut* **67**, 534-541 (2018).
41. M. Rühlemann *et al.*, Consistent alterations in faecal microbiomes of patients with primary sclerosing cholangitis independent of associated colitis. *Aliment Pharmacol Ther* **50**, 580-589 (2019).
42. J. Sabino *et al.*, Primary sclerosing cholangitis is characterised by intestinal dysbiosis independent from IBD. *Gut* **65**, 1681-1689 (2016).
43. M. L. Chen, K. Takeda, M. S. Sundrud, Emerging roles of bile acids in mucosal immunity and inflammation. *Mucosal Immunol* **12**, 851-861 (2019).
44. J. M. Ridlon, D. J. Kang, P. B. Hylemon, Bile salt biotransformations by human intestinal bacteria. *J Lipid Res* **47**, 241-259 (2006).
45. A. Wahlström, S. I. Sayin, H. U. Marschall, F. Bäckhed, Intestinal Crosstalk between Bile Acids and Microbiota and Its Impact on Host Metabolism. *Cell Metab* **24**, 41-50 (2016).
46. J. Y. Chiang, Bile acids: regulation of synthesis. *J Lipid Res* **50**, 1955-1966 (2009).
47. C. Thomas, R. Pellicciari, M. Pruzanski, J. Auwerx, K. Schoonjans, Targeting bile-acid signalling for metabolic diseases. *Nat Rev Drug Discov* **7**, 678-693 (2008).
48. M. J. Monte, J. J. Marin, A. Antelo, J. Vazquez-Tato, Bile acids: chemistry, physiology, and pathophysiology. *World J Gastroenterol* **15**, 804-816 (2009).
49. M. Norlin, K. Wikvall, Enzymes in the conversion of cholesterol into bile acids. *Curr Mol Med* **7**, 199-218 (2007).
50. J. Y. Chiang, Bile acid metabolism and signaling. *Compr Physiol* **3**, 1191-1212 (2013).
51. P. Kurdi, K. Kawanishi, K. Mizutani, A. Yokota, Mechanism of growth inhibition by free bile acids in lactobacilli and bifidobacteria. *J Bacteriol* **188**, 1979-1986 (2006).
52. J. M. Ridlon, D. J. Kang, P. B. Hylemon, J. S. Bajaj, Bile acids and the gut microbiome. *Curr Opin Gastroenterol* **30**, 332-338 (2014).
53. S. N. Cullen, R. W. Chapman, The medical management of primary sclerosing cholangitis. *Semin Liver Dis* **26**, 52-61 (2006).
54. R. W. Chapman, High-dose ursodeoxycholic acid in the treatment of primary sclerosing cholangitis: throwing the urso out with the bathwater? *Hepatology* **50**, 671-673 (2009).
55. U. Beuers *et al.*, Ursodeoxycholic acid for treatment of primary sclerosing cholangitis: a placebo-controlled trial. *Hepatology* **16**, 707-714 (1992).
56. C. B. O'Brien, J. R. Senior, R. Arora-Mirchandani, A. K. Batta, G. Salen, Ursodeoxycholic acid for the treatment of primary sclerosing cholangitis: a 30-month pilot study. *Hepatology* **14**, 838-847 (1991).
57. K. D. Lindor, Ursodiol for primary sclerosing cholangitis. Mayo Primary Sclerosing Cholangitis-Ursodeoxycholic Acid Study Group. *N Engl J Med* **336**, 691-695 (1997).
58. K. D. Lindor *et al.*, High-dose ursodeoxycholic acid for the treatment of primary sclerosing cholangitis. *Hepatology* **50**, 808-814 (2009).
59. G. Rudolph, P. Kloeters-Plachky, D. Rost, A. Stiehl, The incidence of cholangiocarcinoma in primary sclerosing cholangitis after long-time treatment with ursodeoxycholic acid. *Eur J Gastroenterol Hepatol* **19**, 487-491 (2007).
60. C. K. Triantos, N. M. Koukias, V. N. Nikolopoulou, A. K. Burroughs, Meta-analysis: ursodeoxycholic acid for primary sclerosing cholangitis. *Aliment Pharmacol Ther* **34**, 901-910 (2011).
61. J. Smit *et al.*, Homozygous disruption of the murine mdr2 P-glycoprotein gene leads to a complete absence of phospholipid from bile and to liver disease. *Cell* **75**, 451-462 (1993).
62. S. Hohenester *et al.*, A biliary HCO₃⁻ umbrella constitutes a protective mechanism against bile acid-induced injury in human cholangiocytes. *Hepatology* **55**, 173-183 (2012).
63. U. Beuers *et al.*, The biliary HCO₃⁻ umbrella: a unifying hypothesis on pathogenetic and therapeutic aspects of fibrosing cholangiopathies. *Hepatology* **52**, 1489-1496 (2010).
64. A. Gerussi *et al.*, New Therapeutic Targets in Autoimmune Cholangiopathies. *Front Med (Lausanne)* **7**, 117 (2020).

65. P. Fickert *et al.*, norUrsodeoxycholic acid improves cholestasis in primary sclerosing cholangitis. *J Hepatol* **67**, 549-558 (2017).
66. M. E. Himmel, G. Hardenberg, C. A. Piccirillo, T. S. Steiner, M. K. Levings, The role of T-regulatory cells and Toll-like receptors in the pathogenesis of human inflammatory bowel disease. *Immunology* **125**, 145-153 (2008).
67. A. T. Borchers, S. Shimoda, C. Bowlus, C. L. Keen, M. E. Gershwin, Lymphocyte recruitment and homing to the liver in primary biliary cirrhosis and primary sclerosing cholangitis. *Semin Immunopathol* **31**, 309-322 (2009).
68. C. L. Zimmer *et al.*, A biliary immune landscape map of primary sclerosing cholangitis reveals a dominant network of neutrophils and tissue-resident T cells. *Sci Transl Med* **13**, (2021).
69. P. C. Konturek *et al.*, Gut-Liver Axis: How Do Gut Bacteria Influence the Liver? *Med Sci (Basel)* **6**, (2018).
70. C. A. O'Mahony, J. M. Vierling, Etiopathogenesis of primary sclerosing cholangitis. *Semin Liver Dis* **26**, 3-21 (2006).
71. D. Hirayama, T. Iida, H. Nakase, The Phagocytic Function of Macrophage-Enforcing Innate Immunity and Tissue Homeostasis. *Int J Mol Sci* **19**, (2017).
72. C. Rosales, Neutrophil: A Cell with Many Roles in Inflammation or Several Cell Types? *Front Physiol* **9**, 113 (2018).
73. R. G. Cameron, L. M. Blendis, M. G. Neuman, Accumulation of macrophages in primary sclerosing cholangitis. *Clin Biochem* **34**, 195-201 (2001).
74. M. E. Guicciardi *et al.*, Macrophages contribute to the pathogenesis of sclerosing cholangitis in mice. *J Hepatol* **69**, 676-686 (2018).
75. S. D. Kobayashi, N. Malachowa, F. R. DeLeo, Neutrophils and Bacterial Immune Evasion. *J Innate Immun* **10**, 432-441 (2018).
76. N. D. Pennock *et al.*, T cell responses: naive to memory and everything in between. *Adv Physiol Educ* **37**, 273-283 (2013).
77. J. Katt *et al.*, Increased T helper type 17 response to pathogen stimulation in patients with primary sclerosing cholangitis. *Hepatology* **58**, 1084-1093 (2013).
78. M. Sebode *et al.*, Reduced FOXP3(+) regulatory T cells in patients with primary sclerosing cholangitis are associated with IL2RA gene polymorphisms. *J Hepatol* **60**, 1010-1016 (2014).
79. D. Schwinge *et al.*, Dysfunction of hepatic regulatory T cells in experimental sclerosing cholangitis is related to IL-12 signaling. *J Hepatol* **66**, 798-805 (2017).
80. S. Hang *et al.*, Bile acid metabolites control T H 17 and T reg cell differentiation. *Nature* **576**, (2019).
81. W. Li *et al.*, A bacterial bile acid metabolite modulates Treg activity through the nuclear hormone receptor NR4A1. *Cell Host Microbe* **29**, 1366-1377.e1369 (2021).
82. G. Ravichandran *et al.*, Interferon- γ -dependent immune responses contribute to the pathogenesis of sclerosing cholangitis in mice. *Journal of hepatology* **71**, (2019).
83. K. P. Nera, M. K. Kyläniemi, O. Lassila, Regulation of B Cell to Plasma Cell Transition within the Follicular B Cell Response. *Scand J Immunol* **82**, 225-234 (2015).
84. D. P. Harris *et al.*, Reciprocal regulation of polarized cytokine production by effector B and T cells. *Nat Immunol* **1**, 475-482 (2000).
85. A. Mizoguchi, E. Mizoguchi, H. Takedatsu, R. S. Blumberg, A. K. Bhan, Chronic intestinal inflammatory condition generates IL-10-producing regulatory B cell subset characterized by CD1d upregulation. *Immunity* **16**, 219-230 (2002).
86. S. Fillatreau, C. H. Sweeney, M. J. McGeachy, D. Gray, S. M. Anderton, B cells regulate autoimmunity by provision of IL-10. *Nat Immunol* **3**, 944-950 (2002).
87. B. K. Chung *et al.*, Gut and Liver B Cells of Common Clonal Origin in Primary Sclerosing Cholangitis-Inflammatory Bowel Disease. *Hepatol Commun* **2**, 956-967 (2018).
88. A. J. Grant *et al.*, Hepatic expression of secondary lymphoid chemokine (CCL21) promotes the development of portal-associated lymphoid tissue in chronic inflammatory liver disease. *Am J Pathol* **160**, 1445-1455 (2002).
89. M. Botía-Sánchez, M. E. Alarcón-Riquelme, G. Galicia, B Cells and Microbiota in Autoimmunity. *Int J Mol Sci* **22**, (2021).
90. N. W. Palm *et al.*, Immunoglobulin A coating identifies colitogenic bacteria in inflammatory bowel disease. *Cell* **158**, 1000-1010 (2014).
91. A. Bergquist *et al.*, Increased risk of primary sclerosing cholangitis and ulcerative colitis in first-degree relatives of patients with primary sclerosing cholangitis. *Clin Gastroenterol Hepatol* **6**, 939-943 (2008).
92. T. H. Karlsen, E. Melum, A. Franke, The utility of genome-wide association studies in hepatology. *Hepatology* **51**, 1833-1842 (2010).
93. J. Liu *et al.*, Dense genotyping of immune-related disease regions identifies nine new risk loci for primary sclerosing cholangitis. *Nature genetics* **45**, (2013).
94. D. Ellinghaus *et al.*, Analysis of five chronic inflammatory diseases identifies 27 new associations and highlights disease-specific patterns at shared loci. *Nat Genet* **48**, 510-518 (2016).
95. S. G. Ji *et al.*, Genome-wide association study of primary sclerosing cholangitis identifies new risk loci and quantifies the genetic relationship with inflammatory bowel disease. *Nat Genet* **49**, 269-273 (2017).
96. B. Srivastava *et al.*, Fine mapping and replication of genetic risk loci in primary sclerosing cholangitis. *Scand J Gastroenterol* **47**, 820-826 (2012).
97. M. Sharon, R. D. Klausner, B. R. Cullen, R. Chizzonite, W. J. Leonard, Novel interleukin-2 receptor subunit detected by cross-linking under high-affinity conditions. *Science* **234**, 859-863 (1986).

98. K. Sugamura *et al.*, The IL-2/IL-2 receptor system: involvement of a novel receptor subunit, gamma chain, in growth signal transduction. *Tohoku J Exp Med* **168**, 231-237 (1992).
99. T. Takeshita *et al.*, Cloning of the gamma chain of the human IL-2 receptor. *Science* **257**, 379-382 (1992).
100. C. Ye, D. Brand, S. G. Zheng, Targeting IL-2: an unexpected effect in treating immunological diseases. *Signal Transduct Target Ther* **3**, 2 (2018).
101. S. Sakaguchi, T. Yamaguchi, T. Nomura, M. Ono, Regulatory T cells and immune tolerance. *Cell* **133**, 775-787 (2008).
102. W. Liao, J. X. Lin, W. J. Leonard, Interleukin-2 at the crossroads of effector responses, tolerance, and immunotherapy. *Immunity* **38**, 13-25 (2013).
103. S. G. Zheng, J. Wang, P. Wang, J. D. Gray, D. A. Horwitz, IL-2 is essential for TGF-beta to convert naive CD4+CD25-cells to CD25+Foxp3+ regulatory T cells and for expansion of these cells. *J Immunol* **178**, 2018-2027 (2007).
104. O. Boyman, J. Sprent, The role of interleukin-2 during homeostasis and activation of the immune system. *Nat Rev Immunol* **12**, 180-190 (2012).
105. K. K. Farh *et al.*, Genetic and epigenetic fine mapping of causal autoimmune disease variants. *Nature* **518**, 337-343 (2015).
106. H. Huang *et al.*, Fine-mapping inflammatory bowel disease loci to single-variant resolution. *Nature* **547**, 173-178 (2017).
107. S. A. Long *et al.*, Defects in IL-2R signaling contribute to diminished maintenance of FOXP3 expression in CD4(+)CD25(+) regulatory T-cells of type 1 diabetic subjects. *Diabetes* **59**, 407-415 (2010).
108. A. M. Schwartz *et al.*, Multiple single nucleotide polymorphisms in the first intron of the IL2RA gene affect transcription factor binding and enhancer activity. *Gene* **602**, 50-56 (2017).
109. D. R. Simeonov *et al.*, Discovery of stimulation-responsive immune enhancers with CRISPR activation. *Nature* **549**, 111-115 (2017).
110. P. Fickert *et al.*, Characterization of animal models for primary sclerosing cholangitis (PSC). *J Hepatol* **60**, 1290-1303 (2014).
111. Y. Popov, E. Patsenker, P. Fickert, M. Trauner, D. Schuppan, Mdr2 (Abcb4)-/- mice spontaneously develop severe biliary fibrosis via massive dysregulation of pro- and antifibrogenic genes. *J Hepatol* **43**, 1045-1054 (2005).
112. P. Fickert *et al.*, Regurgitation of bile acids from leaky bile ducts causes sclerosing cholangitis in Mdr2 (Abcb4) knockout mice. *Gastroenterology* **127**, 261-274 (2004).
113. P. Fickert *et al.*, A new xenobiotic-induced mouse model of sclerosing cholangitis and biliary fibrosis. *Am J Pathol* **171**, 525-536 (2007).
114. S. Verhulst *et al.*, Infliximab and Dexamethasone Attenuate the Ductular Reaction in Mice. *Sci Rep* **6**, 36586 (2016).
115. L. Jemail *et al.*, Pivotal roles of Kupffer cells in the progression and regression of DDC-induced chronic cholangiopathy. *Sci Rep* **8**, 6415 (2018).
116. I. Okayasu *et al.*, A novel method in the induction of reliable experimental acute and chronic ulcerative colitis in mice. *Gastroenterology* **98**, 694-702 (1990).
117. H. Laroui *et al.*, Dextran sodium sulfate (DSS) induces colitis in mice by forming nano-lipocomplexes with medium-chain-length fatty acids in the colon. *PLoS One* **7**, e32084 (2012).
118. B. Chassaing, J. D. Aitken, M. Malleshappa, M. Vijay-Kumar, Dextran sulfate sodium (DSS)-induced colitis in mice. *Curr Protoc Immunol* **104**, 15.25.11-15.25.14 (2014).
119. D. B. Schauer *et al.*, Genetic and biochemical characterization of *Citrobacter rodentium* sp. nov. *J Clin Microbiol* **33**, 2064-2068 (1995).
120. P. Chandrasekaran *et al.*, Utility of a bacterial infection model to study epithelial-mesenchymal transition, mesenchymal-epithelial transition or tumorigenesis. *Oncogene* **33**, 2639-2654 (2014).
121. L. M. Higgins, G. Frankel, G. Douce, G. Dougan, T. T. MacDonald, *Citrobacter rodentium* infection in mice elicits a mucosal Th1 cytokine response and lesions similar to those in murine inflammatory bowel disease. *Infect Immun* **67**, 3031-3039 (1999).
122. J. W. Collins *et al.*, *Citrobacter rodentium*: infection, inflammation and the microbiota. *Nat Rev Microbiol* **12**, 612-623 (2014).
123. N. Steffens, in *Analysis of the interaction between inflammatory bowel disease and liver pathology in a murine model*. (Dissertation, 2018).
124. F. Mathies, in *Influence of intestinal inflammation on the development of hepatic disease in mice*. (Dissertation, 2017).
125. C. Becker, M. C. Fantini, M. F. Neurath, High resolution colonoscopy in live mice. *Nat Protoc* **1**, 2900-2904 (2006).
126. K. Ishak *et al.*, Histological grading and staging of chronic hepatitis. *Journal of Hepatology* **22**, 696-699 (1995).
127. V. Desmet, M. Gerber, J. Hoofnagle, M. Manns, P. Scheuer, Classification of chronic hepatitis: Diagnosis, grading and staging. *Hepatology* **19**, 1513-1520 (1994).
128. Y. Lapidot *et al.*, Alterations of the salivary and fecal microbiome in patients with primary sclerosing cholangitis. *Hepatol Int* **15**, 191-201 (2021).
129. K. L. Glassner, B. P. Abraham, E. M. M. Quigley, The microbiome and inflammatory bowel disease. *J Allergy Clin Immunol* **145**, 16-27 (2020).
130. J. Y. Chiang, Recent advances in understanding bile acid homeostasis. *F1000Res* **6**, 2029 (2017).
131. I. D. Iliev *et al.*, Interactions between commensal fungi and the C-type lectin receptor Dectin-1 influence colitis. *Science* **336**, 1314-1317 (2012).

132. R. B. Sartor, Microbial influences in inflammatory bowel diseases. *Gastroenterology* **134**, 577-594 (2008).
133. S. Daniel *et al.*, CD8 T cells primed in the gut-associated lymphoid tissue induce immune-mediated cholangitis in mice. *Hepatology (Baltimore, Md.)* **59**, (2014).
134. M. L. Chen *et al.*, Regulatory T cells suppress tumor-specific CD8 T cell cytotoxicity through TGF-beta signals in vivo. *Proc Natl Acad Sci U S A* **102**, 419-424 (2005).
135. N. Chaput *et al.*, Regulatory T cells prevent CD8 T cell maturation by inhibiting CD4 Th cells at tumor sites. *J Immunol* **179**, 4969-4978 (2007).
136. E. B. Okeke, I. Okwor, J. E. Uzonna, Regulatory T cells restrain CD4+ T cells from causing unregulated immune activation and hypersensitivity to lipopolysaccharide challenge. *J Immunol* **193**, 655-662 (2014).
137. M. E. Himmel *et al.*, Human CD4+ FOXP3+ regulatory T cells produce CXCL8 and recruit neutrophils. *Eur J Immunol* **41**, 306-312 (2011).
138. N. Lewkowicz, M. Klink, M. P. Mycko, P. Lewkowicz, Neutrophil--CD4+CD25+ T regulatory cell interactions: a possible new mechanism of infectious tolerance. *Immunobiology* **218**, 455-464 (2013).
139. C. M. Wardell, K. N. MacDonald, M. K. Levings, L. Cook, Cross talk between human regulatory T cells and antigen-presenting cells: Lessons for clinical applications. *Eur J Immunol* **51**, 27-38 (2021).
140. H. W. Lim, P. Hillsamer, A. H. Banham, C. H. Kim, Cutting edge: direct suppression of B cells by CD4+ CD25+ regulatory T cells. *J Immunol* **175**, 4180-4183 (2005).
141. A. Xu *et al.*, TGF-β-Induced Regulatory T Cells Directly Suppress B Cell Responses through a Noncytotoxic Mechanism. *J Immunol* **196**, 3631-3641 (2016).
142. K. Lahl *et al.*, Selective depletion of Foxp3+ regulatory T cells induces a scurfy-like disease. *J Exp Med* **204**, 57-63 (2007).
143. G. Cheng, A. Yu, T. R. Malek, T-cell tolerance and the multi-functional role of IL-2R signaling in T-regulatory cells. *Immunol Rev* **241**, 63-76 (2011).
144. A. Rabiee, M. G. Silveira, Primary sclerosing cholangitis. *Transl Gastroenterol Hepatol* **6**, 29 (2021).
145. O. Y. Mousa *et al.*, Bile Acid Profiles in Primary Sclerosing Cholangitis and Their Ability to Predict Hepatic Decompensation. *Hepatology* **74**, 281-295 (2021).
146. F. Mathies, in *Einfluss einer intestinalen Entzündung auf die Entwicklung von Lebererkrankungen im Mausmodell*. (Dissertation, 2017).
147. J. Tabibian *et al.*, Absence of the intestinal microbiota exacerbates hepatobiliary disease in a murine model of primary sclerosing cholangitis. *Hepatology (Baltimore, Md.)* **63**, (2016).
148. T. Liwinski *et al.*, Alterations of the bile microbiome in primary sclerosing cholangitis. *Gut* **69**, 665-672 (2020).
149. A. W. Thomson, P. A. Knolle, Antigen-presenting cell function in the tolerogenic liver environment. *Nat Rev Immunol* **10**, 753-766 (2010).
150. A. Sica, P. Invernizzi, A. Mantovani, Macrophage plasticity and polarization in liver homeostasis and pathology. *Hepatology* **59**, 2034-2042 (2014).
151. M. Cadamuro, N. Girardi, G. J. Gores, M. Strazzabosco, L. Fabris, The Emerging Role of Macrophages in Chronic Cholangiopathies Featuring Biliary Fibrosis: An Attractive Therapeutic Target for Orphan Diseases. *Front Med (Lausanne)* **7**, 115 (2020).
152. F. Tacke, Targeting hepatic macrophages to treat liver diseases. *J Hepatol* **66**, 1300-1312 (2017).
153. N. Taniki *et al.*, Intestinal barrier regulates immune responses in the liver via IL-10-producing macrophages. *JCI insight* **3**, (2018).
154. E. K. Henriksen *et al.*, Gut and liver T-cells of common clonal origin in primary sclerosing cholangitis-inflammatory bowel disease. *J Hepatol* **66**, 116-122 (2017).
155. A. Y. Rudensky, Regulatory T cells and Foxp3. *Immunol Rev* **241**, 260-268 (2011).
156. J. Wang, M. Siffert, M. Spiliotis, B. Gottstein, Repeated Long-Term DT Application in the DEREK Mouse Induces a Neutralizing Anti-DT Antibody Response. *J Immunol Res* **2016**, 1450398 (2016).
157. I. Eickmeier *et al.*, Influence of CD8 T cell priming in liver and gut on the enterohepatic circulation. *J Hepatol* **60**, 1143-1150 (2014).
158. A. Noble, A. Giorgini, J. A. Leggat, Cytokine-induced IL-10-secreting CD8 T cells represent a phenotypically distinct suppressor T-cell lineage. *Blood* **107**, 4475-4483 (2006).
159. S. Stein *et al.*, IL-17A/F enable cholangiocytes to restrict T cell-driven experimental cholangitis by upregulating PD-L1 expression. *Journal of hepatology* **74**, 919-930 (2021).
160. M. Thapa *et al.*, Blockade of BAFF Reshapes the Hepatic B Cell Receptor Repertoire and Attenuates Autoantibody Production in Cholestatic Liver Disease. *J Immunol* **204**, 3117-3128 (2020).
161. M. Tomura *et al.*, Monitoring cellular movement in vivo with photoconvertible fluorescence protein "Kaede" transgenic mice. *Proc Natl Acad Sci U S A* **105**, 10871-10876 (2008).
162. O. L. Rojas *et al.*, Recirculating Intestinal IgA-Producing Cells Regulate Neuroinflammation via IL-10. *Cell* **176**, 610-624.e618 (2019).
163. Q. Mu *et al.*, Gut Microbiota and Bacterial DNA Suppress Autoimmunity by Stimulating Regulatory B Cells in a Murine Model of Lupus. *Front Immunol* **11**, 593353 (2020).
164. R. Goldberg *et al.*, A Crohn's Disease-associated IL2RA Enhancer Variant Determines the Balance of T Cell Immunity by Regulating Responsiveness to IL-2 Signalling. *J Crohns Colitis* **15**, 2054-2065 (2021).

8.2 List of abbreviations

°C	Degree celsius
μ	Micro
<i>Abcb4</i>	ATP binding cassette subfamily B member 4
ACC	Acceleration
ALP	Alkaline phosphatase
ALT	Alanine aminotransferase
APC	Antigen presenting cell
AST	Aspartate aminotransferase
BA	Bile acids
BACS	Bile acid:CoA synthase
BAT	Bile acid : amino acid transferase
BHI	Brain Heart Infusion
CA	Cholic acid
CD	Crohn's disease
CDCA	Chenodeoxycholic acid
CFU	Colony forming unit
CRISPR	Clustered regularly interspaced short palindromic repeats
CYP	Cytochrome
DCA	Deoxycholic acid
DDC	3,5-diethoxycarbonyl-1,4-dihydrocollidine
DEC	Deceleration
DNA	Deoxyribonucleic acid
dNTPs	Nucleoside triphosphate
DSS	Dextran sulfate sodium
DTX	Diphtheria toxin
EDTA	Ethylenediaminetetraacetic acid
ERCP	Endoscopic retrograde cholangiopancreatography
FACS	Fluorescence-activated cell sorting
FBS	Fetal bovine serum
FGF	Fibroblast growth factor
FIR	Foxp3-IRES-mRFP
FMT	Fecal microbiota transplantation
Foxp3	Forkhead box p3
g	gram
GFP	green fluorescent protein
GGT	Gamma-glutamyl transferase
GWAS	Genome wide association studies

Gy	gray
H&E	Hematoxylin and Eosin
HCA	Hyocholic acid
HDCA	Hyodeoxycholic acid
HLA	Human leukocyte antigen
i.e.	Id est
i.p.	Intraperitoneal
i.v.	Intravenous
IBD	inflammatory bowel disease
IEL	Intraepithelial lymphocytes
IFN	Interferon
Ig	Immunoglobulin
IL	Interleukin
IL-2R	Interleukin 2 receptor
ILCs	Innate lymphoid cells
k	Kilo
l	liter
LB	Lysogeny broth
LCA	Lithocholic acid
M	molar
mAb	monoclonal antibody
MCA	Muricholic acid
MCRP	Magnetic resonance cholangiopancreatography
MDCA	Murideoxycholic acid
<i>Mdr</i>	Multidrug resistance protein
mHAI	Modified hepatic activity index
MHC	Major histocompatibility complex
min	minute
mitoROS	Mitochondrial reactive oxygen species
NK cells	Natural killer cells
<i>norUDCA</i>	24- <i>nor</i> ursodeoxycholic acid
PAMS	Pathogen-associated molecular patterns
PBC	Primary biliary cirrhosis
PBMC	Peripheral blood mononuclear cell
PBS	Phosphate buffered saline
PCR	Polymerase chain reaction
pH	Potential of hydrogen
PMA	Phorbol-12-myristat-13-acetat
PSC	Primary sclerosing cholangitis
RFP	Red fluorescent protein
ROR	Retinoid-related orphan receptor

SCFA	Short chain fatty acids
SEM	Standard error of mean
SNP	Single nucleotide polymorphism
STAT	Signal transducer and activator of transcription
TCR	T cell receptor
Th	T helper
Treg	Regulatory T cells
UC	Ulcerative colitis
UDCA	Ursodeoxycholic acids
wt	Wild type

8.3 List of figures

Figure 1: Induction of a chronic DSS colitis in <i>Mdr2</i> -deficient mice.....	52
Figure 2: Induction of chronic DSS colitis in 24 week old <i>Mdr2</i> -deficient mice.....	53
Figure 3: Induction of DSS colitis in DDC fed mice led to a reduced liver pathology.	55
Figure 4: <i>Citrobacter rodentium</i> infection of <i>Mdr2</i> -deficient mice.....	56
Figure 5: Infection with <i>Citrobacter rodentium</i> of <i>Mdr2</i> -deficient mice led to a reduced liver pathology.....	57
Figure 6: FMT with stool from DDC fed mice, or DDC+DSS fed mice into germ-free wild type mice, did not led to colitis development.....	59
Figure 7: FMT with stool from mice received DDC and DSS led to a stronger DDC induced sclerosing cholestasis compared to a FMT with stool from mice received DDC only.....	60
Figure 8: Unconjugated bile acids were overall reduced in the stool microbiota of <i>Mdr2</i> -deficient mice with DSS colitis.....	62
Figure 9: Induction of DSS colitis in <i>AM^{f/f}Csf1r^{Cre}</i> mice with DDC mediated liver pathology...	64
Figure 10: Severity of liver pathology after induction of DSS colitis in <i>AM^{f/f}Csf1r^{Cre}</i> mice and <i>AM^{+/+}Csf1r^{Cre}</i> littermates with DDC mediated liver pathology.....	65
Figure 11: Depletion of Ly6G ⁺ cells during PSC-associated colitis.....	67
Figure 12: Depletion of Ly6G ⁺ cells during PSC-associated colitis using an anti-Gr1 antibody.....	68
Figure 13: Induction of PSC-associated colitis in a mouse model without T and B cells.....	69
Figure 14: Induction of PSC-associated IBD in a mouse model without T and B cells.	70
Figure 15: Depletion of CD8 ⁺ T cells in <i>Mdr2</i> -deficient mice during chronic colitis induction.....	72
Figure 16: Depletion of CD8 ⁺ T cells in <i>Mdr2</i> -deficient mice during colitis induction results in reduced pathology of the liver.	74
Figure 17: Depletion of Foxp3 ⁺ Treg in <i>Mdr2^{-/-}DEREG</i> mice during acute DSS colitis.	75
Figure 18: Induction of acute DSS colitis in <i>Mdr2^{-/-}DEREG</i> mice.	76
Figure 19: Depletion of Foxp3 ⁺ Treg in <i>Mdr2</i> -deficient mice did not change the observed protective effect after induction of acute DSS colitis.....	77
Figure 20: Depletion of B cells using an anti-CD20 antibody in <i>Mdr2</i> -deficient mice during chronic DSS colitis.....	79
Figure 21: Depletion of B cells in <i>Mdr2</i> -deficient mice impairs the protection in liver pathology during DSS colitis.	80

Figure 22: Generation of a mouse model with an <i>Il2ra</i> ^{SNP}	82
Figure 23: <i>Il2ra</i> ^{SNP} <i>ex vivo</i> isolated Treg show a reduced suppressive capacity <i>in vitro</i>	83
Figure 24: Characterization of the <i>Mdr2</i> ^{-/-} <i>Il2ra</i> ^{SNP_HH} mice in comparison to the <i>Mdr2</i> ^{-/-} <i>Il2ra</i> ^{SNP_Mson} mice.	85
Figure 25: <i>Il2ra</i> ^{SNP} mice developed more severe sclerosing cholangitis compared to <i>Il2ra</i> ^{wt} mice with 14 weeks of age.	87
Figure 26: Analysis of CD4 ⁺ T cells in the livers of <i>Mdr2</i> ^{-/-} <i>Il2ra</i> ^{SNP} mice.....	88
Figure 27: Induction of acute DSS colitis in <i>Mdr2</i> ^{-/-} <i>Il2ra</i> ^{SNP} mice and <i>Mdr2</i> ^{-/-} <i>Il2ra</i> ^{wt} littermates.	90

8.4 List of tables

Table 1: Consumables.....	30
Table 2: Equipment.....	31
Table 3: Reagents for genotyping.....	32
Table 4: Primer sequences for PCR.....	32
Table 5: Reagents for cell isolation and <i>in vitro</i> assays	32
Table 6: Reagents for flow cytometry	33
Table 7: Buffers and solutions for genotyping	33
Table 8: Buffers and solutions for cell isolation and flow cytometry.....	33
Table 9: Buffers and solutions for FMT	34
Table 10: Buffers and solutions for histology.....	34
Table 11: Mouse models	35
Table 12: Antibodies for surface and intracellular staining.....	35
Table 13: Antibodies and chemicals for animal experiments and <i>in vitro</i> assays.....	36
Table 14: Kits	36
Table 15: Software.....	36
Table 16: Master mix <i>Mdr2</i>	37
Table 17: Master mix <i>Rag1</i>	38
Table 18: Master mix <i>Il2ra</i> ^{SNP}	38
Table 19: Master mix <i>Fir</i>	38
Table 20: Master mix <i>Tiger (wild type)</i>	39
Table 21: Master mix <i>Tiger (GFP)</i>	39
Table 22: Master mix <i>Il17Kat</i>	39
Table 23: Mdr2 program.....	40
Table 24: Il2raSNP program.....	40
Table 25: Touchdown program	40

8.5 Acknowledgment

I would like to express my sincere gratitude to Prof. Samuel Huber, who gave me the opportunity to work in his laboratory on this exciting project. I would also like to express my deepest appreciation to Dr. Tanja Bedke for the excellent supervision. Without their guidance, encouragement and continuous support, this dissertation would not have been achievable. I would also like to thank Prof. Nicola Gagliani for his expert input, his constant interest and invaluable discussions.

Thanks a lot to Prof. Julia Kehr who kindly offered to review my dissertation. In this regard, I would also like to thank Prof. Susanne Dobler and Prof. Wolfgang Streit, who offered to complete my defense committee.

I am especially thankful for the great working atmosphere, the team spirit and the constant discussion in the AG Huber. Thank you to all members and former members of the lab: Dr. Tanja Bedke, Dr. Penelope Pelczar, Dr. Shiwa Soukou-Wargalla, Dr. Mikolaj Nawrocki, Dr. Andres Machicote, Dr. Babett Steglich, Dr. Anastasios Giannou, Dr. Lis Velasquez, Dr. Antonella Fazio, Dr. Marius Böttcher, Dr. Jöran Lücke, Dr. Mustafa Shiri, Dr. Laura Garcia Perez, Dr. Can Ergen-Behr, Morsal Sabihi, Franziska Bertram, Loreen Heuer, Rongrong Jia, Beibei Liu, Tao Zhang, Martina Corazza, Philipa Loose, Anissa Franke, Simon Bohmann, Jan Kempfski, Lennart Bauditz, Sandra Wende, Cathleen Haueis, Amanda Pidgornij, Leya Eckermann, Tom Blankenburg, Jaana Helmuth und Francis Huber. Also a great thanks to the whole AG Gagliani, AG Bosurgi and AG Adlung for collaborations, discussions and help whenever needed. Thank you so much, for the great years, the constant support and the fun in the lab. Without you, I would not be where I am today.

I would like to thank Dr. Tanja Bedke and Morsal Sabihi for proofreading this dissertation.

Last but not least I would like to thank my family and friends for always being so encouraging. I am particularly thankful for the support of Jakob. Thank you for always having my back, helping me through ups and downs, and showing so much enthusiasm for what I am doing.

Thank you all, for your great support!

8.6 Curriculum vitae

Entfällt aus datenschutzrechtlichen Gründen.

8.7 Eidesstattliche Erklärung

Hiermit erkläre ich an Eides statt, dass ich die vorliegende Dissertationsschrift selbst verfasst und keine anderen als die angegebenen Quellen und Hilfsmittel benutzt habe.

8.8 Statement under oath

I hereby declare upon oath that I have written the present dissertation independently and have not used further resources and aids than those stated.

A handwritten signature in black ink, appearing to be 'F. Stumme', with a horizontal line extending to the right.

Hamburg, March 2022

8.9 Confirmation of linguistic correctness

I hereby declare, that I have read the doctoral thesis from Friederike Stumme titled “Analysis of the connection between primary sclerosing cholangitis and inflammatory bowel disease“ and confirm its linguistic correctness in English.

A handwritten signature in black ink, appearing to be 'Morsal Sabihi', with a large, stylized flourish at the end.

(Morsal Sabihi)

Hamburg, March 2022